UNIVERSIDADE DE LISBOA
FACULDADE DE CIÊNCIAS
DEPARTAMENTO DE QUÍMICA E BIOQUÍMICA

Study of the effect of electrochemical gradients on the function of cytochrome *c* oxidase using molecular simulation methods

Catarina Gusmão Beira Salgueiro Grazina

Mestrado em Bioquímica
Bioquímica Médica

Dissertação orientada por:
Dr António Baptista, Dr Francisco Pinto

2016

UNIVERSIDADE DE LISBOA

FACULDADE DE CIÊNCIAS

DEPARTAMENTO DE QUÍMICA E BIOQUÍMICA

Study of the effect of electrochemical gradients on the function of cytochrome *c* oxidase using molecular simulation methods

Catarina Gusmão Beira Salgueiro Grazina

Mestrado em Bioquímica
Especialização em Bioquímica Médica

Dissertação orientada por:
Dr António Baptista, Dr Francisco Pinto

2016

ABSTRACT

Cytochrome *c* oxidase (Ccox) is an enzyme that acts as the terminal enzyme of the respiratory chain in eukaryotes and in aerobic prokaryotes. It is an integral membrane protein, also known as complex IV of the mitochondrial respiratory chain, and belongs to the heme-copper oxidase superfamily. Ccox is a membrane-bound redox-driven proton pump that plays the role of an energy transducer that uses the potential energy of electron transfer to move protons across the membrane, against an electrochemical gradient and couples that process with dioxygen reduction to water. The vectorial electron transfer and proton pumping that occur generate a membrane potential, and the H^+ consumption generates a pH gradient. Both of these give rise to an electrochemical proton gradient, also known as protonmotive force. Given the importance of these parameters, for this thesis, we have decided to make the necessary changes to the Poisson-Boltzmann/Monte Carlo method and apply it to the study of the effect on Cytochrome *c* oxidase. However, we have also applied our model to bacteriorhodopsin (bR) in order to confirm and validate the changes that we have introduced to the method.

The work in this thesis is based on an implementation of this new method, consisting on its testing and preliminary application. It is the first time that these kind of computational methods have been applied to the study of membrane potential in Ccox.

Before the inclusion of the membrane potential, the study of the titration behavior of titrable residues in Ccox showed that the titration of many of these residues was influenced by the pH gradient. However, our results show that some residues are highly influenced by the membrane potential, and some of them even become insensitive to the pH gradient. Given the results obtained for three key residues in the Ccox system, GLU-286_i, TYC- 288_i, and LYS-362_i we have concluded that it is unlikely that these residues are involved in a regulation mechanism, since they do not titrate at physiological values, when a membrane potential is present.

Taking into account that the work presented in this thesis is essentially of implementation of a new method, the results presented here should be considered as a validation of the implementation and as an ensemble of preliminary results and conclusions that we intend to further explore, since it was not possible to do it in the time period established for the realization of this thesis. We intend to perform some future analyses to determine other biological implications of the presence of the membrane potential in Cytochrome *c* oxidase, being that the final objective of this work is the integration of this new method, presented here, in constant pH molecular dynamics simulations.

Key-words: Cytochrome c oxidase, Bacteriorhodopsin, membrane potential, protonmotive force, pH gradient

RESUMO

A Citocromo *c* oxidase (Ccox) é um enzima que actua como enzima terminal na cadeia respiratória mitocondrial em organismos eucariotas e procariotas aeróbios. Este enzima é uma proteína de membrana integral, também conhecida como complexo IV da cadeia respiratória mitocondrial, que pertence à superfamília heme-cobre oxidase. A Ccox actua como uma bomba de protões e também desempenha a função de transdutor de energia que utiliza a energia potencial que resulta da transferência de electrões para bombear protões através da membrana em que está inserida, que separa a matriz mitocondrial do espaço intermembranar mitocondrial. Esta transferência de protões é realizada contra um gradiente electroquímico e está acoplada à redução de moléculas de dioxigénio a moléculas de água. A transferência de electrões é vectorial, o que significa que acontece de forma unidireccional. Esta transferência de electrões e o bombeamento de protões através da membrana mitocondrial interna tem como consequência a geração de um potencial de membrana. Além disso, o consumo de protões leva à formação de um gradiente de pH. Ambos estes factores, o potencial de membrana e o gradiente de pH originam um gradiente electroquímico de protões que é, normalmente denominado de força motriz gerada por protões.

O trabalho apresentado nesta tese é essencialmente a validação e aplicação preliminar da implementação deste novo método que considera a influência do potencial de membrana em sistemas biológicos, sendo que esta foi a primeira vez que um estudo computacional da influência do potencial de membrana foi aplicado à Citocromo *c* oxidase. Alguns autores, como Ullmann e o seu grupo, já investigaram a importância e a influência do potencial de membrana e do gradiente de pH em sistemas biológicos. Este grupo, através da utilização de métodos computacionais, determinou que estes factores têm uma grande influência no comportamento e titulação de resíduos tituláveis na Bacteriorodopsina (bR). Esta proteína é bastante conhecida e foi utilizada por nós, nesta tese, como modelo para a validação do nosso novo método de Poisson-Boltzmann/ Monte Carlo que, para além do gradiente de pH, também inclui o potencial de membrana. Para a bR decidimos também testar quatro valores (4, 6, 8 e 10) diferentes de constantes dielétricas a atribuir à proteína. Com os resultados obtidos verificámos que, na maior parte dos resíduos, não havia diferenças significativas entre os valores de constantes dielétricas testados. Assim, como o valor de 10 foi utilizado num dos trabalhos anteriores em que nos baseámos para comparar resultados, decidimos usar este valor para todos os testes feitos. Desta forma, o mesmo valor de constante dieléctrica foi também atribuído à Citocromo *c* oxidase. Os resultados obtidos para a bR através do nosso método apresentam algumas diferenças face aos resultados obtidos pelo Ullmann e o seu grupo. Estas diferenças pouco significativas, que foram observadas aquando da comparação dos resultados obtidos, podem ter origem em vários factores. Para além de termos introduzido algumas alterações ao método usado por este grupo também os campos de forças utilizados nos cálculos moleculares são diferentes, uma vez que as cargas parciais e os raios atómicos variam entre campos de forças: Ullmann e os seus colaboradores usaram um campo de forças denominado CHARM22 enquanto o nosso método utiliza o GROMOS 54A7. Outra razão para a existência de algumas diferenças é a forma como os resíduos tituláveis foram atribuídos a cada lado da membrana: nós usamos um critério geométrico enquanto Ullmann e os seus colaboradores se basearam em redes de ligações por pontes de hidrogénio. Finalmente, outra razão possível é o facto de nós termos usado uma membrana explícita em que os lípidos carregados podem influenciar o comportamento dos resíduos, enquanto Ullmann e os seus colaboradores usaram "dummy atoms" que não têm carga atribuída e, por isso, não têm a capacidade de estabilizar ou destabilizar as formas protonadas ou desprotonadas que os resíduos proteicos adquirem durante a titulação na presença do gradiente de pH e do potencial de membrana. Devido à importância do papel da Ccox na respiração

celular, decidimos aplicar a esta proteína o nosso novo método e comparar os nossos resultados, na presença do potencial de membrana, com resultados obtidos em trabalhos anteriores, desenvolvidos no grupo de Simulação Molecular do ITQB, em que apenas foi contabilizado o efeito do gradiente de pH. Para incluir o efeito da força motriz gerada por protões foram testados dois valores: 150 mV e 200 mV. O valor de 150 mV foi testado porque é, aproximadamente, o valor observado deste parâmetro em várias condições biológicas, enquanto o valor de 200 mV foi testado uma vez que é o valor máximo, geralmente, associado a este parâmetro. No entanto, após os testes iniciais verificámos que não havia diferenças significativas na utilização destes dois valores. Assim, confirmámos que a variação do potencial de membrana entre estes valores seria insignificante e, sendo assim, seria indiferente a utilização de qualquer um deles, sendo que o erro associado à utilização deste parâmetro era reduzido. Decidimos utilizar os resultados a 150 mV como termo de comparação com os resultados obtidos para a influência do gradiente de pH, uma vez que este é o valor associado à Citocromo *c* oxidase em condições biológicas. Antes da inclusão do potencial de membrana, foi verificado, pelo grupo de Simulação Molecular do ITQB, que o comportamento dos resíduos tituláveis da Ccox era influenciado pelo gradiente de pH. No entanto, os resultados obtidos através deste novo método mostram que alguns desses resíduos se tornam insensíveis ao gradiente de pH quando há um potencial de membrana presente e que a presença deste potencial influencia de forma muito mais acentuada o comportamento dos resíduos tituláveis. Nestes trabalhos anteriores foi sugerido que três dos resíduos cujo comportamento era influenciado pelo gradiente de pH, a valores de pH fisiológicos (GLU-286_i, TYC-288_i, LYS-362_i), poderiam desempenhar um papel importante num mecanismo regulador próprio da Ccox. No entanto, com a introdução do potencial de membrana, o comportamento desses resíduos sofreu grandes alterações e estes deixaram de titular a valores de pH fisiológicos. Tendo em conta que em condições biológicas normais o potencial de membrana está sempre presente, uma das conclusões que retirámos do trabalho aqui apresentado foi que é pouco provável que estes resíduos, considerados resíduos-chave na Ccox, estejam envolvidos nesse mecanismo regulador. Para além disto, os nossos resultados mostram claramente que a presença de um potencial de membrana, neste tipo de estudos, tem uma grande influência no comportamento dos resíduos tituláveis. Estes factos levam-nos a acreditar que muitos dos valores de $\mathrm{p}K_a$ determinado através de métodos experimentais ou computacionais, na ausência de um potencial de membrana, podem não ser verificados em condições fisiológicas.

Tendo em conta o facto de o trabalho apresentado nesta tese ser essencialmente o primeiro passo após a implementação de um novo método, os resultados aqui apresentados devem ser considerados como uma validação da implementação deste método e como um conjunto de resultados e de conclusões preliminares que tencionamos continuar a explorar de uma forma mais aprofundada, uma vez que não foi possível de o fazer no tempo estabelecido para a realização desta tese. Temos previstas algumas análises futuras para determinação de outras implicações biológicas da presença do potencial de membrana na Citocromo *c* oxidase, sendo que o objectivo final é integrar esta nova metodologia, aqui apresentada, em simulações de dinâmica molecular a pH constante.

Palavras-Chave: Citocromo c oxidase, Bacteriorodopsina, potencial de membrana, força motriz gerada por protões, gradiente de pH

ACKNOWLEDGMENTS

I would like to thank to the Molecular Simulation Group at ITQB for receiving me during this year.

I would also like to thank to one of my supervisors, Dr. António Baptista for all the help, patience and availability in teaching me all the necessary subjects for the work we have developed.

I also thank my co-supervisor, Dr. Francisco Pinto, for all the availability and support.

I would also like to thank to Drª Sara Campos. Even though her name is not on this thesis as my co- supervisor, she was fundamental during this entire process and helped me since the beginning.

I also thank Pedro, Luis, Sofia and Davide for receiving me so well and helping me with fruitful discussions and suggestions. Especially Pedro for all the technical support he has provided.

I thank my parents, my grandparents and my brother for their support without which this would not have been possible to accomplish, for always believing in my capabilities, dealing with my stress crisis and support my decisions.

Last but not least, I want to thank all my family and friends for their support. In particular, I want to acknowledge Marisa Magalhães, Inês Mavioso and Maria Cordeiro for all the lunches and support they have provided during this period.

CONTENT

LIST OF FIGURES

LIST OF ABBREVIATIONS

NADH- Nicotinamide adenine dinucleotide

$FADH_2$- Flavin adenine dinucleotide

ATP- Adenosine-5′-triphosphate

ADP- Adenosine-5′-diphosphate

P_i- Inorganic phosphate

mRNA- Messenger RNA

ETC- Electron Transport Chain

pmf- Protonmotive force

R- The gas constant (8.3 kJ $mol^{-1}K^{-1}$)

T- Temperature

mV- Millivolts

m- Cation charge

F- Faraday constant (0.0965 kJ $mol^{-1}mV^{-1}$)

V- Membrane potential

MCU- Mitochondrial Calcium Uniporter

bR- Bacteriorhodopsin

kDa- Kilo Dalton

RTP-Retinal Schiff base

ROS- Reactive oxygen species

Ccox- Cytochrome *c* Oxidase

Cu- Copper ion

cyt c- Cytochrome *c*

TYC-288_i- Tyrosine covalently bonded to one of the histidine ligands of Cu_B

DNA- Deoxyribonucleic acid

MM- Molecular Mechanics

MD- Molecular Dynamics

PB- Poisson Boltzmann

MC- Monte Carlo

FF- Force Field

PEF- Potential Energy Function

LPBE- Linearized Poisson Boltzmann Equation

I- Ionic strength

k_B- Boltzmann constant

PBE- Poisson Boltzmann Equation

CE- Continuum electrostatics

Å- Angstrom

K- Kelvin

Δp- Protonmotive force (mV)

Δψ- Membrane potential

ΔpH- pH gradient across the membrane

ΔG - Gibbs energy change (kJ mol^{-1})

pH_P- pH on the side of the membrane to which protons are pumped

pH_N- pH on the side of the membrane from which protons are pumped

pH_{top}- pH at the side above the membrane

pH_{bot}- pH ate the side bellow the membrane

PRA-554- A-propionate from heme a

PRD-555- D-propionate from heme a

PRA-557- A-propionate from heme a_3

PRD-558- A-propionate from heme a_3

CHAPTER 1: INTRODUCTION

Biological membrane´s main function is to separate different compartments with different compositions. In order to do that, these membranes have a selective permeability that allows the cells to have a very tight control of their chemical composition. However, ionic channels and proton pumps allow an increase in that level of control by tolerating the exchange of bigger molecules and molecules with different features. In normal conditions, if two compartments with different concentrations of a certain solute are separated by a permeable membrane, that solute will tend to be transported to the side of the membrane in which it is in a lower concentration, until an equilibrium is achieved. If two compartments with ions of opposite charges are separated by a permeable membrane it generates an electric gradient across the membrane, also known as membrane´s potential. As such, the direction in which each ion is transported depends on its chemical gradient, due to the difference between its concentration on each side of the membrane, and it also depends on its electric gradient, also known as electrochemical potential (Quintas, Halpern e Freire 2008). This electrochemical driving force is always present in biological systems since the constant flow of energy and matter retains the systems in a constant non-equilibrium condition.

Membrane proteins constitute important interfaces that are responsible for the communication and for the mediation of the exchange of matter and information between the cell, or organelle, with the exterior medium. These proteins are encoded by 26% of the human genome (Fagerberg, et al. 2010) and are the main drug targets used for therapeutic purposes. All living cells exhibit a transmembrane potential difference or voltage across their membrane, generated by unequal electrochemical ion gradients across the bilayer (Yang e Brackenbury 2013). In recent years, it has been experimentally demonstrated that this membrane potential affects the conformation, function and transmitted signals of the membranes and that it plays a crucial role in biological energy transduction where an electrochemical gradient is generated by proton pumps (Cramer e Knaff 1991).

The electron transport chain coupled with oxidative phosphorylation is one of the most complex and effective energy transduction mechanisms. The electron transport chain is located in the mitochondrial internal membrane and is formed by four protein complexes that are responsible for the transport of electrons and generation of a proton gradient. NADH and $FADH_2$ molecules transfer, respectively, electrons to both the complexes I and II. These electrons are then transferred, by the transporter coenzyme Q, also known as ubiquinone, to the complex III. This complex then reduces the cytochrome *c* electron transporter and it donates its electrons to the complex IV that reduces O_2 molecules to H_2O. The energy generated by the electron flow is used to pump protons to the space between the internal and external mitochondrial membranes, against the concentration gradient, generating a proton gradient. The electron transport chain also includes a fifth complex responsible for the degradation of the proton gradient and ATP synthesis. This process is responsible for the conversion of electrochemical energy in chemiosmotic energy, which is then converted in chemical energy under the form of ATP molecules from ADP and P_i, releasing one water molecule (McKee e Mckee 2009).

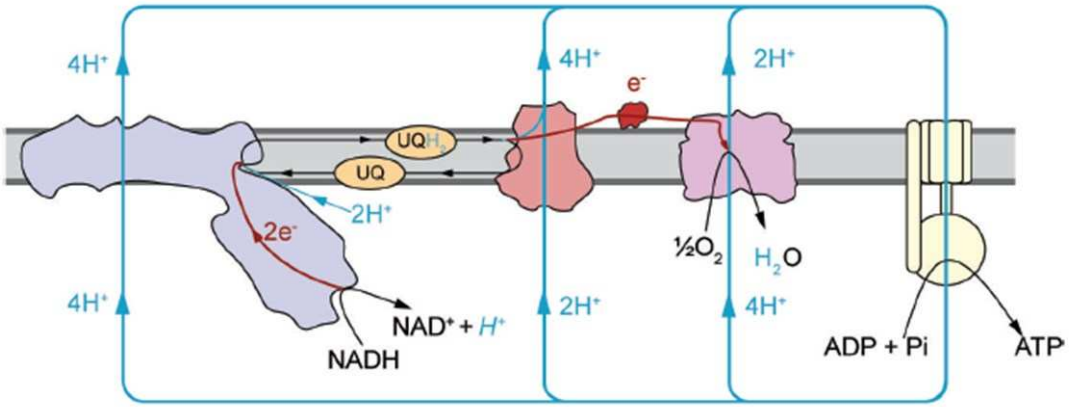

Figure 1.1: Overview of the chemiosmotic model (Nicholls e Ferguson 2013)

Despite the importance that the membrane potential and concentration gradients have in the understanding of the function of membrane proteins, these features are ignored in most of the experimental works, since it is extremely difficult to set up the systems in a way that allows the proper adjustment of these parameters (Bombarda, Torsten e Ullmann 2006). The influence of membrane potential and concentration gradients across the membrane in the function of membrane proteins can be addressed by electrophysiological methods using *in vitro* systems such as vesicles and black lipid membranes and *in vivo* systems such as *Xenopus* oocytes. In *in vivo* studies, the mRNA encoding for membrane proteins is injected in *Xenopus* oocytes in order to gain insights into the electrophysiology of membrane protein (Nicholls e Ferguson 2013).

1.1 Proton pumps

A proton pump is an integral membrane protein that is able to move protons across the biological membrane in which it is inserted. All energy transducing membranes possess several distinguishing features and they all contain a primary proton pump that differs with the energy source used by the membrane and a conserved secondary proton pump, the ATP synthase or the H^+-translocating ATPase. When these pumps function in isolation in a membrane, they hydrolyse ATP to ADP and Pi and pump protons in the same direction as the primary pump. However, based on the chemiosmotic theory, developed by the British biochemist Peter Mitchell in 1961, the primary proton pump generates an electrochemical gradient of protons large enough to force protons back through the secondary pump so that it works in the reverse order and synthesises ATP from ADP and Pi (Nicholls e Ferguson 2013). This chemiosmotic model (Figure 1.1), also known as Mitchell´s model, has two important features:

i. When electrons pass through the electron transport chain (ETC), protons are transported from the matrix to the intermembrane space. During this process, an electric potential difference ($\Delta\psi$) and a proton gradient (ΔpH) are generated across the mitochondrial inner membrane. The electrochemical gradient that arises in this process is known as the protonmotive force (Δp);
ii. Protons that are in excess in the intermembrane space can be transported back to the matrix through a special channel in the inner membrane that contains an ATP synthase activity and ATP synthesis occurs.

Mitchell has also suggested that the free energy release of electron transport across the ETC and ATP synthesis are coupled by the protonmotive force (McKee e Mckee 2009). The electron flow within primary pumps is tightly coupled to proton translocation, thus both pump types (primary and secondary) work in a concerted way. The proton electrochemical gradient is given the symbol μ_{H^+} and has two components: one that accounts for the concentration difference of protons across the membrane, ΔpH, and one that accounts for the difference in electrical potential between the two aqueous phases separated by the membrane, the membrane potential, Δψ. A bioenergetic convention is to convert μ_{H^+} into units of electrical potential (usually millivolts) and to refer to this as the protonmotive force (pmf) expressed by the symbol Δp. The critical stages of chemiosmotic energy transduction involve the interconversions of ΔG between the different forms. Isolated mitochondria can achieve equilibrium between the protonmotive force and ATP synthesis if reactions that hydrolyse ATP are absent (Nicholls e Ferguson 2013).

In the absence of a membrane potential, the Gibbs energy ΔG change for the transfer of 1 mol of solute across a membrane from a concentration $[X]_A$ to a concentration$[X]_B$ is given by:

$$\Delta G = 2.3RTlog_{10}\frac{[X]_B}{[X]_A} \qquad \textbf{eq. 1.1}$$

The transfer of a charged species driven by a membrane potential in the absence of a concentration gradient, the Gibbs energy change when 1 mol of cation, X^{m+}, is transported down an electrical potential of Δψ, mV, is given by:

$$\Delta G = -mF\Delta\psi \qquad \textbf{eq. 1.2}$$

The ion will be affected by both concentration and electrical gradients, and the ΔG when 1 mol of X^{m+} is transported down an electrical potential of Δψ mV from a concentration of $[X^{m+}]_A$ to $[X^{m+}]_B$ is given by the electrochemical equation:

$$\Delta G = -mF\Delta\psi + 2.3RT\log_{10}\left\{\frac{[X^{m+}]_B}{[X^{m+}]_A}\right\} \qquad \textbf{eq. 1.3}$$

ΔG in this equation is often expressed as the ion electrochemical gradient. In the specific case of the proton electrochemical gradient, $\Delta\tilde{\mu}_{H^+}$, eq. 1.4 can be considerably simplified because pH is a logarithmic function of $[H^+]$:

$$\Delta\tilde{\mu}_{H^+} = -F\Delta\psi + 2.3RT\Delta pH \qquad \textbf{eq.1.4}$$

ΔpH is defined as the pH in the P-phase, the side of the membrane to which protons are pumped, minus the pH in the N-phase, the side of the membrane from which protons are pumped. This means that in a respiring mitochondrion, ΔpH is usually negative. Δψ is also defined as P-phase minus N-phase and is usually positive. Mitchell defined the term protonmotive force (pmf or Δp) in units of voltage, where:

$$\Delta p = -\frac{\Delta\tilde{\mu}_{H^+}}{F} \qquad \textbf{eq.1.5}$$

As with all Gibbs energy changes, an ion distribution is at equilibrium across a membrane when ΔG, and hence $\Delta\tilde{\mu}_{H^+}$, for the ion transport process is zero. This means that at equilibrium, the ion electrochemical potential becomes:

$$\Delta G = 0 = -mF\Delta\psi + 2.3RT\log_{10}\left\{\frac{[X^{m+}]_B}{[X^{m+}]_A}\right\} \qquad \textbf{eq.1.6}$$

This rearranges to give the equilibrium Nernst equation, relating the equilibrium distribution of an ion to the membrane potential:

$$\Delta\psi = 2.3\frac{RT}{mF}log_{10}\left\{\frac{[X^{m+}]_B}{[X^{m+}]_A}\right\} \qquad \textbf{eq.1.7}$$

An ion can achieve an electrochemical equilibrium when its concentration is uneven on the two sides of the membrane. The Nernst potential is the value of $\Delta\psi$ at which an ion gradient is at equilibrium (eq.1.7). Membrane potential influences all ions distributed across a membrane and it also affects the distribution of a second ion. If the second ion is only transported by a simple electrical uniporter, it will diffuse until it reaches its electrochemical equilibrium and that ion distribution will enable the membrane potential to be calculated (Eq.1.7). The mitochondrial membrane potential is not influenced by the distribution of the second ion since the latter is present at low concentration. This occurs because a steady-state proton translocation is established and any transient decrease in membrane potential is compensated by the proton pumping. This effect is the principle for the determination of $\Delta\psi$ across energy-transducing membranes.

There are two ways to generate a membrane potential:

i. By the action of an electrogenic ion pump, such as the ones that operate in energy-transducing membranes;

ii. By the addition to one side of a membrane of a salt with a cation and an anion that have different permeabilities. The more permeable species will diffuse through the membrane ahead of the other ion creating a *diffusion potential*. These diffusion potentials can be generated through the addition of external KCl in the presence of valinomycin. The valinomycin provides permeability for K^+ generating a $\Delta\psi$, positive inside. The magnitude of the diffusion potential can be calculated from the Nernst equation (Eq.1.7). Such diffusion potentials are usually transient because the other ion, such as Cl^-, permeates slowly across the membrane and the KCl concentration will become equal on the two sides of the membrane, and also due to the rapid movement of counter-ions. In eukaryotic plasma membranes the slow transport processes enable potentials to be sustained for several hours. When this happens, the diffusion potentials due to the maintained concentration gradients across the plasma membrane play the prominent role in the determination of the membrane potential, in experimental procedures. However they are not physiologically significant, most of the times (Nicholls e Ferguson 2013).

1.1.1 Experimental measurement of protonmotive force components

The electrical circuit model of the proton circuit is often used to the measurement of Δp that has been used for different purposes. The quantification of Δp was essential to establish the thermodynamic viability of the chemiosmotic theory. The qualitative determination of $\Delta\psi$, the principal component of Δp (in Cytochrome *c* oxidase), has been extensively used as a parameter on respiration assays. In cellular applications and in combination with the application of Ohm's law ($I = V/R$), the determination of this parameter has enabled the quantification of the conductance of the inner membrane, through proton conductance. Other more sophisticated semiquantitative techniques have been used to determine whether an intervention results in a subtle increase or decrease in Δp, that has been employed as a complement in respiratory experiments. Parallel determination of respiration rates and its relation with Δp (or Δψ) provides the most insightful information on the proton circuit (Nicholls e Ferguson 2013).

1.1.2 Estimates of the protonmotive force

In 1969 Mitchell and Moyle employed pH- and K^+-selective electrodes in an initially anaerobic, low K^+ incubation to make the first determination of Δp in mitochondria. They added valinomycin to allow K^+ to equilibrate. $\Delta\psi$ was calculated from the K^+ uptake and ΔpH was calculated from proton extrusion and calculating the associated internal acidification from the buffering capacity of the matrix. The value obtained for Δp for mitochondria respiring under 'open circuit' conditions in the absence of ATP synthesis was 228 mV. However this value is overestimated because too low a value was taken for the matrix volume resulting in the amplification of the gradients (Mitchell e Moyle 1969). The technique was modified for radioactive assay and excluding the use of valinomycin since it results in the fixation of Δψ at a value corresponding to the Nernst equilibrium for the pre-existing K^+gradient across the membrane. Most of the change in Δp is reflected in changes in ΔpH, and it is crucial that this parameter is also measured to give a meaningful estimate of Δp (D. Nicholls 1974).

1.1.3 Indicators of membrane potential and ΔpH

Some extrinsic indicators of the membrane potential such as phosphonium ions as well as other lipophilic cations and anions with extensive π-orbital systems allow charge to be delocalised throughout the structure, and membrane permeant, can achieve a Nernst equilibrium across energy transducing membranes and can thus be used to monitor $\Delta\psi$. Many of these compounds have characteristic absorption spectra in the visible region, and their planar structure allows them to aggregate and form stacks when at high concentrations reducing their ability to absorb light, a phenomenon known as quenching. This can be used to monitor the uptake of the probes by mitochondria from the decrease in total absorbance, or emission if the probe is fluorescent. However, there are some things to take into consideration when using probes, such as the fact that some probes are mitochondrial inhibitors (Scaduro e Grotyohann 1999). There are also some integral membrane constituents that respond to the electrical field by altering their spectral properties and are used as intrinsic indicators of membrane potential. However, the most widely studied of these intrinsic probes are the carotenoids of photosynthetic energy-transducing membranes that are only found in both chloroplasts and photosynthetic bacteria. Another limitation of this technique is that because

carotenoids are integral membrane components, they only detect the field in their near environment, which does not necessarily correspond to the bulk-phase membrane potential difference (Smith 1990).

Weak bases can be used as ΔpH indicators in assays similar to the radioactive ones used in the estimates of the pmf. ΔpH can also be estimated from the fluorescence quenching of acridine dyes, which are weak bases and as such will tend to accumulate on the acidic side of the membrane where their fluorescence may be quenched. They can be useful qualitative probes however there are often problems in the quantification of the quenching in terms of a pH gradient (Nicholls e Ferguson 2013).

1.1.4 Factors controlling the contribution of Δψ and ΔpH to Δp

Some of the factors that regulate the contribution of Δψ and ΔpH to the Δp are represented in Figure 1.2. In figure 1.2a, we have a state of zero protonmotive force. If we add to this system an isolated working H^+ pump, it generates a protonmotive force of around 200 mV, in which Δψ is the main component. The system will remain in this steady state while in the absence of a significant flow of other ions (Figure 1.2b). If we add to the system an electrically permeant ion, such as Ca^{2+} or K^+plus valinomycin (Figure 1.2c), their accumulation will dissolve the membrane potential resulting in a decrease of the Δp value. As a consequence, there is an increase in the extrusion of protons in order to reestablish the protonmotive force. This compensation will lead to an increase of the ΔpH contributions in around 60 mV. Since the respiratory chain can only achieve the same total Δp as before, the final Δψ must be nearly 60 mV. The addition of a permeant weak acid, such as Pi, results in its accumulation, in the mitochondrial matrix, and in the redistribution of other solutes present, which will neutralize the ΔpH. The dissipation of the pH gradient allows the respiratory chain to restore the Δψ and also further Ca^{2+} uptake, through a mitochondrial calcium uniporter (MCU) (Figure 1.2d) (Nicholls e Ferguson 2013)

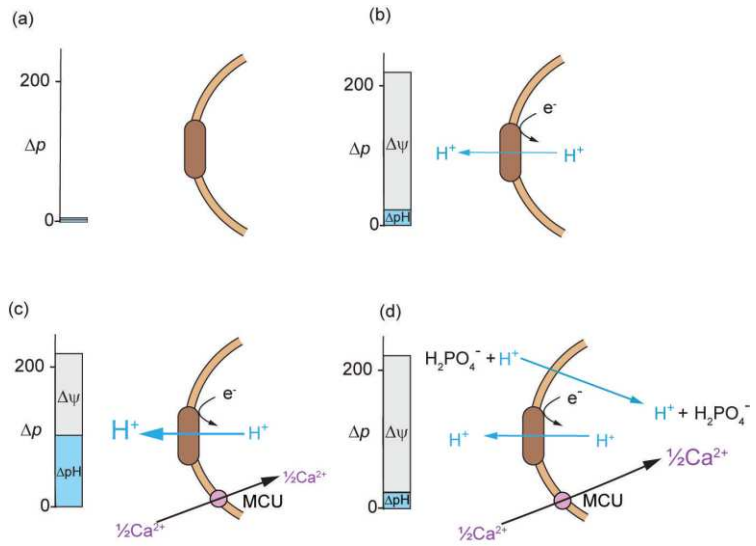

Figure 1.2: Factors that control the contribution of Δψ and ΔpH to Δp **(a)**non-respiring mitochondrion **(b)**respiration leads to a high Δψ and low ΔpH **(c)**addition of the Ca^{2+}leads to a decrease in Δψ which allows a further proton extrusion leading to an increase of ΔpH **(d) a**ddition of a permeant weak acid such as Pi results in its accumulation, in the mitochondrial matrix, with a proton driven by ΔpH which will neutralize the ΔpH and re-establish Δψ allowing further Ca^{2+} uptake (Nicholls e Ferguson 2013)

1.2 Bacteriorhodopsin

Membrane protein bacteriorhodopsin (bR) is widely used as a model system because it has been studied extensively at every aspects of characterization, structure, thermodynamics and kinetics and is now the best characterized membrane protein (J. Lanyi 1999) (J. Lanyi 2004). Also bR's great simplicity in comparison with other proton translocating bioenergetic proteins makes it an ideal model for the study of vectorial proton translocation (Baudry, et al. 2001).

Bacteriorhodopsin is a 26 kDa transmembrane protein that acts as the light-driven, voltage sensitive proton pump in the plasmatic membrane, in other words it pumps protons across the membrane using the energy of light (Calimet e Ullmann 2004). This protein comprehends seven α-helices that surround an all-trans-retinal chromophore linked via a protonated Schiff base to residue Lys-216. Upon light absorption, the retinal (RTP) experiences an isomerization process that results in the translocation of a proton from the cytoplasmic side to the extracellular side of the membrane (Ebrey 1993) (J. Lanyi 1999). This light dependent proton pump creates a transmembrane electrochemical H^+ potential that can then be used for ATP synthesis (Kayushin e Skulachev 1974). Under physiological conditions, bR pumps protons against an electrochemical potential gradient (Bombarda, Torsten e Ullmann 2006) and this vectorial proton translocation through membranes is a fundamental energy conversion process in biological cells (Baudry, et al. 2001). The dynamics of the excited state of the retinal in bR and of all-trans- and 13-cis-retinal Schiff base and the effect of the protein environment on the rate of its photoisomerization have been experimentally investigated (Logunov, El-Sayed e Song 1996) (Song, El-Sayed e Lanyi 1993).

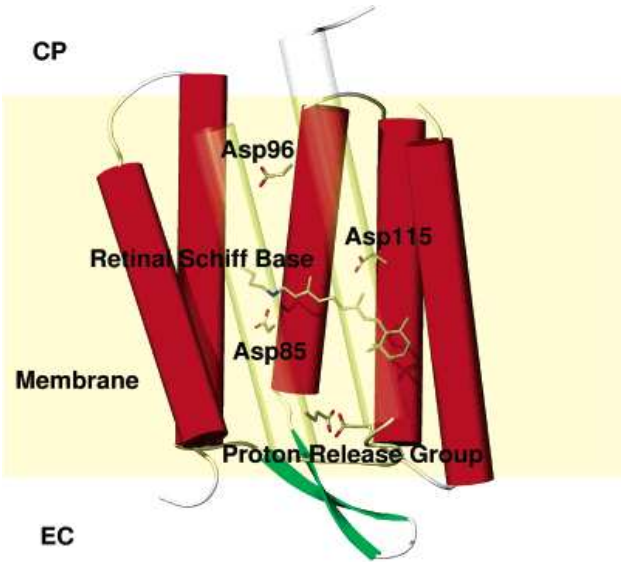

Figure 1.3 Bacteriorhodopsin structure (Bombarda, Torsten e Ullmann 2006)

Over the last years, experimental methods have provided crystal structures of bR at high resolution (Henderson, et al. 1990) (Grigorieff, et al. 1996) (Kimura, et al. 1997). These structures, together with the experimental data on bR's function, provide insight into the proton pathway in bR, but not into the pump mechanism. Although this crystal structures may not reveal the dynamics of the pump mechanism, they provide structural guiding points that allow the realization of molecular dynamics simulations and the confirmation of the structures obtained through these methods. These

theoretical and computational studies of bR allow the study of the proton translocation as the dynamic process that it represents. These types of studies can be achieved only through modeling, since proton translocation involves time scales below the resolution of observation through experimental methods, but accessible to molecular modeling (Xu, Sheves e Schulten 1995). Recent crystallographic studies have identified internal and some external water molecules (Pebay-Peyroula , et al. 1997) (Belrhali , et al. 1999). These theoretical studies have been able to determine that internal water molecules are probable key players in proton pumping (Baudry, et al. 2001).

In order to get a deeper insight on the influence of a transmembrane pH gradient on the protonation probabilities of proton pumps, Ullmann and co-workers have developed a theoretical method based on continuum electrostatics and titration calculations and this method was applied to bR (Calimet e Ullmann 2004). However, as refered above, other studies have demonstrated that the membrane potential is the main component of the pmf (in the Ccox system which is the main focus of this thesis) and, as such, its presence should have a larger influence on the function of these proton pumps (Mitchell e Moyle 1969). Some years later, Ullman and co-workers have updated their method in order to include this membrane potential and yet again they have used bR as a model to test their new method and compared it with their previous work done when taking into account only the influence of the pH gradient (Bombarda, Torsten e Ullmann 2006). Based on experimental data (Nagel, et al. 1998), they assume the membrane potential to be a simple function of ΔpH :

$$\Delta\psi(pH) = a\left({}^{RT}/_{F}\right)\ln(10)(pH_{EC} - pH_{CP}) \qquad \textbf{eq. 1.8}$$

where, a , takes the value of 0.5 as a factor that scales the increase of the membrane potential with increasing ΔpH.

With this work they have been able to determine that the membrane potential and the pH gradient are important parameters in proton pumps, as they both influence the protonation behavior of bR. The presence of these parameters has also proven to influence the energetics of the individual proton transfer steps and the protonation of certain key residues (Bombarda, Torsten e Ullmann 2006).

1.3 Cytochrome c oxidase

The complex structure and function of aerobic organisms is based on their ability to produce great amounts of energy under the form of ATP. This capacity is sustained by their ability to use O_2 as the final electron acceptor in the respiratory chain. Oxygen has several features that justify its energy-generating capacity: it is very abundant in almost every environment on earth, it diffuses easily through cell membranes and it is highly reactive which allows it to accept electrons in a very short time scale. This highly reactive feature of oxygen is responsible for its tendency to form highly destructive metabolites: reactive oxygen species (ROS) (McKee e Mckee 2009). These species can lead to cell death and degenerative diseases that can be induced by the effect of membrane potential in cytochrome *c* oxidase (Ccox). Apoptotic cell death can occur from changes in mitochondrial integrity initiated by these ROS that leads to the release of cytochrome *c* that is followed by a decrease of the mitochondrial membrane potential (Kadenbach, et al. 2004).

The cytochromes were the first components of the mitochondrial respiratory chain to be detected, due to their distinctive, redox-sensitive, visible spectra. An individual cytochrome displays one major absorption band in its oxidized form, whereas most cytochromes show three absorption bands when reduced (Nicholls e Ferguson 2013).

The sequence of electron carriers in the mitochondrial respiratory chain (Figure 1.1) was established in the 1960s through a combination of experimental techniques as oxygen electrode and spectroscopic techniques (Nicholls e Ferguson 2013). Cytochrome *c* oxidase is an enzyme that acts as the terminal enzyme of the respiratory chain in eukaryotes and in aerobic prokaryotes. It is an integral membrane protein, also known as complex IV of the mitochondrial respiratory chain, and belongs to the heme-copper oxidase superfamily which can be divided in three different families: A, B and C. This division is done according to the differences in the pathways and mechanisms of proton transfer. On this thesis we will focus on the type A family which includes the most studied type of Ccoxs such as the bovine heart mitochondria, the *Paracoccus denitrificans* and the *Rhodobacter sphaeroides* enzymes (Oliveira, et al. 2014). These Ccoxs contain two subunits in the functional core:

i. The catalytic oxygen-reduction site subunit, subunit I, includes a low spin heme *a* group and a heterodinuclear center, the binuclear center, which is deeply buried in the core and includes a high spin heme a_3 and a copper ion (Cu_B) (Siletsky 2013);

ii. The second subunit, subunit II, includes a binuclear copper center (Cu_A) that forms a redox center which receives electrons from cyt *c* and transfers them to the BNC through heme *a* (Oliveira, et al. 2014).

It is thought that both chemical and pumped protons are transported from the N-side of the membrane to the BNC through proton conducting pathways: the D-, the K- and, in certain situations, an H-pathway. These pathways are situated in subunit I. The D-pathway starts in a highly conserved aspartate residue (ASP-132) and leads to another highly conserved residue (GLU-286) near the heme-copper centre, through a chain of hydrogen-bonded waters (Svensson-Ek, et al. 2002). The K-pathway leads from the N-side of the protein to the immediacy of the binuclear center and includes some highly conserved residues: a lysine (LYS-362) and two threonines (THR-352 and THR-359) (Gennis, Multiple proton-conducting pathways in cytochrome oxidase and proposed role for the active-site tyrosine 1998). The entry of this channel includes a glutamic acid residue (GLU-101) of the subunit II (Hofacker e Schulten 1998). The H-pathway is believed to be present only in mammalian Ccox (Yoshikawa, Muramoto e Shinzawa-Ioth 2011) and it is supposed to be exclusively used for the transfer of pumped protons (Shimokata, et al. 2007). It is assumed that this channel is used for pumping protons from the N-side of the membrane to the Aspartic acid residue (ASP-51) on the P-side of the membrane (Muramoto, et al. 2007).

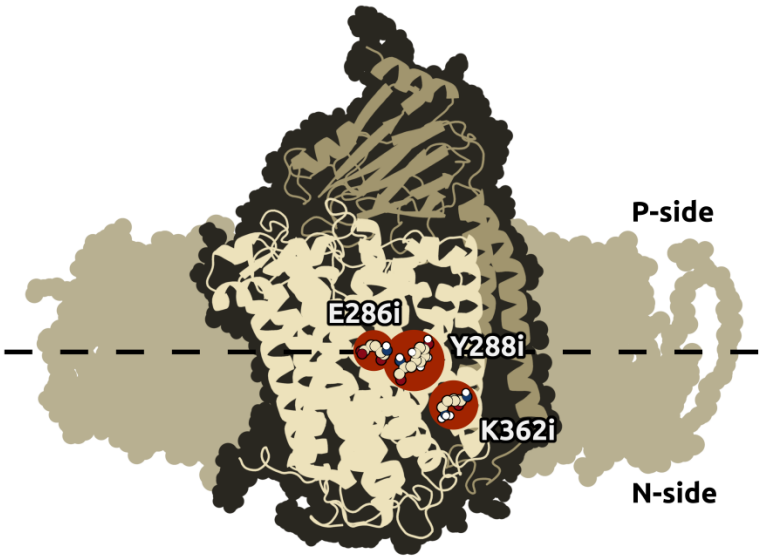

Figure 1.4: Cytochrome *c* oxidase structure

Ccox is a membrane-bound redox-driven proton pump that plays the role of an energy transducer that uses the potential energy of electron transfer to move protons across the membrane, against an electrochemical gradient and couples that process with dioxygen (O_2) reduction to water (Mills e Ferguson-Miller 2002). In order to do that, Ccox takes up four electrons from the reduced cytochrome *c* in the positively charged space of the membrane (in mitochondria it corresponds to the intermembrane space) and eight protons from the negatively charged side. Four of these eight protons are used to reduce one O_2 molecule and form two water molecules (Wikstrom 1977) (Brzezinski e Gennis 2008). The remaining protons are pumped from the negative to the positive side of the membrane (Oliveira, et al. 2014). This process is translated by the following equation:

$$4\ cyt\ c_P^{Red} + 8\ H_N^+ + \ O_2\ \rightarrow 2\ H_2O + 4\ H_P^+ + 4\ cyt\ c_P^{Ox} \qquad \textbf{eq.1.9}$$

The vectorial electron transfer and proton pumping that occurs generates a membrane potential $\Delta\psi$ and the H^+ consumption generates a pH gradient ΔpH. Both of these give rise to an electrochemical proton gradient, also known as protonmotive force, pmf, as previously explained, that is the driving force of oxidative phosphorylation (Mitchell e Moyle 1969) (Wikstrom 1977). The protonmotive force, at physiologic temperature, is given by:

$$\Delta p = \Delta\psi - 60\Delta pH \quad \text{mV} \qquad \textbf{eq. 1.10}$$

Energisation of mitochondria is associated with the development of a pmf around 200 mV that shifts the enzyme into a more low-spin conformation resulting in associated modifications in spectral, redox and kinetic properties (Wikstrom 1977). However the pmf can assume different, lower, values according to the type of electron acceptors available and type of substrate for growth. In the case

where O_2 is the final acceptor, as it happens in biological conditions, pmf is around 150 mV (Tran e Unden 1998). Thus we can estimate the membrane potential through the equation:

$$\Delta\psi = \Delta\mathrm{p} + 60\Delta pH \qquad \textbf{eq.1.11}$$

Taking this information into consideration, we have decided to test two different values for the pmf: 150 and 200 mV, in order to get a better understanding on how the range of Δψ varies at a given ΔpH:

$$\Delta\psi = (150 + 60\Delta pH) \quad \mathrm{mV} \qquad \textbf{eq.1.12}$$

$$\Delta\psi = (200 + 60\Delta pH) \quad \mathrm{mV} \qquad \textbf{eq.1.13}$$

1.4 Objectives and scope of this work

Simulation methods that are based in the semi-empirical potential energy functions are gaining an increasing importance and are playing a crucial role in the study of biological macromolecules. With the development of more affordable and powerful computers, it is now possible to study the dynamic properties of macromolecules, or biological complexes, on the nanosecond time scale with low economical costs. Simulations have become important complements to more conventional experimental approaches, because they provide detailed structural information on the dynamic properties of macromolecules and the conformational transitions that can be difficult to detect in traditional experimental procedures. In the past decades, some groups have been able to perform molecular simulations of DNA (Levitt, et al. 1995), native proteins (Levitt e Sharon 1988), peptides (Daggett e Levitt 1992), unfolding of proteins (Alonso e Daggett 1995), protein-DNA complexes (Levitt, et al. 1995) and proton pumps (Oliveira, et al. 2016) (Magalhães, et al. 2016) that are in good agreement with experimental results. Some of the studies done with these methods have been used to get a better insight in proton pumping mechanisms, especially in the Ccox system. An overview of these studies can be found in (Oliveira, et al. 2016).

Previous works done by the simulation group at ITQB (Magalhães, et al. 2016) and by Ullmann and co-workers (Calimet e Ullmann 2004) have studied the influence of the pH gradient on the protonation probabilities of bR and Ccox, where they only took in consideration the contribution of the chemical potential and they have shown that ΔpH can significantly affect the titration of several residues, meaning that this is an important feature to take into consideration. However some studies have shown that, in Ccox, this component is not as significant as the membrane potential, which is why on this thesis we are focusing on this particular component of the electrochemical gradient (Mitchell e Moyle 1969). Ullmann and co-workers have also studied the protonation probabilities of

bR in the presence of a membrane potential (Bombarda, Torsten e Ullmann 2006). Given the importance of these parameters, for this thesis, we have decided to make the necessary changes in Ullmann´s method and apply it to the study of the effect on Cytochrome *c* oxidase. However, we have also applied our model to bR in order to confirm and validate the changes that we have introduced to the method. Since the membrane potential is considered the main component of the pmf, in this thesis we focus on the study of the influence of both the pH gradient and membrane potential of Ccox.

The work in this thesis is based on the implementation of a new method, that takes into consideration the membrane potential, and it was the first time that this kind of computational method have been applied to the study of membrane potential in Ccox. Taking these facts into consideration, the results presented here should be considered as a test to the implementation of the method and as an ensemble of primary results and conclusions that we intend to further explore, since it was not possible to do it in the time period established for this thesis. The final objective is to integrate this methodology in Constant -pH Molecular Dynamics simulations (explained in chapter 2).

CHAPTER 2: THEORY AND METHODS

Since the past century computation techniques have played an important role in science and engineering. Computer-based techniques have become crucial in molecular biology, since they frequently represent the only possible way to study the behavior of a complex biological system. The study of very complex and large biological systems requires the application of different approaches, that can go from comparative analysis of sequences and structural databases to the analysis of networks of interdependence between cell components and processes, that can be achieved through coarse-grained modeling to atomically detailed simulations, and finally to molecular quantum mechanics (Liwo 2013). However, many of the problems and systems we would like to study are too large to be considered by quantum mechanics, since these methods account for all the electrons in a system which means that a large amount of particles must be considered and that is very time-consuming. Molecular mechanics is an economical alternative to quantum mechanical methods both time and money wise. Molecular modeling involves theoretical methods and computational techniques used to model or study the structure and behavior of molecules. This technique is used for studying many different molecular systems ranging from small chemical systems to large biological molecules (Leach 2001).

2.1 Statistical Mechanics

When studying complex biomolecular systems, thermodynamic properties that are usually measured by experimental procedures as average properties, are averaged over an ensemble of particles and also averaged over the time of the measurement (Leach 2001) (Hinchliffe 2008). Computation methods also allow the calculation of the average values of properties by simulating the dynamic behavior of the system at the microscopic level. The force acting on each atom can be calculated and the acceleration can be determined. The simulation generates representative configurations of these systems in such a way that accurate values of structural and thermodynamic properties can be obtained. This means that, at equilibrium conditions, the trajectory averages can represent the equilibrium properties of the system (Allen e Tildesley 1987) (van Gunsteren, Hunenberger, et al. 1995). Therefore, following the natural evolution of the system makes it possible to predict the static and dynamic properties directly from the underlying interactions between the molecules (Becker, et al. 2001).

The bridge between the microscopic behavior and macroscopic properties of molecular systems follows the laws of statistical mechanics which allow us to express thermodynamic properties in terms of microscopic quantities (Hoover 1991). This is accomplished by the application of probability rules to the macroscopic thermodynamic properties of bulk matter of the systems (Ben-Naim 1992). Statistical mechanics tells us that, instead of following the temporal evolution of a few particles, we can alternatively consider the microscopic states populated by the large ensemble of particles making up the system, which follow specific probability rules that depend on thermodynamic parameters of the system like temperature, pressure, pH, etc (Ben-Naim 1992). The ergodic principle states that, for a system in equilibrium, the time average of a certain property is the same as its ensemble average. In other words, the averaged value over the ensemble is exactly the same as the time average that would be calculated by studying the time evolution of the original system

(Hinchliffe 2008) (Rapaport 2004). This makes possible to devise non-temporal molecular simulation methods that allow us to generate a statistically representative ensemble of configurations of the system in order to obtain good ensemble averages, without having to follow its dynamics. Due to these two possible approaches, molecular modeling methods can be dynamic (like MM/MD of section 2.3), non-dynamic (PB/MC of section 2.5), or a mixture of both (constant-pH MD of section 2.8.

2.2 Molecular Mechanics

Molecular mechanics (MM) is the study of the energetics of atoms in a system using a non-quantum description. The ultimate aim of this method is to predict the energy associated with a given conformation of a molecule. This method allows the prediction of equilibrium geometries and transition states and relative energies between conformers or between different molecules. In this method the Born-Oppenheimer approximation is assumed, which means that, since the electrons can adapt to the nuclei positions very quickly, the electronic motions are ignored and we can assume only the nuclei positions. This is a huge improvement when compared to the quantum mechanical methods relatively to the time scale that is necessary to simulate a large complex system.

A biological system can be described computationally by the creation of a realistic atomic model, a force field (FF). A force field has two components: a set of equations that describe the potential energies and forces, and the parameters used in this set of equations. Over the last decades, several FFs have been developed following different approaches and focusing on reproducing different properties of a molecular system. In the “All-atom” FFs all the atoms in the system, including hydrogen molecules, are explicitly treated. In the case of the “united-atom” FFs the aliphatic hydrogens are incorporated into the atom to which they are bonded. Finally, in the “coarse-grain” FFs, the functional groups in the molecular systems are represented by simpler coarse particles rather than individual atoms. The choice of the FF is not a straightforward task and depends directly on several factors, such as, the simulation time and the properties we want to study. However a force field is only truly defined when the parameters used in the potential energy function (PEF) equation are specified. These parameters can be determined by fitting them to results of ab initio quantum calculations on small molecular clusters or by fitting them to experimental data such as crystal structure, nuclear magnetic resonance, among others (van Gunsteren e Beredndsen, Computer simulation of molecular dynamics: Methodology, applications and perspectives in chemistry 1990). For the work in this thesis, we have used the GROMOS 54A7 (Schmid, et al. 2011) force field. This FF uses the “united-atom” approach described above, and due to the reduction in the number of interactions sites, is able to decrease the computational time.

2.2.1 Potential Energy Function

The potential energy function (PEF) is a simple, empirically derived mathematical expression that gives the energy of the system as a function of the positions of the atoms and it is the way MM uses to describe the protein and its interactions. This function describes the total energy of a molecule as a sum of all the contributions: bonded (Bond length stretching, bond angle bending and dihedral (or torsion) angle twisting) and non-bonded interactions (van der Waals interactions and electrostatic terms) (figure 2.1) (Levitt, et al. 1995).

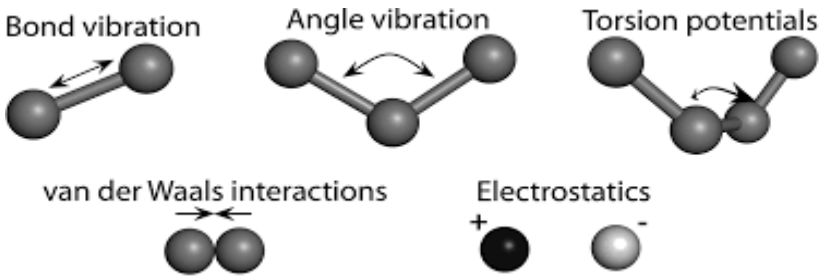

Figure 2.1: Interactions considered in MM models

In the FFs mentioned above, the potential energy of a system V(r^n) composed of *n* particles is calculated as a function of the atomic position (***r***) of each particle and, usually, takes the form presented in equation 2.1:

$$V(r^n) = V_{bonds} + V_{angles} + V_{\substack{improper \\ dihedrals}} + V_{\substack{proper \\ dihedrals}} + V_{\substack{van \\ der \\ Waals}} + V_{electrostatics} \qquad \textbf{eq.2.1}$$

As can be seen, the potential energy function is formed by six individual terms that describe the bonded (equations eq.2.2 to eq.2.5) and non-bonded (equations eq.2.6 and eq.2.7) contributions. In the GROMOS 54A7 FF, these terms are:

$$V_{bonds} = \sum_{bonds} \frac{1}{4} k_b (b^2 - b_0^2)^2 \qquad \textbf{eq.2.2}$$

$$V_{angles} = \sum_{\substack{bond \\ angles}} \frac{1}{2} k_\theta (\cos\theta - \cos\theta_0)^2 \qquad \textbf{eq.2.3}$$

$$V_{\substack{improper \\ dihedrals}} = \sum_{\substack{improper \\ dihedrals}} \frac{1}{2} k_\xi (\xi - \xi_0)^2 \qquad \textbf{eq.2.4}$$

$$V_{\substack{proper \\ dihedrals}} = \sum_{\substack{proper \\ dihedrals}} k_\varphi [(1 + \cos(\delta)\cos(m\varphi)] \qquad \textbf{eq.2.5}$$

$$V_{\substack{van \\ der \\ Waals}} = \sum_{\substack{pairs \\ i,j}} 4\varepsilon_{i,j} \left[\left(\frac{\sigma_{i,j}}{r_{i,j}} \right)^{12} - \left(\frac{\sigma_{i,j}}{r_{i,j}} \right)^{6} \right] \qquad \textbf{eq.2.6}$$

$$V_{electrostatics} = \sum_{\substack{pairs \\ i,j}} \frac{q_i q_j}{4\pi\varepsilon_0 \varepsilon_r} \frac{1}{r_{i,j}} \qquad \textbf{eq.2.7}$$

The first four terms in the potential energy function describe the bonded interactions acting between atoms that are separated by one, two or three covalent bonds, respectively. The bond length stretching contribution (figure 2.1), described by equation 2.2, where the energy between two bonded atoms is defined by a force constant (k_b) and by the difference between the bond length values (b) and

a reference bond length (b_0). The bond stretching is modeled by a harmonic quadratic potential that does not allow bond breaking.

The second term describes bond angle bending, represented by equation 2.3, and takes a similar form to bond length stretching since the angles between atoms are also modeled by a harmonic potential where k_θ is the force constant and θ_0 is the reference angle.

The third and fourth term describe dihedral angle twisting and can represent torsional "true" dihedral angles and 'improper' dihedral angles. Equation 2.4 describes the improper dihedral angles potential that are not allowed to make transitions. This potential maintains the atoms restricted to a plane and avoids transitions to a configuration of opposite chirality. These interactions are modeled by a harmonic potential where k_ξ is the force constant and ξ_0 the reference angle. Finally, equation 2.5 represents the proper dihedrals angle potential, and describes a 360 degrees rotation of a central bond in a four atom system. In this case, the proper dihedrals φ are modeled by a sinusoidal term where k_φ is the force constant, *m* the multiplicity and δ the phase shift. The multiplicity describes the periodicity of the trigonometric function, whereas the phase shift describes the dihedrals at which the energy maxima/minima occur.

The two remaining terms in the potential energy function deal with non-bonded interactions that allow for interactions between pairs of atoms separated by three or more bonds along the covalent structure, that are modeled as a function of the distance between atoms. These are the van der Waals (eq.2.6) and the electrostatic Coulombic (eq.2.7) interactions (Oostenbrink 2004). The van der Waals interactions are represented by the Lennard-Jones function, which has a term to account for increasing repulsion as the electron clouds of atoms overlap, and a term to account for the weak dispersion attraction that exists between all atoms, where $\mathrm{r_{ij}}$ is the separation of the atoms. The electrostatic terms are represented by the Coulomb potential, which can be attractive or repulsive depending on the signs of the partial charge parameters, q_i, which are assigned to all atoms.

In Equation 2.6, σ corresponds to the distance between the two atoms for which the potential interaction energy is zero, and ε is the minimum potential energy for a pair of atoms. It is important to refer that both σ and ε are unique for each pair of atoms. The van der Waals interactions are presumably calculated for all atom pairs, but, in order to reduce the computational cost of the simulation, the use of a cutoff radius is common.

In equation 2.7, the Coulombic interactions between two atoms (*i* and *j*) depend on the atomic partial charges of the interacting atoms (q_i and q_j), the distance between them (r_{ij}) and on the vacuum (ε_0) and relative permittivity of the medium ($\varepsilon = \varepsilon_0\varepsilon_r$ is called the permittivity). These interactions decay proportionally to $1/r_{ij}$. However, in order to reduce the computational cost of the columbic interactions the use of a cutoff criterion is frequent, in a similar way to the procedure for the van der Waals term.

2.3. Molecular Mechanics / Molecular Dynamics

Molecular Mechanics / Molecular Dynamics (MM/MD) methods are used to simulate the dynamic behavior of molecules modeled with a MM FF, following the first, dynamic, approach, described in section 2.1. MD applies the Newton's equations of motion to the atoms of a molecular

system, generating a representative ensemble of configurations. This method also allows the calculation of a specific trajectory which corresponds to the changes of positions and velocities of the atoms along the simulation time, resulting in a dynamic description of the system. With this method, it is possible to explore the conformational space of our system and predict its preferred conformations. The forces derived from the PEF allow us to calculate the acceleration of each particle at instant *t* using Newton's second law. However, the motions of all particles are coupled which makes the problem impossible to solve analytically, being necessary the use of numerical methods (Hinchliffe 2008) (Allen e Tildesley 1987). Basically, these methods integrate the equations of motion in very small steps and the force on each particle is a result of its interaction with other particles. One possible integration method is the leap-frog algorithm developed by Hockney in 1974. This algorithm uses the positions r_i at instant t and the velocities at instant $t - \frac{\Delta t}{2}$ and calculates the new positions and velocities according with equations 2.8 and 2.9 (Allen e Tildesley 1987) (Leach 2001):

$$r_i(t + \Delta t) = r_i(t) + v_i\left(t + \frac{\Delta t}{2}\right)\Delta t \qquad \textbf{eq.2.8}$$

$$v_i\left(t + \frac{\Delta t}{2}\right) = v_i\left(t - \frac{\Delta t}{2}\right) + \frac{F_i(t)}{m_i}\Delta t \qquad \textbf{eq.2.9}$$

2.4 Continuum electrostatics

The knowledge of protein properties at the atomic scale is very important since proteins are involved in every functional part of biological systems. Among inter and intramolecular forces, electrostatic interactions are a principal determinant of protein properties, such as function and stability, due to their strength and long-range nature. Electrostatic interactions are fundamental in several processes such as diffusional effects on enzymatic reactions, in the catalytic mechanism and especially in processes where charge alteration occurs, such as phosphorylation (Martel, Baptista e Petersen 1996). These interactions are also highly associated with the effect of pH on proteins, due to the charge alteration of titrable residues. Because of the importance of these interactions, their proper treatment in molecular modeling studies is essential in the prediction of the function and structure of native and novel proteins. There are two major approaches to model these interactions. In one approach, the system is modeled at atomic scale using a MM FF (section 2.2) and is simulated using, for example, a MM/MD method (section 2.3). In the other approach, the electrostatic interactions are treated approximately using classical continuum electrostatics, where the solute is an irregularly-shaped low dielectric object that contains embedded atomic charges, immersed in the solvent, a high-dielectric medium (figure 2.2). The boundary between these interfaces is a surface defined by the atomic coordinates and radii of the macromolecule (D. Bashford, Macroscopic electrostatic models for protonation states in proteins 2004). The solute charges can have fixed values or be associated with titrable sites that exchange protons with the solvent.

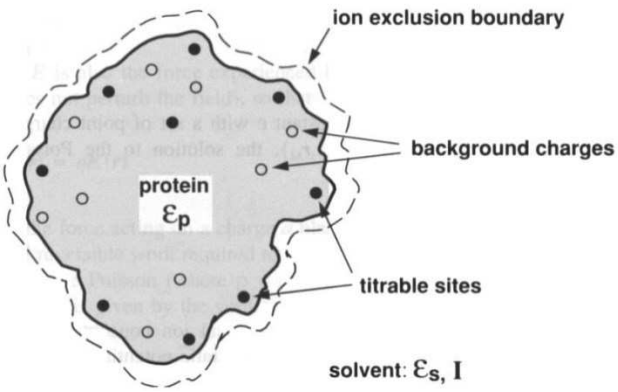

Figure 2.2: Continuum electrostatics model of a protein in solution (Martel, Baptista e Petersen 1996)

2.4.1. Poisson-Boltzmann model

The most common continuum electrostatic is the Poisson-Boltzmann (PB) approach (Fogolari, Brigo e Molinari 2002). To perform a PB calculation it is necessary to determine the electrostatic potential of the system that is considered a continuous function in space. In order to do that, some approximations are needed: as mentioned above, the protein is considered a continuous region with a value of a dielectric constant, ε_{in} and the solvent, usually water, is treated implicitly with a high dielectric constant,ε_{out}. This approximation describes the instantaneous reorganization of dipoles, and the higher its value the more reorganizable the medium. The solvent has a high value of dielectric constant, usually 80, for water, since it can adapt its conformation very easily. Unlike the solvent, the protein has a lower dielectric constant, since its ability to reorganize is lower. The PB model also considers the atomic charges of the solute in the calculation of the electrostatic potential and the ions in solution are treated in an implicit manner through the use of ionic strength. This model treats electrostatic interactions with the linearized Poisson-Boltzmann equation (LPBE):

$$\nabla.[\varepsilon(r)\nabla\phi(r)] - \kappa^2(r)\varepsilon(r)\phi(r) = -\rho(r) \qquad \textbf{eq.2.10}$$

r represents the vectorial positions of all protein atoms, ε(r) is the permittivity, ϕ(r) is the electrostatic potential, ρ(r) is the charge density and κ(r) is the reciprocal Debye length (eq 2.11), that indicates the magnitude of the thickness of the neutralizing layer of solution ions.

$$\kappa(r) = \begin{cases} \left(\frac{2e^2 I}{\varepsilon_{out}\kappa_B T}\right)^{1/2} & \text{if } r \text{ is in an ion accessible region} \\ 0 & \text{Otherwise} \end{cases} \qquad \textbf{eq.2.11}$$

I is the ionic strength of the solvent, ε_{out} is the dielectric constant of the solvent, k_{B} is the Boltzmann constant, e is the unitary charge and T is the absolute temperature. κ(r) is zero when the r is a region inaccessible to ions (inside the ion exclusion boundary in figure 2.2). If I is zero, the LPBE takes the form of the Poisson equation (PE):

$$\nabla.[\varepsilon(r)\nabla\phi(r)] = -\rho(r) \qquad \textbf{eq.2.12}$$

The LPBE and PBE are used to estimate the electrostatic potential at different positions of the system, which is, usually, done using a numerical method like finite differences (Bashford e Karplus, pKa´s of ionizable groups in proteins: atomic detail from a continuum electrostatic model 1990). When the electrostatic potential has been obtained for all points in space, the continuum electrostatic energy of the system can be easily computed as:

$$\mathcal{U} = \frac{1}{2}\sum_{j=1}^{M} q_j\phi(r_j) \qquad \textbf{eq.2.13}$$

where r_j is the position of each of the M charges on the solute.

The electrostatic energies can be used to estimate the protonation Gibbs free energy of a titrable site, the free energy difference between a reference protonation state and another state. In order to do this calculation, the use of a thermodynamic cycle is necessary.

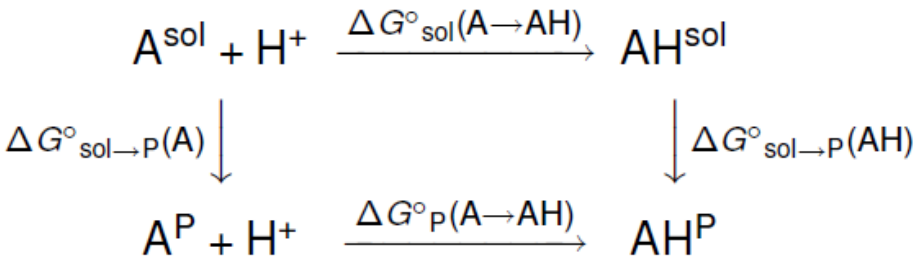

Figure 2.3: Thermodynamic cycle representation

In the thermodynamic cycle A^{sol} and AH^{sol} represent, respectively, the deprotonated and protonated site in the solvent, and A^{P} and AH^{P} represent, respectively, the deprotonated and protonated site in the protein (or other solute) environment. The standard free energy difference of protonating the site in the protein is given by:

$$\begin{aligned}\Delta G_P(A \to AH) &= \Delta G_{sol}(A \to AH) + \Delta G_{sol\to P}(AH) - \Delta G_{sol\to P}(A) \\ &= \Delta G_{sol\to P}(A \to AH) + \Delta\Delta G_{sol\to P}(A \to AH)\end{aligned} \qquad \textbf{eq.2.14}$$

This Gibbs free energy can be used to calculate to the respective pK_a value:

$$pK_a(P) = pK_a(sol) + \frac{1}{2.3k_BT}\Delta\Delta G_{sol\to P}(AH \to A)$$

$$= pK_{int} + \frac{1}{2.3k_BT}\Delta G_{interact}(P) \qquad \textbf{eq.2.15}$$

$pK_a(P)$ is the pK_a of the site in the protein environment and $pK_a(sol)$ is the pK_a of the titrable site in solution (pK_{mod}). pK_{int} is given by the pK_{mod} and the interaction of the titrable site with all other charges in the protein present in residues that are not titrating and with all other titrating sites when they are all neutral, as such it is pH-independent. $\Delta G_{interact}(P)$ depends on the pH and considers the contribution of the interaction of the site with all other titrating sites in the protein. If all these differences of free energies are approximated as differences of continuum electrostatic energies $\mathcal{U}$ (eq.2.13), all these site-specific quantities can be estimated from LPBE calculations. The same can be done for all the interaction free energies between the sites (Bashford e Karplus, pKa´s of ionizable groups in proteins: atomic detail from a continuum electrostatic model 1990).

With these previous calculations it is possible to calculate the free energy of changing from a reference state to a determined state a:

$$\Delta G(a) = -2.3k_BT\sum_i a_i\gamma_i pK_{int,i} + \sum_i\sum_{j\neq i} a_i a_j \Delta W_{ij} \qquad \textbf{eq.2.16}$$

The global protonation state of a protein (or other solute) can be written as a vector $a = (a_1, a_2 \ldots)$, with as many terms as titrable sites in the protein, where a_i is 0 if the site *i* is neutral and 1 if site *i* is charged. $\Delta G(a)$ is the free energy of the change, γ_i is the charge of site *i* when it is ionized and ΔW_{ij} is the interaction free energy between ionized sites *i* and *j*.

When we consider for each site its tautomeric state (the exact chemical placement of its titrable proton), the vector *a* must be replaced with a more general vector *x* that also indicates that tautomerism. Although the inclusion of tautomerism introduces more complexity, the protonation free energy relative to a reference state can still be written as a sum over individual sites and pairs of sites (Machuqueiro e Baptista, Is the prediction of pKa values by constant-pH molecular dynamics being hindered by inherited problems? 2011):

$$\Delta G(x) = \sum_i g_i(x_i) + \sum_i\sum_{j<i} g_{ij}(x_i, x_j) \qquad \textbf{eq.2.17}$$

Similarly to the case without tautomerism, the terms g_i and g_{ij} can be obtained using LPBE calculations.

2.5 Poisson-Boltzmann/Monte Carlo

We know from statistical mechanics that the probability of existence of a protonation state *x* at a given pH is given by (Machuqueiro e Baptista, Is the prediction of pKa values by constant-pH molecular dynamics being hindered by inherited problems? 2011):

$$p(x) = \exp[-\Delta n(x) \ln(10)\, pH - \Delta G(x)/k_B T]\ \mathrm{p}(0) \quad \textbf{eq.2.18}$$

where $\Delta n(x)$ corresponds to the change in the number of bound protons from the reference state, whose probability is $\mathrm{p}(0)$. The pH arises from the fact that the Boltzmann factor includes the term $n(x)\mu_{H^+}/k_B T$, where μ_{H^+} is the chemical potential of protons in the solution reservoir. Since we know this probability rule, we can adopt the non-dynamic approach mentioned in section 2.2, using, for example, the Monte Carlo (MC) method (Metropolis, et al. 1953) (Allen e Tildesley 1987).

The Monte Carlo method is always valid, does not require any type of additional criteria and the computation time increases linearly with the number of titrable sites. This is a sampling method that undergoes through all sites iteratively and evaluates random protonation changes. When the system changes from a protonation state x to x', the new state x' is accepted if $L(x') \leq L(x)$ or with a probability of $e^{-L(x')+L(x)}$ if $L(x') > L(x)$, where $L(x) = \Delta n(x) \ln(10)\, pH + \Delta G(x)/k_B T$. This logic obeys the Metropolis criterion (Metropolis, et al. 1953). After a certain number of MC steps a correct sample of the possible states is obtained. With the sampling obtained it is possible to determine several features: a final protonation state from the MC run, which should be representative of the used conformation, the average protonation of each titrating site and an estimated $\mathrm{pK_a}$ for each titrable residue from its titration curve, if calculations are made at different pH values.

2.6 Poisson-Boltzmann/Monte Carlo with pH gradient

In previous works (Calimet e Ullmann 2004) (Magalhães, et al. 2016), the PB/MC calculation method explained above was modified in order to include a pH gradient, ΔpH, which results in two pH values that are then assigned to either side of the membrane: $\mathrm{pH_N}$ and $\mathrm{pH_P}$ (see section 1.1). The assignment of sites to either the P- or N-side of the membrane can be performed by using their position relative to the membrane midpoint (Magalhães, et al. 2016) or their connectivity to the surface through hydrogen-bond networks (Calimet e Ullmann 2004).

2.7 Poisson-Boltzmann/Monte Carlo with membrane potential

In order to take the membrane potential into consideration some changes in the typical PB/MC calculations are necessary. We set up the system as a protein embedded in a membrane subjected to a membrane potential Δψ. The bulk potential is set to zero on side I of the membrane and on side II the membrane potential can be set to the convenient value (V), according to the system under appreciation. This system can be described by the modified PB equation (Roux 1997) (Grabe, et al. 2004):

$$-\nabla.[\varepsilon(r)\nabla\phi(r)] + \bar{\kappa}^2(r)[\phi(r) - V\Theta(r)] = \rho_f(r) \quad \textbf{eq.2.19}$$

where $\phi(r)$, $\varepsilon(r)$ and $\rho_f(r)$ correspond to the electrostatic potential, permittivity and solute charge density at point *r* and $\bar{\kappa}^2(r) = \kappa^2(r)\varepsilon_{out}$. The parameter $\Theta(r)$ can be either 0 or 1 whether the point *r* is found on side I or side II of the membrane, respectively.

The electrostatic potential ϕ can be divided in:

$$\phi(r) = \phi_f(r) + \phi_m(r) \qquad \textbf{eq.2.20}$$

where both $\phi_f(r)$ and $\phi_m(r)$ satisfy the equations 2.21 and 2.22:

$$-\nabla.\left[\varepsilon(r)\nabla\phi_f(r)\right] + \bar{\kappa}^2(r)\phi_f(r) = \rho_f(r) \qquad \textbf{eq.2.21}$$

$$-\nabla.\left[\varepsilon(r)\nabla\phi_m(r)\right] + \bar{\kappa}^2(r)\phi_m(r) = \rho_m(r) \qquad \textbf{eq.2.22}$$

The PB equation (eq.2.21) is the one that describes the system in the absence of membrane potential and in which ϕ_f accounts for the potential only due to charge density ρ_f, and can be computed using a standard PB solver. The PB equation 2.22 accounts for the contribution due to membrane potential, in which ϕ_m is the electrostatic potential created by the ionic charge density "displacement":

$$\rho_m(r) = \bar{\kappa}^2(r)\,\Theta(r)V \qquad \textbf{eq.2.23}$$

that results from the membrane potential V. Once the potentials ϕ_f and ϕ_m are determined, the total electrostatic energy of the system can be considered as (Roux 1997):

$$\mathcal{U}^* = \mathcal{U} + \int \rho_f(r)\phi_m(r)dr + \frac{1}{2}CV^2 \qquad \textbf{eq.2.24}$$

$$\mathcal{U} = \frac{1}{2}\int \rho_f(r)\phi_f(r)dr \qquad \textbf{eq.2.25}$$

$\mathcal{U}$ represents the electrostatic energy in the absence of membrane potential (equivalent to eq.2.13) and *C* (eq.2.26) respresents the capacitance of the system, that is defined by the dielectric media and ion-exclusion conditions:

$$C = \int \frac{\rho_m(r)}{V}\left[1 - \frac{\phi_m(r)}{V}\right]dr \qquad \textbf{eq.2.26}$$

Equation 2.22 must be solved with a PB solver in order to produce a true potential. This can be done in practice by discarding the protein charges and assigning to each finite-difference voxel a point charge $q=\rho_m/v$, where v is the voxel volume.

2.7.1 Boundary Conditions

The resolution of the PB equation requires the specification of the boundary conditions. The Dirichlet conditions are the ones usually adopted in finite difference calculations where the value of the potential is initially assigned and fixed to each voxel at the box walls. This assignment can be done with PB solvers providing at least one of them for the common case where the potential disappears at infinity. However this does not work for the situation in equation 2.22 because the potential at infinity along the membrane should tend to zero on side I and to V on side II while reflecting the infinite membrane along the other directions. In this case, we assign the potential at the walls with the values obtained for a perfectly planar membrane (Grabe, et al. 2004) (Roux 1997).

2.7.2 Protonation free energies

When no membrane potential is present, the standard Gibbs free energy can be captured by the electrostatic energies $\mathcal{U}$ of the PB model (Machuqueiro e Baptista, Is the prediction of pKa values by constant-pH molecular dynamics being hindered by inherited problems? 2011):

$$\Delta G(x) = \Delta\tilde{G}(x) + \mathcal{U}(x) - \mathcal{U}(0) - \sum_{i=1}^{N}\tilde{\mathcal{U}}_i(x_i) + \sum_{i=1}^{N}\tilde{\mathcal{U}}_i(0) \quad \textbf{eq.2.27}$$

where 0 represents the chosen reference protonation state, the tilted quantities refer to a set of model compounds and the non-tilted quantities refer to the solute being considered.

When a membrane potential is present, the electrostatic interactions of the membrane system must be replaced by their counterparts $\mathcal{U}^*$:

$$\Delta G^*(x) = \Delta\tilde{G}(x) + \mathcal{U}^*(x) - \mathcal{U}^*(0) - \sum_{i=1}^{N}\tilde{\mathcal{U}}_i(x_i) + \sum_{i=1}^{N}\tilde{\mathcal{U}}_i(0) \quad \textbf{eq.2.28}$$

From here, through a series of theoretical deductions done during the implementation of this method, we get :

$$\Delta G^*(x) = \Delta G(x) + \sum_i V\Delta Q_i(x_i) \quad \textbf{eq. 2.29}$$

where

$$\Delta Q_i(x_i) = \sum_{a\in i}[q_a(x_i) - q_a(0)]\,\phi_m(r_a)/V \quad \textbf{eq. 2.30}$$

is the change of an effective charge of protonable site *i.*

From this and equation 2.17, we see that, in order to include the effect of the membrane potential in usual PB/MC calculations, it is only necessary to add $V\Delta Q_i(x_i)$ to each individual site of $\Delta G(x)$:

$$\Delta G^*(x) = \sum_i g_i^*(x_i) + \sum_i \sum_{j<i} g_{ij}(x_i, x_j) \qquad \textbf{eq.2.31}$$

$$g_i^*(x_i) = g_i(x_i) + \sum_{a\epsilon i}[q_a(x_i) - q_a(0)]\phi_m(r_a) \qquad \textbf{eq.2.32}$$

An alternative, but equivalent, derivation can be found in (Bombarda, Torsten e Ullmann 2006).

2.7.3 Protonation equilibrium

In order to include the membrane potential effect, there are some changes that need to be done in equation 2.18, in section 2.5: $\Delta G(x)$ has to be replaced with $\Delta G^*(x)$, the proton chemical potential must be replaced by the electrochemical potential to reflect the membrane potential influence in the protons in bulk solution, and we need to replace the single pH value with the site specific pH_i value in order to account for the fact that each site can be influenced by the reservoir I or II. Thus the equation becomes:

$$p(x) = \exp[-\sum_i \Delta n_i(x_i) \ln(10)\, pH_i^* - \Delta G^*(x)/k_B T]\, p(0) \qquad \textbf{eq.2.33}$$

$$pH_i^* = pH_i - \frac{\psi_i e}{k_B T \ln(10)} \qquad \textbf{eq.2.34}$$

Where pH_i and ψ_i are the corresponding values to pH and ψ values of the respective reservoir.

$$pH_i^* = \begin{cases} pH_I & \text{if } i \text{ exchanges with I} \\ pH_{II} - \frac{\psi_i e}{k_B T \ln(10)} & \text{if } i \text{ exchanges with II} \end{cases} \qquad \textbf{eq.2.35}$$

An alternative, but equivalent, derivation can be found in (Bombarda, Torsten e Ullmann 2006).

2.8 Constant pH-MD

Until recently there was no computational method that allowed the treatment of pH and its effect on biomolecular structures and function. MM/MD methods (see section 2.3) do not allow a change in the protonation state during the simulation. PB/MC methods (see section 2.5) do not take

into account the structural reorganization and protonation conformation coupling events. However both approaches share a certain complementarity regarding the treatment of protonation/ deprotonation events: MM/MD methods can be used to determine structural dynamics but require the use of a fixed protonation state, while PB/MC-based approaches can be used to address multiple protonation equilibrium but require the use of a rigid protein structure. Recently, an alternative methodology that takes into account the complementarity of standard MM/MD and PB/MC methods was developed by Baptista et al (Baptista, Teixeira e Soares, Constant-pH molecular dynamics using stochastic titration 2002): the stochastic constant-pH MD method. In this method, protonation states are similarly obtained from PB/MC calculations. The coupling between the MM/MD and PB/MC algorithms ensures a proper Markov sampling from the correct thermodynamic ensemble. The stochastic titration method allows the explicit inclusion of the solvent, which makes it the perfect candidate for the explicit modeling of lipid membranes. The method works in a cycle with three main steps: the first step is a PB/MC calculation that samples a suitable protonation state for the first conformation of the system, at the intended pH; the next step is a short MM/MD segment with frozen solute to let the water molecules adapt to the new protonation state, allowing the solvent to relax to the newly presented charges coming from PB/MC calculations; the final MM/MD step is the production run with the system unfrozen. The last conformation is then used as input to the first step of the next cycle.

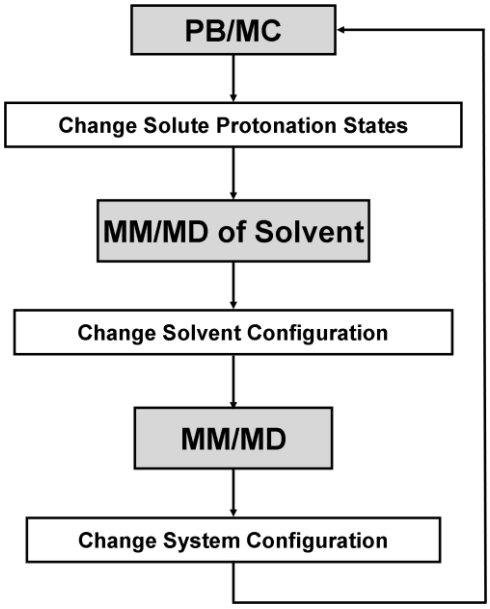

Figure 2.4: Scheme of the stochastic constant-pH MD algorithm (Baptista, Teixeira e Soares, Constant-pH molecular dynamics using stochastic titration 2002)

2.9 Methodological setup used in this work

The structural setups for both Ccox and bR were done as explained, in detail, in (Magalhães, et al. 2016). The original structures used correspond to the fully oxidized state of Ccox and to the ground state of bR.

Finite difference Poisson-Boltzmann calculations were performed using an in-house altered MEAD 2.2.9 (Bashford e Gerwert, Electrostatic calculations of the pKa values of ionizable groups in Bacteriorhodopsin 1992) version, in order to include the effect of the membrane potential, as described in section 2.7.2. For the bR standard calculations the multiflex tool from MEAD was used in a three step focusing procedure for the protein and membrane system. The first grid was composed of 151^3 points, each spaced 1.0 Å, the second grid composed of 81^3 points, each spaced 0.5 Å and with the third grid composed of 101^3 points each spaced 0.2 Å. A two-step focusing procedure was used for the model compounds using the same grid points. For the bR membrane potential calculation (eq. 2.22) a grid composed of 151^3 points, each spaced 1.0 Å, a second grid composed of 201^3 points, each spaced 0.5 Å and a third grid composed of 351^3 points each spaced 0.2 Å, was used. For the Ccox standard calculations (eq. 2.21) the first grid was composed of 161 points, each spaced 2.0 Å, the second grid composed of 81^3 points, each spaced 0.5 Å and with the third grid composed of 101^3 points each spaced 0.2 Å. A two-step focusing procedure was used for the model compounds using 61^3 grid points spaced 1.0 Å and 0.25 Å for the first and second grids, respectively. For the Ccox membrane potential calculation (eq. 2.22) a grid composed of 161^3 points, each spaced 1.0 Å, a second grid composed of 241^3 points, each spaced 0.5 Å and a third grid composed of 501^3 points each spaced 0.2 Å. In all PB calculations with membrane, dummy atoms were used to extend the bilayer until the walls of the larger grid.

Protein and lipid atoms were assigned partial charges from the GROMOS 54A7 force field description, mentioned in section 2.2, and their radii were derived from Lennard-Jones parameters as previously described (equation 2.6) (Teixeira, Cunha, et al. 2005). The retinal charges and radii used were the same used in (Magalhães, et al. 2016)**.** Proton isomerism was included as tautomeres for the neutral forms of all titratable sites and as rotamers for water molecules and serine and threonine residues, as described elsewhere (Teixeira, Cunha, et al. 2005) (Baptista e Soares, Some Theoretical and Computational Aspects of theInclusion of Proton Isomerism in the Protonation Equilibrium of Proteins 2001) (Oliveira, et al. 2016). The pK values of the model compounds were the ones previously used by (Oliveira, et al. 2014). The molecular surface was defined with a solvent probe radius of 1.4 Å, and a Stern ion-exclusion layer of 2.0 Å. A temperature of 300 K and an ionic strength of 0.1 M were used. A dielectric constant of 80 was assigned to the solvent. The dielectric constant of non-solvent regions, when applied at the molecular level, is an empirical parameter that is used in an attempt to capture all factors not explicitly included in the model, such as, structural reorganization, being highly dependent on the nature of the model used (Eberini, et al. 2004) (Schutz e Warshel 2001). Our PB/MC method, usually, needs a moderately large dielectric constant in the absence of full structural sampling, requiring a value of 6 or 8 (Eberini, et al. 2004) (Teixeira, Vila-Viçosa, et al. 2014). Thus, since the PB/MC calculations are performed in the present work using a single rigid structure, a dielectric constant of 10 was chosen, for Ccox and bR, even though several values have been tested for bR (4, 6, 8 and 10). Besides, a value of 10 was found to accurately reproduce the protonated state of the retinal in the ground state of bacteriorhodopsin, in previous works that have used our method, without the inclusion of the membrane potential (Magalhães, et al. 2016).

Monte Carlo (MC) calculations were performed using the newest version of our in-house program PETIT (Baptista, Martel e Soares, Simulation of Electron-Proton Coupling With a Monte Carlo Method: Application to Cytochrome c3 Using Continuum Electrostatics 1999) (Baptista e Soares, Some Theoretical and Computational Aspects of the Inclusion of Proton Isomerism in the Protonation Equilibrium of Proteins 2001). This recent implementation was modified in order to include three new parameters, as explained in sections 2.7.2 and 2.7.3: the first is ΔpH, which is added to, or subtracted from the selected pH value (pHinput ± ΔpH/2), resulting in two pH values that are then assigned to either side of the membrane: pH_N and pH_P; the second is an additional input file which contains all titratable sites in the protein and their respective assignment to either side of the membrane; the third is Δψ, where a value of 0 is assigned to one side of the membrane, and a value of membrane potential (V), is assigned to the other side. The assignment of sites to either the P- or N-side of the membrane was performed by applying a geometric criterion, as referred in section 2.6, where a membrane midpoint was calculated using the average z coordinates of the phosphorus atoms of the lipids closest to the protein. Sites were then assigned to either the P- or N-side of the membrane depending on whether they were above or below the calculated midpoint. The only site which had to be manually assigned due to its location near the midpoint was GLU-286I, in Ccox system. Since the side chain of this residue is facing down towards the N-side in all x-ray structures (Kaila, et al. 2008), we decided to assign it to this side. Calculations were performed for all combinations of pH values in the 0–14 range using an interval of 0.1 pH units. Each MC run consisted of 10^3 equilibration steps followed by 10^5 production steps, with one step corresponding to a cycle of single trial protonation moves on each site plus a cycle of double trial moves on each pair of strongly-coupled sites (with an interaction above 2 pK_a units). Trial moves were evaluated with a Metropolis scheme (Metropolis, et al. 1953) using the Poisson-Boltzmann protonation energy terms, the pH of the solution and the membrane potential assigned to each system, according to eq. 2.33 as previously described (Calimet e Ullmann 2004) (Baptista e Soares, Some Theoretical and Computational Aspects of theInclusion of Proton Isomerism in the Protonation Equilibrium of Proteins 2001).

CHAPTER 3: RESULTS AND DISCUSSION

3.1 Bacteriorhodopsin: method validation

As it has been referred in section 1.2, membrane protein bacteriorhodopsin (bR) is widely used as a model system because every aspect of characterization, structure, thermodynamics and kinetics have been studied in an extensive manner. Thus, this is now the best characterized membrane protein (J. Lanyi 1999) (J. Lanyi 2004). This protein has been the object of study of some other works, over the years. As such, we have chosen to use bR as a method validation, since the method we use in this thesis is similar to others used in this system, even though it includes the membrane potential, while the previous ones only include the pH gradient (Calimet e Ullmann 2004) (Magalhães, et al. 2016).

In this thesis, we have evaluated the contribution of the membrane potential to the protonmotive force and, also, in what manner this membrane potential varies with the pH gradient. In order to apply this method to the main system of this work, Ccox, we have used bR as a way to certify the in-house developed method. Since similar work has been done for bR, we can confirm the results obtained (Bombarda, Torsten e Ullmann 2006). We have plotted the equation 1.8 (section 1.2) obtained by (Bombarda, Torsten e Ullmann 2006), in order to determine the membrane potential as a function of pH_{top} (corresponds to the extracellular side (EC) in (Bombarda, Torsten e Ullmann 2006)) and pH_{bot} (corresponds to the cytoplasmic side (CP) in (Bombarda, Torsten e Ullmann 2006)). As a result we have obtained figure 3.1.

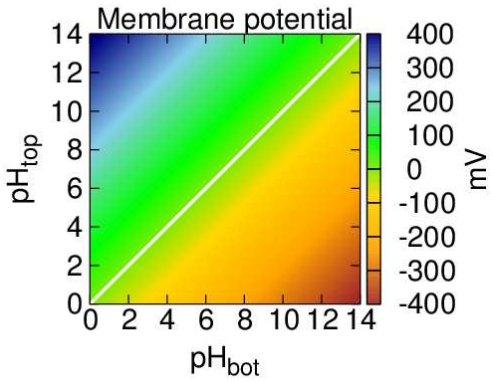

Figure 3.1: Membrane potential as a function of pH_{top} and pH_{bot}.

In order to determine how the titration of key residues are influenced by the membrane potential, titration profiles of the bR residues were evaluated. These profiles may deviate from the standard sigmoidal behavior due to electrostatic interactions with other residues, the inclusion of different pH values on both sides of the membrane and, in addition to this, the presence of a membrane potential across the membrane. The titration behavior of residues was plotted in two-dimensional titrations curves, where the color-box represents the protonation state of the titrable site (1 corresponds to a fully protonated state, while 0 corresponds to a fully deprotonated state) (presented in Appendix A). Three types of titration behavior were observed:

i. residues that, in general, do not titrate at any pH gradient (TYR-57, TYR-79, ARG-82, ARG-134, ARG-164 and TYR-185);

ii. residues whose titration is only affected by the pH of the side of the membrane they are assigned to (ARG-7, LYS-30, ASP-36, ASP-38, LYS-40, LYS-41, TYR-43, GLU-74, ASP-102, ASP-104, LYS-129, TYR-133, LYS-159, GLU-161, GLU-166, LYS-172, ARG-225 and ARG-227);

iii. residues whose titration is influenced by the pH-gradient (GLU-9, TYR-26, TYR-64, TYR-83, ASP-85, ASP-96, ASP-115, TYR-131, TYR-147, TYR-150, GLU-194, ARG-175, GLU-204, ASP-212 and the retinal titrable site RTP-216);

From the plots obtained for the titration profiles we can see that many residues are influenced by the pH gradient, however some are more influenced than others. Some residue titrations are highly influenced by the pH gradient (ASP-85, TYR-83, ASP-96, ASP-115, GLU-194, GLU-204, ASP-212 and RTP-216).

There are some residues that differ from the results presented by Ullmann and co-workers (Bombarda, Torsten e Ullmann 2006). Some of the differences observed might be generated by the use of different force fields: in (Bombarda, Torsten e Ullmann 2006) they have used the CHARMM force field, while we have used the GROMOS force field. These FFs have different sets of atomic partial charges, with the latter usually resulting in higher dipoles. This means that, when compared to the results of (Bombarda 2006), the charged forms of titrable sites may be more or less stabilized in our calculations than in theirs, depending on whether nearby dipoles are oriented in a favorable or unfavorable way. Furthermore, although the atomic radii are not indicated in (Bombarda, Torsten e Ullmann 2006), they were presumably also derived from CHARMM22 parameters, and will be generally different from ours and will result in a slightly different molecular surface. This means that, when compared to the results of (Bombarda, Torsten e Ullmann 2006), the charged forms of titrable sites may be more or less stabilized in our calculations than in theirs, depending on whether they are more or less exposed to solvent, which may happen at the surface or at interior cavities assigned with high dielectric constant. Therefore, the dipolar stabilization and the solvation of charged forms in our calculations may be lower or higher than in (Bombarda, Torsten e Ullmann 2006), and may even have opposite effects on a given site. Other important difference between the two methods is the assignment of sites to either the P- or N-side of the membrane: in our method we have used a simple geometric criterion, which has been explained in section 2.9, while Ullmann and co-workers have used hydrogen-bond networks (Bombarda, Torsten e Ullmann 2006). Finally, one last difference between the two methods is that we have used explicit lipids in the membrane, which have charged regions, while in (Bombarda, Torsten e Ullmann 2006) they have used dummy atoms. These lipid charges can influence the titration behavior of residues buried in the protein.

In the work developed in this thesis, as explained above, we had to establish the value of the dielectric constant for both the protein and the solvent. In order to do that we have decided to run all the simulations with four different ε_{in} values for the protein (4, 6, 8 and 10), keeping the value of the water constant (ε_{out}=80). From the start, we know that our PB/MC method, usually, needs a

moderately large dielectric constant in the absence of full structural sampling, as referred in section 2.9 (Eberini, et al. 2004) (Teixeira, Vila-Viçosa, et al. 2014).

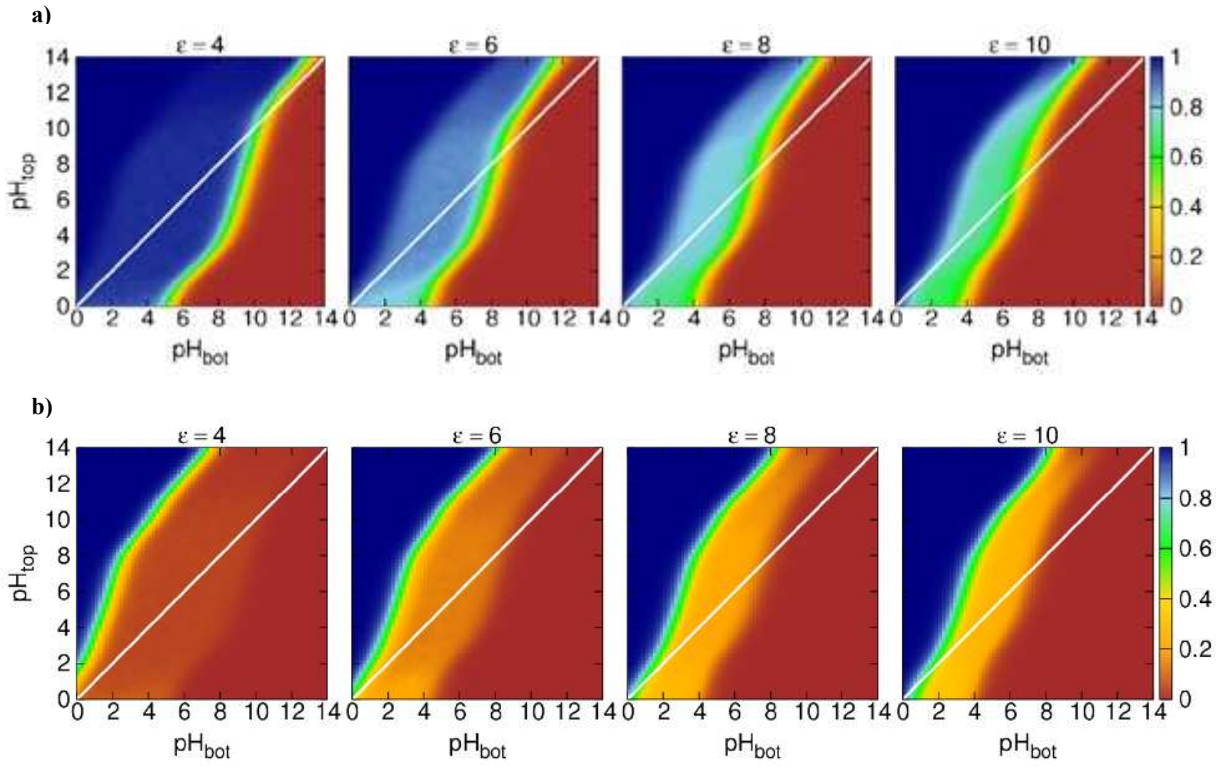

Figure 3.2: Influence of the dielectric constant in the titration profiles of **a)** GLU-194 and **b)** GLU-204.

On the titration plots, presented in Appendix A, no significant difference is observed between the four tested values, for most of the cases. Some of the larger differences verified due to the value of dielectric constant used are represented in figure 3.2. Although ε_{in}=4 was the value used by Ullmann and co-workers (Bombarda, Torsten e Ullmann 2006), in this thesis, the value of 10 was chosen since it was found to accurately reproduce the protonated state of the retinal in the ground state of bacteriorhodopsin, in previous works (Magalhães, et al. 2016).

In the case of GLU-9, our results (figure 3.3a)) reveal that this residue is more frequently in the protonated state than in Ullmann´s case, however the shape of its variation with ΔpH is the same that the one presented by Ullmann (figure 3.3b)). Our results may be due to the fact that GLU-9 is a superficial residue, which means that it is in a close proximity with the higher dielectric value of the solvent. These high values of ε have the ability to stabilize charged forms. As explained above in this section, the atomic radii used in (Bombarda, Torsten e Ullmann 2006) were presumably derived from CHARMM22 parameters, while ours were derived from GROMOS. Thus, these radii will be generally different from ours and will result in a slightly different molecular surface. This means that the charged forms of titrable sites may be more or less stable in our calculations, depending on whether they are more or less exposed to solvent, which may happen at the surface or at interior cavities assigned with high dielectric constant. Thus, a few slightly larger atoms at the surface near GLU-9 may displace the equilibrium towards the neutral form, as observed.

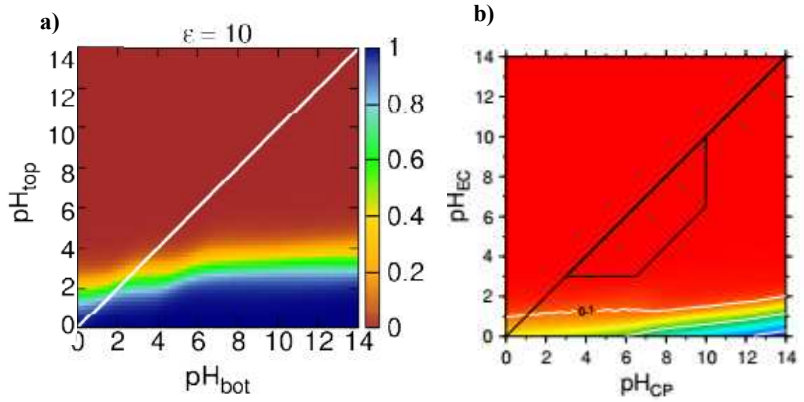

Figure 3.3: Protonation probabilities in dependence of a pH gradient and a membrane potential in GLU-9 **a)** obtained by our method **b)** obtained by (Bombarda, Torsten e Ullmann 2006)

The other residues in which we observed greater differences between our results and Ullmann´s are all buried inside the protein. In all these cases, our residues are more often in the charged, deprotonated form, than in Ullmann´s case. In the cases of ASP-85 (figures 3.4a)) and 3.4b)) and ASP-115 (figures 3.4c) and 3.4d)) the titration plots maintain the same shape and they continue to exhibit a great level of coupling between them: when ASP-85 is protonated, ASP-115 tends to be deprotonated and vice-versa. In (Bombarda, Torsten e Ullmann 2006) they were able to determine that ASP-115 is located in close proximity to a cavity, present inside the protein, with a dielectric constant value of 80. As explained earlier, a higher stabilization of the protonated form (Bombarda, Torsten e Ullmann 2006) may be related to a lower proximity of these residues to the high dielectric constant. Due to the differences between the force fields used, as explained above, our system may display a larger cavity in this region, which would explain the observed differences.

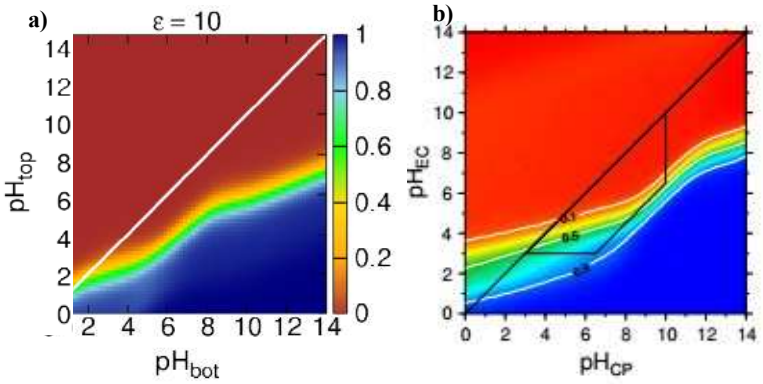

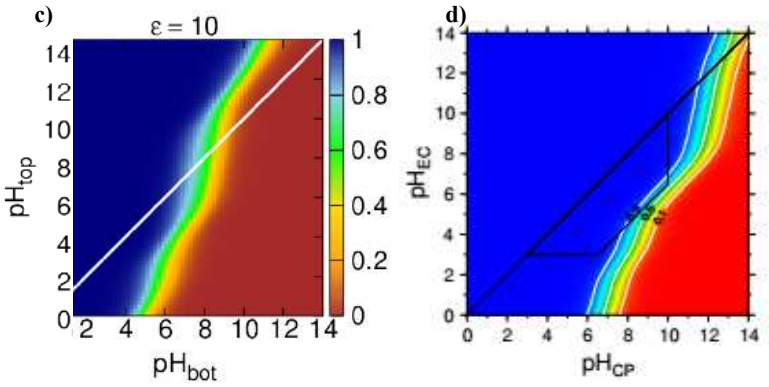

Figure 3.4: Protonation probabilities in dependence of a pH gradient and a membrane potential **a)** ASP-85 obtained by our method **b)** ASP-85 obtained by (Bombarda, Torsten e Ullmann 2006) **c)** ASP-115 obtained by our method **d)** ASP-115 obtained by (Bombarda, Torsten e Ullmann 2006)

Relatively to the residues ASP-96 (figures 3.5a) and 3.5b)), GLU-194 (figures 3.5c) and 3.5d)) and the Retinal Schiff base covalently bound to LYS-216 (RTP-216) (figures 3.5e) and 3.5f)), it is verified the same situation described in the previous case. In our simulations, all the titration shapes display a larger charged presence than in Ullmann´s study. This suggests a better stabilization of the charged form by nearby dipoles or cavities.

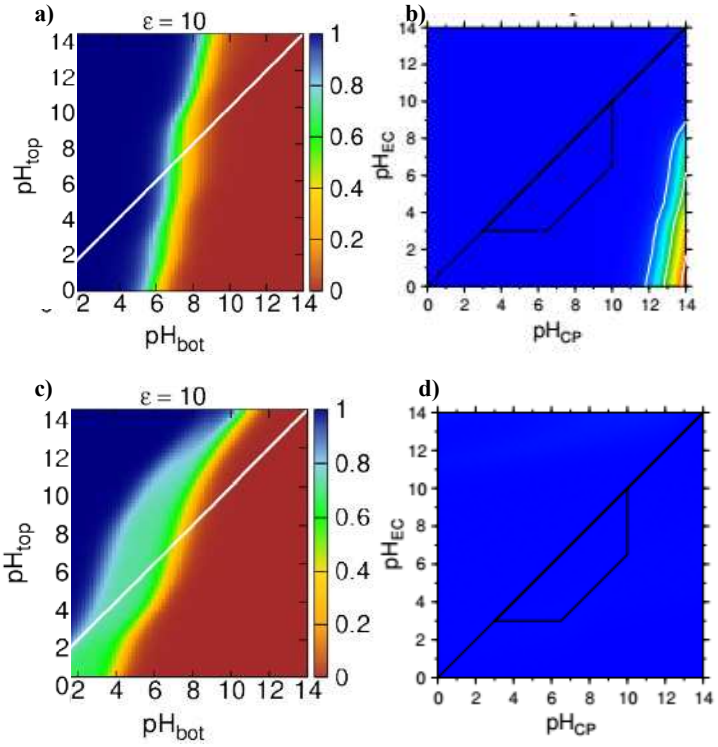

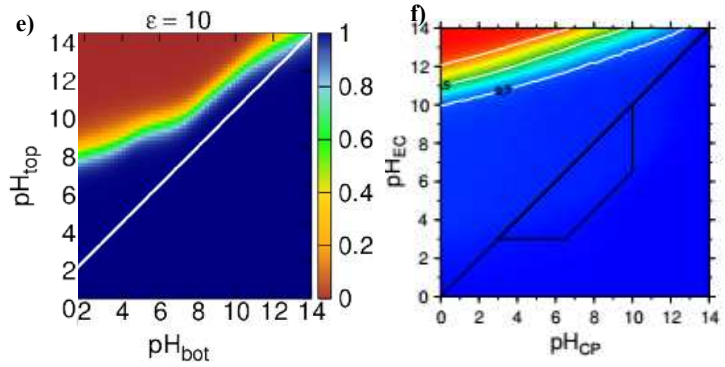

Figure 3.5: Protonation probabilities in dependence of a pH gradient and a membrane potential **a)** ASP-96 obtained by our method **b)** ASP-96 obtained by (Bombarda, Torsten e Ullmann 2006) **c)** GLU-194 obtained by our method **d)** GLU-194 obtained by (Bombarda, Torsten e Ullmann 2006) **e)** RTP-216 obtained by our method **f)** RTP-216 obtained by (Bombarda, Torsten e Ullmann 2006)

The residue that exhibits a larger difference between these two methods is GLU-204 (figure 3.6). This is simply due to the fact that this residue has been assigned to different sides of the membrane. In order to do the assignment of the residues, Ullmann and co-workers have used a hydrogen bond network while our criterion was geometrical (Bombarda, Torsten e Ullmann 2006), as referred in the final section of chapter 2.

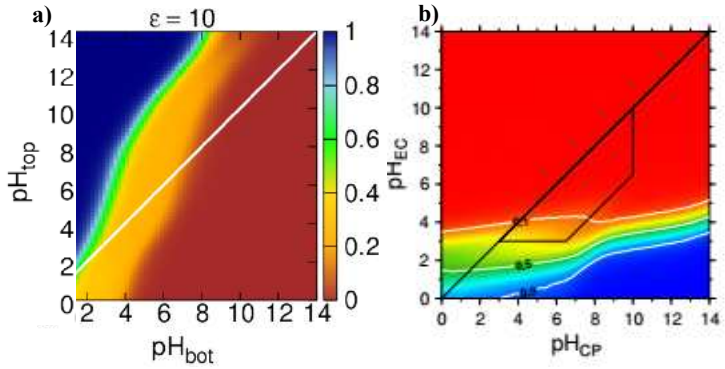

Figure 3.6: Protonation probabilities in dependence of a pH gradient and a membrane potential **a)** GLU-204 obtained by our method **b)** GLU-204 obtained by (Bombarda, Torsten e Ullmann 2006)

As found by Ullmann and co-workers (Calimet e Ullmann 2004) (Bombarda, Torsten e Ullmann 2006), when we compare our results with the work in (Magalhães, et al. 2016), we verify that the membrane potential has some influence in the results obtained. However, with the exception of some cases, this influence is not very significant. This is due to the fact that the value for the membrane potential, in this system is relatively low, as it is shown in figure 3.1.

The majority of the results we have obtained display no differences from the results presented in (Bombarda, Torsten e Ullmann 2006) and the differences obtained can be explained by several parameters, as discussed above. However, the exact reasons for the differences are difficult to evaluate: the proximity to charges that are able to stabilize nearby titrable residues, the presence of small cavities that can stabilize the charged form due to the high ε_{out} (80) and the distance to the interface with the solvent that is able to stabilize the charged form. Thus, this overall agreement with an analogous implementation, make us feel comfortable to use our method and apply it to other biological systems, in this case, Ccox.

3.2 Cytochrome *c* oxidase

In this chapter, we have evaluated the contribution of the membrane potential to the protonmotive force and, also, in what manner this membrane potential fluctuates with the pH gradient in the Ccox system. We have plotted the equation 1.10 (section 1.3) obtained from (Nicholls e Ferguson 2013), in order to determine the membrane potential as a function of pH_{top} (corresponds to the pH_P explained in chapter1) and pH_{bot} (corresponds to the pH_N explained in chapter1). In order to determine how the titration of key residues are influenced by the membrane potential, titration profiles of the Ccox residues were evaluated. Two pmf values were tested in order to evaluate the magnitude of the influence of the membrane potential (figure 3.7), with a dielectric constant of 10 for the protein, as used for bR. A value of pmf of 150 mV (eq.1.12, section 1.3) was used since it has been associated with biological conditions (Tran e Unden 1998) and a value of 200 mV (equation 1.13, section 1.3) was used since it has been seen that this value is associated with a state of energisation of mitochondria (Wikstrom 1977).

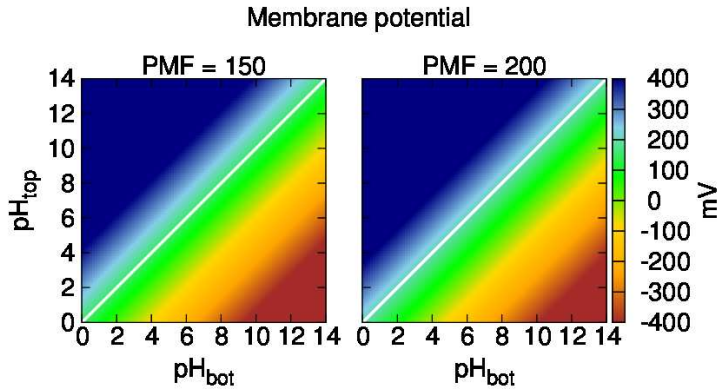

Figure 3.7: Membrane potential as a function of pH_{top} and pH_{bot} in both pmf values tested. Although the similar color range was used for comparison with bR, the values, in Ccox, vary between -600 mV and 1000 mV.

With the utilization of both these pmf values, we screened through pH_{top} and pH_{bot}. Based on the titration plots, presented in Appendix B, we can verify that there are no substantial differences between the two tested pmf values, which assure us that our calculations are not significantly affected by the uncertainty associated with this parameter. The titration behavior of residues was plotted in two-dimensional titrations curves, where the color-box represents the protonation state of the titrable site (1 corresponds to a fully protonated state, while 0 corresponds to a fully deprotonated state) (presented in Appendix B). We present the two cases where a larger difference has been observed: ARG-188_i (figure 3.8) and HIS-195_i (figure 3.9) (the index values i and ii correspond to subunits I and II, respectively).

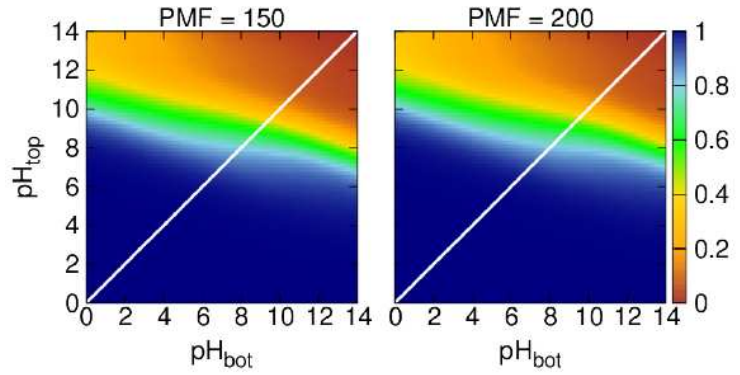

Figure 3.8: Protonation probabilities of ASP-188$_i$ with different pmf values.

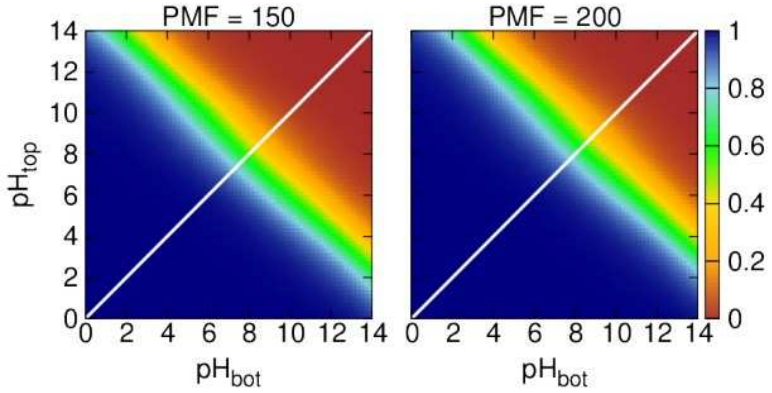

Figure 3.9: Protonation probabilities of HIS-195$_i$ with different pmf values.

Although there are no significant differences between the two pmf values, in this thesis, the value of 150 mV was chosen since it is closer to the ones associated with several biological conditions, section 1.3 (Tran e Unden 1998).

In previous works (Magalhães, et al. 2016) the effect of the pH gradient across the membrane on the titration behavior of residues in Ccox has been studied. It was determined that the pH gradient has a significant influence on the titration of several residues (Magalhães, et al. 2016). In order to determine how the titration of key residues are influenced by the membrane potential, titration profiles of the Ccox residues were evaluated, as it was done for bR, section 3.1. Some of the profiles obtained also deviate from the standard sigmoidal behavior due to electrostatic interactions with other residues, the inclusion of different pH values on both sides of the membrane and, in addition to this, the presence of a membrane potential across the membrane, as was observed for bR. Four types of titration behavior were observed:

i. residues that, in general, do not titrate at any pH gradient (In subunit I: NTPHE-17, HIS-26, LYS-27, TYR-33, GLU-54, HIS-67, GLU-69, LYS-74, HIS-93, TYR-122, HIS-127, TYR-146, HIS-223, LYS-224, ASP-256, ASP-271, TYR-275, HIS-277, TYC-288, HIS-300, LYS-307, LYS-308, TYR-313, TYR-336, TYR-347, LYS-362, GLU-376, LYS-378, ASP-407, TYR-409, TYR-414, TYR-415, TYR-422, TYR-437, LYS-442, GLU-450, HIS-456, HIS-472, ARG-476, ARG-482, TYR-483, TYR-486, GLU-488, TYR-517, ARG-521, TYR-530, GLU-533, HIS-534, ASP-536, GLU-548, HIS-549, PRA-554, PRD-

555, PRA-557, PRD-558. In subunit II: NTLEU-30, GLU-31, HIS-55, HIS-84, LYS-86, LYS-89, ARG-93, ASP-133, LYS-137, TYR-141, TYR-144, TYR-147, TYR-149, ASP-151, GLU-157, TYR-159, ASP-169, GLU-175, GLU-177, GLU-182, GLU-189, ASP-195, ASP-214, LYS-227, ASP-229, GLU-243, ARG-244, TYR-262, LYS-268, GLU-272, TYR-275, GLU-280, HIS-282, HIS-285, CTHIS-285);

ii. residues whose titration is only affected by the pH of the side of the membrane they are assigned to (In subunit I: ARG-19, ASP-28, GLU-66, GLU-86, ASP-132, ARG-216, ARG-257, ARG-446, ARG-524, CTPHE-551. In subunit II: ARG-35, GLU-128, GLU-131, GLU-148, GLU-152, GLU-153, ARG-171, TYR-185, LYS-204, GLU-245, GLU-273, HIS-283, HIS-284);

iii. residues whose titration is influenced by the pH-gradient (in subunit I: TYR-50, ARG-52, ARG-137, TYR-175, GLU-182, ASP-188, ARG-408, TYR-410, TYR-448, ARG-481, ASP-485, GLU-539. In subunit II: ASP-58, ARG-82, GLU-85, ARG-87, HIS-96, GLU-101, ARG-187, ASP-188, ARG-234, ARG-241);

iv. residues whose titration is influenced by both pH_{top} and pH_{bot} (In subunit I: TYR-143, TYR-185, HIS-195, GLU-286, TYR-318, LYS-454. In subunit II: TYR-78).

Based on the titration plots obtained with our method, we can see that, with a few exceptions, most of the titrable sites display large differences relatively to their titration behavior obtained without the presence of a membrane potential (Magalhães, et al. 2016). This large differences caused by the presence of a membrane potential are not verified in the bR system, where the influence of the membrane potential is not that significant, when compared to the pH gradient (Calimet e Ullmann 2004) (Bombarda, Torsten e Ullmann 2006). From the plots presented in Appendix B, we have chosen three titrable sites (figure 3.10) where the presence of a membrane potential has had significant influence in the titration behavior of these sites.

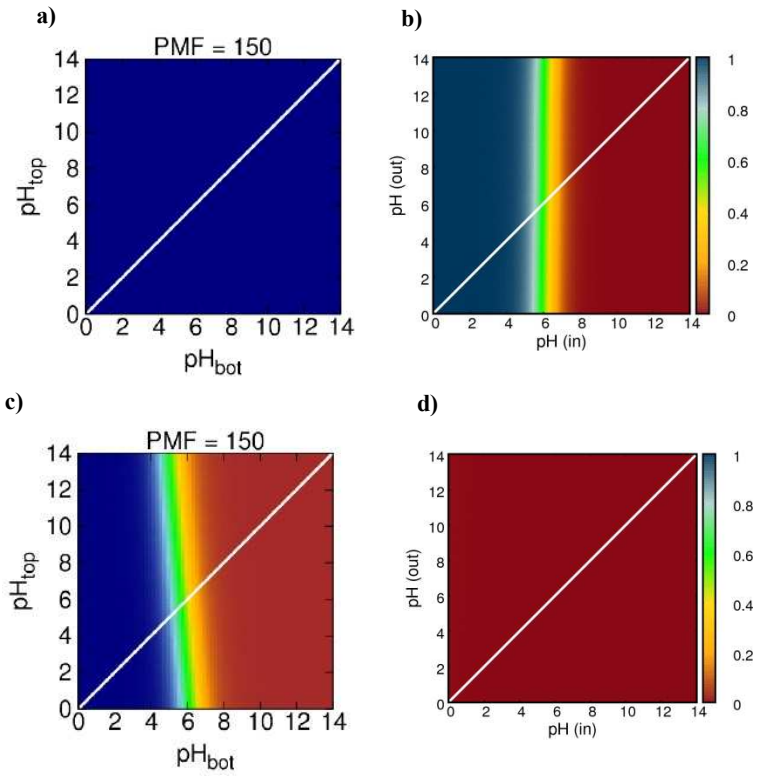

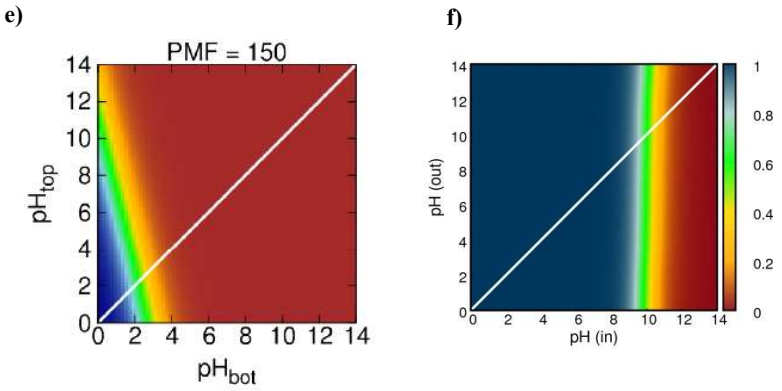

Figure 3.10: Protonation probabilities **a)** NTPHE-17_i in dependence of a pH gradient and a membrane potential **b)** NTPHE-17_i in dependence of a pH gradient obtained by (Magalhães, et al. 2016) **c)** GLU-539_i in dependence of a pH gradient and a membrane potential **d)** GLU-539_i in dependence of a pH gradient obtained by (Magalhães, et al. 2016) **e)** TYR-78_{ii} in dependence of a pH gradient and a membrane potential **f)** TYR-78_{ii} in dependence of a pH gradient obtained by (Magalhães, et al. 2016)

However, as explained in sections 1.2 and 1.3 and illustrated by figures 3.1 and 3.7, the membrane potential contribution to the pmf is greater in Ccox than in bR. This explains why the effect of the membrane potential is greater in Ccox (when comparing our results with (Magalhães, et al. 2016)), than in bR (when comparing (Calimet e Ullmann 2004) with (Bombarda, Torsten e Ullmann 2006)). In other words, the membrane potential contribution to the pmf is greater in Ccox, than in bR. Since the behavior of every titrable site in Ccox changes in the presence of the membrane potential, it would be interesting to investigate if there is any relation between the magnitude of these differences and the relative position of the sites in the protein. Some analyses of studies that can be done in order to determine if there is any trend are: if they are buried in the interior of the protein, if they are at the surface, in which side of the membrane they are located or if they have any internal water molecules in their close proximity. This may be addressed in future works.

Among the changes that are caused by the presence of a membrane potential, there are a few residues that are more intriguing: TYR-143_i, TYR-185_i, HIS-195_i, GLU-286_i, TYR-318_i, LYS-454_i and TYR-78_{ii}. Before the inclusion of the membrane potential in the study of the titration behavior of residues TYR-143_i (figures 3.11 a) and b)), HIS-195_i(figures 3.11 c) and d)), GLU-286_i (figures 3.11 e) and f)), TYR-318_i (figures 3.11 g) and h)) and LYS-454_i (figures 3.11 i) and j)), results obtained in previous works showed that the titration of these residues was influenced by the pH gradient (Magalhães, et al. 2016) , with the titration region (color-changing band) tilted to the right (right column, figure 3.11). In our results we see an inversion in the titration behavior, with the color-changing band tilted to the left (left column, figure 3.11). Since the pH gradient varies (increases or decreases) away from the diagonal white line where the pH gradient is zero, a color-changing band with a slope similar to the diagonal indicates a titration strongly dependent on the gradient, while a slope perpendicular to the diagonal indicates a titration insensitive to the gradient. Therefore, our results indicate that some residues have become less sensitive, or even completely insensitive, to the pH gradient, in the presence of the membrane potential. Also, TYR-143_i, HIS-195_i and GLU-286_i are more frequently in the charged form. In the case of TYR-185_i (figures 3.12 a) and b)) and TYR-78_{ii} (figures 3.12 c) and d)), residues whose titration behavior was found, in (Magalhães, et al. 2016),

to be dependent only on the pH of the side of the membrane they were assigned to, have now become sensitive to the membrane potential and depend on pH in a more complex way.

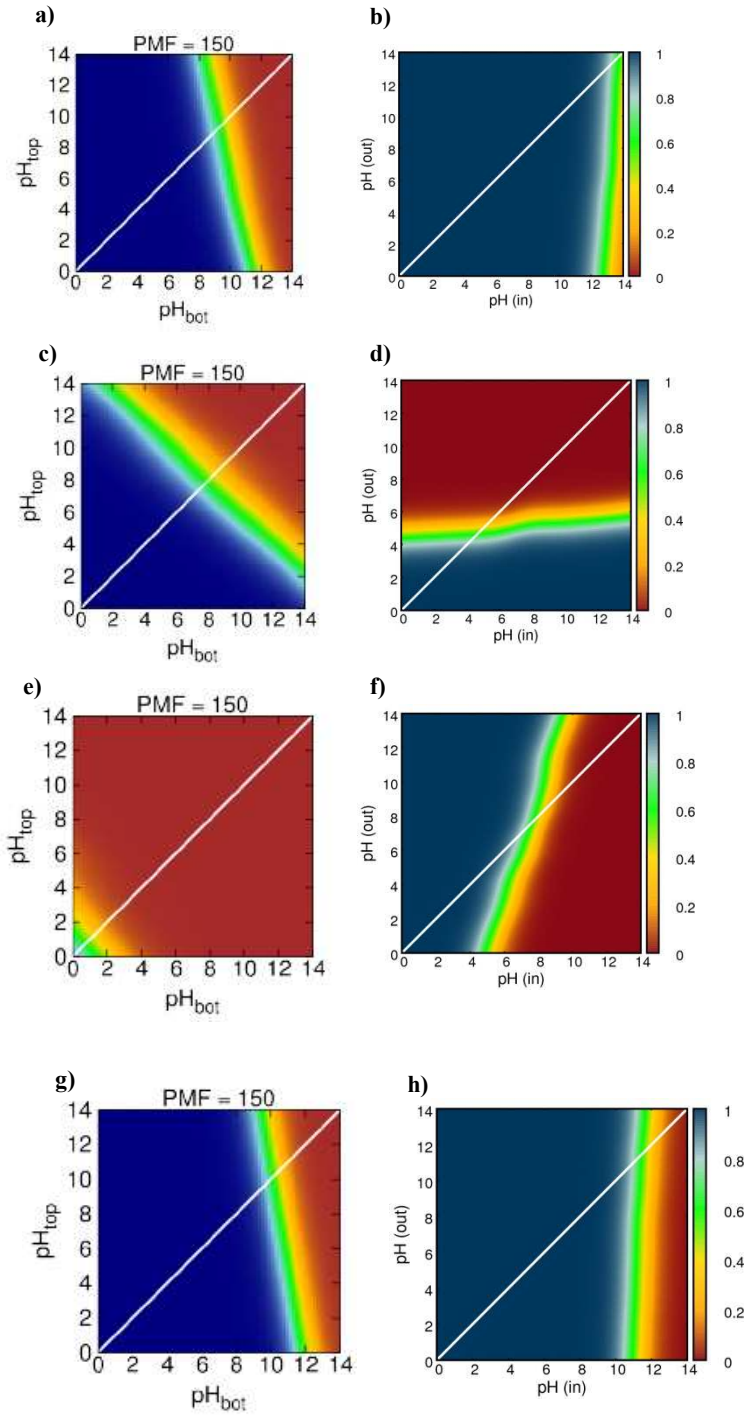

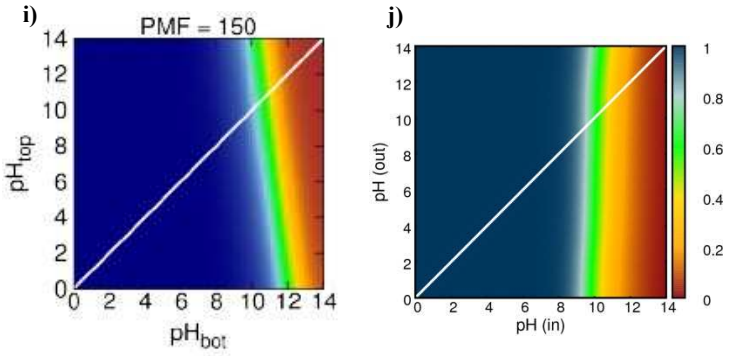

Figure 3.11: Protonation probabilities **a)**TYR-143$_i$ in dependence of a pH gradient and a membrane potential **b)**TYR-143$_i$ in dependence of a pH gradient obtained by (Magalhães, et al. 2016) **c)**HIS-195$_i$ in dependence of a pH gradient and a membrane potential **d)**HIS-195$_i$in dependence of a pH gradient obtained by (Magalhães, et al. 2016) **e)**GLU-286$_i$in dependence of a pH gradient and a membrane potential **f)**GLU-286$_i$in dependence of a pH gradient obtained by (Magalhães, et al. 2016) **g)**TYR-318$_i$in dependence of a pH gradient and a membrane potential **h)**TYR-318$_i$in dependence of a pH gradient obtained by (Magalhães, et al. 2016) **i)** LYS-454$_i$in dependence of a pH gradient and a membrane potential **j)**LYS-454$_i$in dependence of a pH gradient obtained by (Magalhães, et al. 2016)

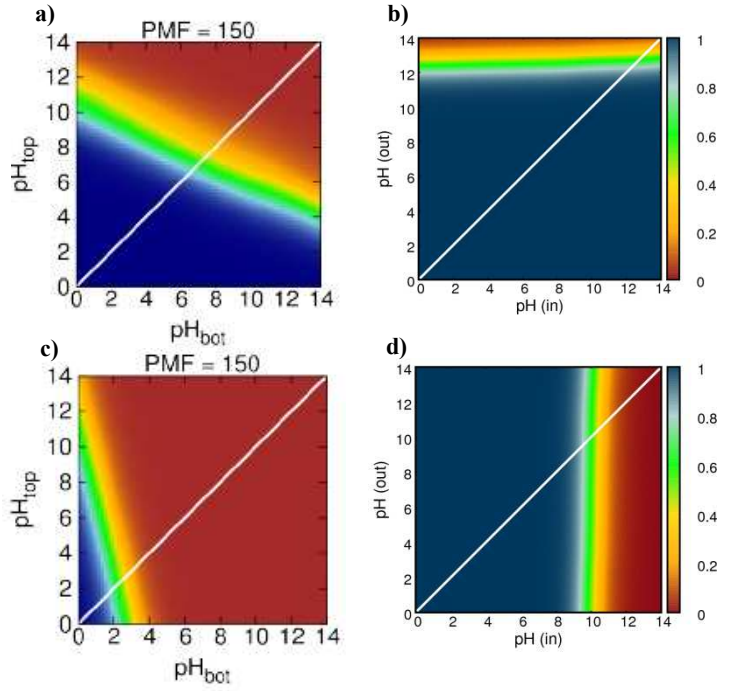

Figure 3.12: Protonation probabilities **a)** TYR-185$_i$ in dependence of a pH gradient and a membrane potential **b)** TYR-185$_i$ in dependence of a pH gradient obtained by (Magalhães, et al. 2016) **c)** TYR-78$_{ii}$ in dependence of a pH gradient and a membrane potential **d)** TYR-78$_{ii}$ in dependence of a pH gradient obtained by (Magalhães, et al. 2016)

The effect observed in figures 3.11 and 3.12 should be further investigated in future studies, in order to determine why the titrable sites become less sensitive to the pH gradient. The investigation of this extreme exchange of behavior can probably be best understood with the type of analyses mentioned above.

In the work done in (Magalhães, et al. 2016) it was suggested that three key residues in Ccox, whose titration was influenced by the pH gradient at physiological pH values, GLU-286$_i$, TYC- 288$_i$, and LYS-362$_i$, are part of a regulatory mechanism to control the proton flow. GLU-286$_i$ (figure 3.13) is located at the end of the D-channel, near the active site of Ccox and it is believed that it serves as a regulator of the flow of chemical and pumped protons, see section 1.3. TYC- 288$_i$ (figure 3.14) is

a highly conserved residue and is the terminal residue in the K-channel (Pereira, Santana e Teixeira 2001). It is assumed that this residue is involved in the catalytic process of Ccox, by donating a hydrogen atom to facilitate the breaking of the O–O bond (Gennis, Multiple proton-conducting pathways in cytochrome oxidase and a proposed role for the active-site tyrosine 1998). LYS-362$_i$, (figure 3.15) is a highly conserved residue located in a hydrophobic environment (Magalhães, et al. 2016) near the entrance of the K-channel.

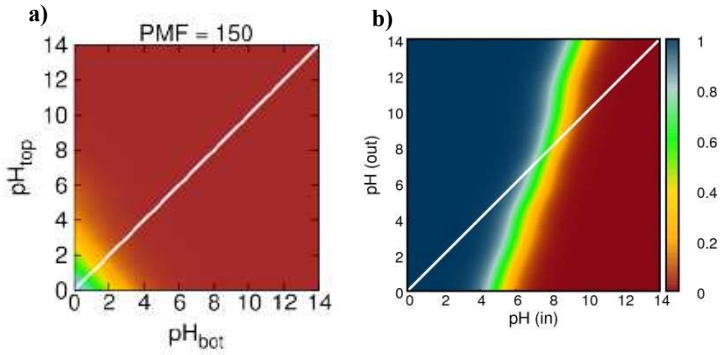

Figure 3.13: Protonation probabilities of GLU-286$_i$**a)** in dependence of a pH gradient and a membrane potential **b)** in dependence of a pH gradient obtained by (Magalhães, et al. 2016)

As we can see through the comparison of the images in figure 3.13, the residue GLU-286$_i$, in the presence of a membrane potential, changes from being a site that titrates in physiological conditions to a residue that do not titrate at those values, being in the charged form most of the time.

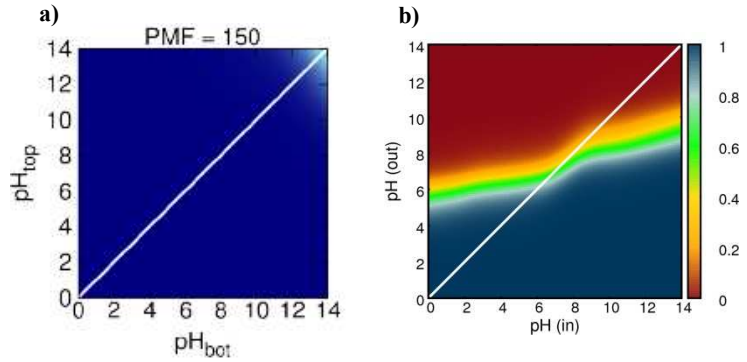

Figure 3.14: Protonation probabilities of TYC- 288$_i$**a)** in dependence of a pH gradient and a membrane potential **b)** in dependence of a pH gradient obtained by (Magalhães, et al. 2016)

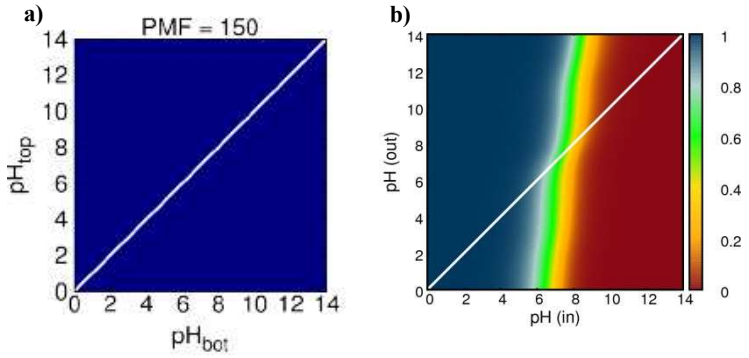

Figure 3.15: Protonation probabilities of LYS- 362_i **a)** in dependence of a pH gradient and a membrane potential **b)** in dependence of a pH gradient obtained by (Magalhães, et al. 2016)

As for the TYC- 288_i and LYS-362_i residues we can see the opposite titration behavior. In the presence of a membrane potential, they change from being sites that titrates in physiological conditions to become residues that do not titrate at all, being in the protonated form all the time.

Given that the results obtained in (Magalhães, et al. 2016) for these three key residues in the Ccox system were computed including only a pH gradient, we can probably assume that the suggestion that these residues are involved in a regulation mechanism is unlikely when a membrane potential is present. The influence of these residues on such a mechanism is probably only relevant if the membrane potential is dissipated. However, in most physiological conditions, a membrane potential is present.

The results obtained using our method show that the membrane potential has a great influence on the titrating behavior of all the titrable sites in Ccox. They also show that some of the residues that are believed to have a large influence on the function and regulation mechanisms in Ccox are highly sensitive to the presence of the main component of the pmf in Ccox, the membrane potential. These overall observations lead us to believe that all the previous pK_a calculations done for these residues, in the absence of a membrane potential (Gunner, et al. 2013) (Woelke, et al. 2013) (Magalhães, et al. 2016), are unlikely to be representative in the physiological context, where, as referred earlier, a membrane potential is always present. Furthermore, since many experimental studies are also done in the absence of a membrane potential, even some experimental pK_a values may be unrealistic for physiological conditions.

CHAPTER 4: CONCLUDING REMARKS

As referred in the previous chapter, the membrane protein bacteriorhodopsin was used as a model system to validate our in-house method, since the method we use in this thesis is similar to others used in this system in order to determine the influence of the pH gradient and the membrane potential (Calimet e Ullmann 2004) (Bombarda, Torsten e Ullmann 2006) (Magalhães, et al. 2016). In general, the results obtained for bR were similar with the ones obtained in similar studies. The exact reasons of differences observed are difficult to evaluate: the proximity to charges that are able to stabilize nearby titrable residues, the presence of small cavities that can stabilize the charged form due to the high ε_{out} (80), and the determination of the distance to the surface that is able to stabilize the charged form. Thus, this overall agreement with an analogous implementation, make us feel comfortable to use our method and apply it to other biological systems, in this case, Ccox. In order to do that we tested four different values for the dielectric constant of bR (4, 6, 8 and 10), keeping the value of the water constant (ε_{out}=80). On the titration plots obtained, no significant difference is observed between the four tested values, for most of the cases. Thus, the value of 10 was chosen since it was found to accurately reproduce the protonated state of the retinal in the ground state of bacteriorhodopsin, in previous works (Magalhães, et al. 2016).

Following this test using bR, we studied the effects of the pH gradient and the membrane potential on the protonation states of residues in cytochrome c oxidase. By including both these parameters in our in-house developed PB/MC method, we found three different types of titration behavior in both bacteriorhodopsin and Ccox: residues that, in general, do not titrate at any pH gradient, residues whose titration is only affected by the pH of the side of the membrane they are assigned to and residues whose titration is influenced by the pH-gradient. One additional titration behavior was found in Ccox: residues whose titration is influenced by both $\mathrm{pH_{top}}$ and $\mathrm{pH_{bot}}$, but not by the pH gradient. In Ccox we can see that, with a few exceptions, most of the titrable sites display large differences relatively to their titration behavior obtained without the presence of a membrane potential (Magalhães, et al. 2016). These large differences caused by the presence of a membrane potential are not verified in the bR system, where the influence of the membrane potential is not as significant, when compared to the pH gradient (Calimet e Ullmann 2004) (Bombarda, Torsten e Ullmann 2006).

In order to determine how the titration of key residues are influenced by the membrane potential, titration profiles of the Ccox residues were evaluated. Two pmf values were tested in order to evaluate the magnitude of the influence of the membrane potential: 150 mV and 200mV. We verified that there are no substantial differences between them and the value of pmf of 150 mV was selected since it has been associated with several biological conditions (Tran e Unden 1998).

Before the inclusion of the membrane potential, the study of the titration behavior of titrable residues in Ccox showed that the titration of many residues was influenced by the pH gradient (Magalhães, et al. 2016). However, our results show that some residues titration has become more complex and some of them have become insensitive to the pH gradient, with the inclusion of a membrane potential.

Given the results obtained for three key residues in the Ccox system, GLU-286_i, TYC- 288_i, and LYS-362_i (Magalhães, et al. 2016), we have concluded that the previous suggestion that these residues are involved in a regulation mechanism is unlikely, since they do not titrate at physiological

values, when a membrane potential is present. Also, our results show that the membrane potential has a great influence on the titrating behavior of all the titrable sites in Ccox, which lead us to believe that all the previous pK_a calculations done for these residues, in the absence of a membrane potential (Gunner, et al. 2013) (Woelke, et al. 2013) (Magalhães, et al. 2016), are unlikely to be accurate in the physiological context. This may also be the case for experimental pK_a values measured on the absence of membrane potential.

4.1 Future perspectives

It is important to remember that the work done in this thesis was mainly a validation and preliminary application of a new method developed in-house in order to include the membrane potential effect in biological systems. We were able to apply it to the Ccox system, which was our main goal in the beginning; however, we have only approached the surface of the many consequences that the inclusion of the membrane potential can generate. Having said that, I would like to suggest some future approaches that can be applied to the deeper study of the Ccox system:

i) As referred in section 3.2, it would be interesting to establish a connection between the magnitude of the membrane potential influence in the titration behavior of the residues and the relative position of those residues in the protein (if they are buried inside the protein, if they are at the surface, to which side of the membrane they are assigned to, are just some examples);

ii) Also referred in section 3.2, it would be interesting to get a better understanding of the inversion of the titration behavior that was verified in some residues (TYR-143_i, TYR-185_i, HIS-195_i, GLU-286_i, TYR-318_i, LYS-454_i and TYR-78_{ii}) and confirm how they have become insensitive to the pH gradient, when a membrane potential is present;

iii) It would also be important to test more dielectric constant values for Ccox (4, 6, 8), as it was done for bR, since that, in the presence of the membrane potential, larger differences can rise between these values.

iv) As it was done in previous works, in the absence of the membrane potential (Magalhães, et al. 2016), it would be interesting to determine if there are any correlations between sites: if the titration of one site is coupled to the titration of another site;

v) Test different ΔpH:V combinations obtained by experimental procedures using different types of electron acceptors (Tran e Unden 1998);

vi) Repeat the calculations done in this thesis for the reduced state of Ccox, since in this thesis we have only studied the fully oxidized state;

vii) Finally, the ultimate goal is to apply this method to Ccox in constant-pH MD calculations.

CHAPTER 5: REFERENCES

Alder, B. J., and T. E. Wainwright. "Studies in molecular dynamics." (J Chem Phys) 31, 459-466 (1959).

Allen, M. P., and D. J. Tildesley . *Computer Simulation of Liquids.* New York: Oxford University Press, 1987.

Alonso, D. O. V., and V Daggett. "Molecular Dynamics Simulations of Protein Unfolding: Characterization of Partially Unfolded States of Ubiquitin in 60% Methanol." (J Mol Biol) 247, 501 (1995).

Baptista , A M. "Theoretical methods for the simulation of proteins at constant pH. PhD thesis." Instituto de Tecnologia Química e Biológica, Universidade Nova de Lisboa, Lisboa, 1998.

Baptista, A M, and C M Soares. "Some Theoretical and Computational Aspects of the Inclusion of Proton Isomerism in the Protonation Equilibrium of Proteins." (J Phys Chem B) 105, 293-309 (2001).

Baptista, A M, and C M Soares. "Some Theoretical and Computational Aspects of theInclusion of Proton Isomerism in the Protonation Equilibrium of Proteins." (J Phys Chem B) 105, 293-309 (2001).

Baptista, A M, P J Martel, and C M Soares. "Simulation of Electron-Proton Coupling With a Monte Carlo Method: Application to Cytochrome c3 Using Continuum Electrostatics." (Biophys J) 76, 2978-2998 (1999).

Baptista, A M, V H Teixeira, and C M Soares. "Constant-pH molecular dynamics using stochastic titration." (J Chem Phys) 117, 4184 (2002).

Bashford, D. "Macroscopic electrostatic models for protonation states in proteins." (Front Biosci) 9: 1082-1099 (2004).

Bashford, D, and K Gerwert. "Electrostatic calculations of the pKa values of ionizable groups in Bacteriorhodopsin." (J Mol Biol) 224, 473-486 (1992).

Bashford, D, and M Karplus. "pKa´s of ionizable groups in proteins: atomic detail from a continuum electrostatic model." (Biochemistry) 29(44), 10219-25 (1990).

Bashford, D., and D. A. Case. "Generalized Born Models of Macromolecular Solvation Effects." (Annu Rev Phys Chem) 51: p. 129- 152 (2000).

Baudry, J., E. Tajkhorshid, F. Molnar, J. Phillips, and K. Schulten. "Molecular Dynamics Study of Bacteriorhodopsin and the Purple Membrane." (J Phys Chem) 105, 5 (2001).

Becker, U.M., A.D. Mackerrel Jr, B. Roux, and M. Watanabe. *Computational Biochemistry and Biophysics.* New York: Marcel Dekker Inc, 2001.

Belrhali , H, et al. "Protein, lipid and water organization in bacteriorhodopsin crystals: a molecular view of the purple membrane at 1.9 A resolution." (Structure) 7(8):909-17 (1999).

Ben-Naim, A. *Statistical thermodynamics for chemists and biochemists.* New York: Plenum Press, 1992.

Berendsen, H. J. C., J. P. M. Postma, W. F. van Gunsteren, A. DiNola, and J. R. Haak. "Molecular dynamics with coupling to an external bath." (J Chem Phys) 81, 8:3684-3690 (1984).

Bombarda, Elisa, Becker Torsten, and G. Matthias Ullmann. "Influence of the Membrane Potential on the Protonation of Bacteriorhodopsin: Insights from the Electrostatic Calculations into the Regulation of Proton Pumping." (J Am Chem Soc) 128, 12129-12139 (2006).

Brzezinski, P, and RB Gennis. "Cytochrome c oxidase: exciting progress and remaining mysteries." (J Bioener Biomembr) 40:521-531 (2008).

Calimet, N, and G. M. Ullmann. "Influence of a transmembrane pH gradient on protonation probabilities of bacteriorhodopsin:the structural basis of the back-pressure effect." (J Mol Biol) 339, 571-589 (2004).

Cramer, W. A., and D. B. Knaff. *Energy Transduction in Biological Membranes.* New York: Springer, 1991.

Daggett, V, and M Levitt. "Molecular Dynamics Simulations of Helix Denaturation." (J Mol Biol) 223, 1121 (1992).

Eberini, I, A M Baptista, E Gianazza, F Fraternali, and T Beringhelli. "Reorganization in Apo- and Holo-β-Lactoglobulin upon Protonation of Glu89: Molecular Dynamics and pKa Calculations." (Proteins: Struct, Funct, and Bioinf) 54, 744-758 (2004).

Ebrey, T. *Termodynamics of Membranes, Receptors and Channels.* New York: CRC Press, 1993.

Fagerberg, L, K Jonasson, G von Heijne, M Unlén, and L Berglund. "Prediction of the human membrane proteome." (Proteomics) 10:1141-1149 (2010).

Fogolari, F, A Brigo, and H Molinari. "The Poisson-Boltzmann equation for biomolecular electrostatics: a tool for structural biology." (J Mol Recognit) 15:377-392 (2002).

Gennis, R B. "Multiple proton-conducting pathways in cytochrome oxidase and a proposed role for the active-site tyrosine." (Biochim Biophys Acta-Bioenergetics) vol. 1365, no. 1, pp. 241–248 (1998).

Gennis, R B. "Multiple proton-conducting pathways in cytochrome oxidase and proposed role for the active-site tyrosine." (Biochim Biophys Acta) 1365, 241-248 (1998).

Grabe, M, H Lecar, Yuh Nung Jan, and Lily Yeh Jan. "A quantitative assessment of models for voltage-dependent gating of ion channels." (Proc Natl Acad Sci USA) 101, 17640–17645 (2004).

Grigorieff, N, TA Ceska, KH Downing, JM Baldwin, and R Henderson. "Electron-crystallographic refinement of the structure of bacteriorhodopsin." (J Mol Biol) 259(3):393-421 (1996).

Gunner, M, M Amin, X Zhu, and J Lu. "Molecular mechanisms for generating transmembrane proton gradients." (Biochim Biophys Acta -Bioenergetics) vol. 1827, no. 8, pp. 892–913 (2013).

Henderson, R, JM Baldwin, TA Ceska, F Zemlin, E Beckmann, and KH Downing. "Model for the

structure of bacteriorhodopsin based on high-resolution electron cryo-microscopy." (J Mol Biol) 213(4):899-929 (1990).

Hess, B., H. Bekker, H. J. C. Berendsen, and J. G. E. M. Fraaije. "LINCS: a linear constraint solver for molecular simulations." (J Comput Chem) 18:1463 (1997).

Hinchliffe, A. *Molecular Modelling for Beginners.* UK: John Wiley & Sons Ltd, 2008.

Hofacker, I, and K Schulten. "Oxygen and proton pathways in cytochrome c oxidase." (Proteins) 30, 100-107 (1998).

Hoover, W. G. *Computational Statistical Mechanics.* Vol. 11 of the Studies in Modern Thermodynamics Series. Elsevier, 1991.

Kadenbach, B, S Arnold, I Lee, and M Huttemann. "The possible role of cytochrome c oxidase in stress-induced apoptosis and degenerative diseases." (Biochim Biophys Acta) 1655, 400-408 (2004).

Kaila, V R, M Verkhovsky, G Hummer, and M Wikstrom. "Prevention of Leak in the Proton Pump of Cytochrome c Oxidase." (Biochim Biophys Acta - Bioenergetics) 1777, 890-892 (2008).

Kayushin, Lev P., and Vladimir P. Skulachev. "Bacteriorhodopsin as an electrogenic proton pump: reconstitution of bacteriorhodopsin proteolipossomes generating Δψ and ΔpH." (FEBS Letters) 39, 39-41 (1974).

Kimura, Y, et al. "Surface of bacteriorhodopsin revealed by high-resolution electron crystallography." (Nature) 389(6647):206-11 (1997).

Lanyi, J. K. "Progress toward an explicit mechanistic model for the light-driven pump, bacteriorhodopsin." (FEBS Lett) 464: 103-107 (1999).

Lanyi, JK. "Bacteriorhodopsin." (Annu Rev Physiol) 66:665-88 (2004).

Leach, A. R. *Molecular modelling: principles and applications.* London: Pearson Education Limited, 2001.

Levitt, M, and R Sharon. "Accurate Simulation of Protein Dynamics in Solution." (Proc Natl Acad Sci) 85, 7557 (1988).

Levitt, Michael, M Hirshberg, R Sharon, and V Daggett. "Potential energy function and parameters for simulations of the molecular dynamics of proteins and nucleic acids in solution." (Elsevier) 91, 215-231 (1995).

Liwo, Adam. *Computational Methods to Study the Structure and Dynamics of Biomolecules and Biomolecular Processes: From Bioinformatics to Molecular Quantum Mechanics* . Springer, 2013.

Logunov, S., M. El-Sayed, and L. Song. "Catalysis of the retinal subpicosecond photoisomerization process in acid purple bacteriorhodopsin and some bacteriorhodopsin mutants by chloride ions." (Biophys J) 71, 3, 1545-1553 (1996).

Machuqueiro, M, and A M Baptista. "Acidic range titration of HEWL using a constant-pH molecular dynamics method." (Proteins: Struct Funct Bioinf) 72, 289 (2008).

Machuqueiro, M, and A M Baptista. "Is the prediction of pKa values by constant-pH molecular dynamics being hindered by inherited problems?" (Proteins: Struct, Funct and Bioinf) 79 (12), 3437-3447 (2011).

Magalhães, P, A S F Oliveira, S R R Campos, C M Soares, and A M Baptista. "Effect of a pH gradient on the protonation states of cytochrome c oxidase: a CE/MC study." (To be published) 2016.

Martel, P., A. Baptista, and S. Petersen. "Protein electrostatics." (Elsevier) 2 (1996).

McKee, T, and J Mckee. *Biochemistry: The Molecular Basis of Life.* Oxford University Press, 2009.

Metropolis, N, AW Rosenbluth, MN Rosenbluth, A. H. Teller , and E. Teller. "Equation of state calculations by fast computing machines." (J Chem Phys) 21, 1087-1092 (1953).

Mills, Denise A., and Shelagh Ferguson-Miller. "Influence of structure, pH and membrane potential on proton movement in cytochrome oxidase." (Biochim Biophys Acta) 1555, 96-100 (2002).

Mitchell, P, and J Moyle. "Estimation of membrane potential and pH difference across the cristae membrane of rat liver mitochondria." (Eur J Biochem) 7, 471-484 (1969).

Miyamoto, S, and P A Kollman. "SETTLE: an analytical version of the SHAKE and RATTLE algorithm for rigid water models." (J Comput Chem) 13:952 (1992).

Muramoto, K, et al. "A histidine residue acting as a controlling site for dioxygen reduction and proton pumping by cytochrome c oxidase." (Proc Natl Acad Sci USA) 104, 7881-7886 (2007).

Nagel, G, B Kelety, B Mockel, G Buldt, and E Bamberg. "Voltage dependence of proton pumping by bacteriorhodopsin is regulated by the voltage-sensitive ratio of M1 to M2." (Biophys J) 74 (1): 403-412 (1998).

Nicholls, D. G. "The influence of respiration and ATP hydrolysis on the proton electrochemical potential gradient across the inner membrane of rat liver mitochondria as determined by ion distribution." (Eur J Biochem) 50, 305-315 (1974).

Nicholls, David, and Stuart Ferguson. *Bioenergetics.* Vol. 4. Elsevier, 2013.

Oliveira, A S F , S R R Campos, A M Baptista, and C M Soares. "Coupling between protonation and conformation in cytochrome c oxidase: Insights from constant-pH MD simulations." (Biochim Biophys Acta) 1857, 759-771 (2016).

Oliveira, ASF, JM Damas, AM Baptista, and CM Soares. "Exploring O2 Diffusion in A-Type Cytochrome c Oxidases: Molecular Dynamics Simulations Uncover Two Alternative Channels towards the Binuclear site." (PLoS Comput Biol) 10(12): e1004010. doi:10.1371 (2014).

Oostenbrink, C. et al. "A biomolecular force field based on the free enthalpy of hydration and solvation: the GROMOS force-field parameter sets 53A5 and 53A6." (J Comput Chem) 25(13): p. 1656-76 (2004).

Pebay-Peyroula , E, G Rummel , JP Rosenbusch , and EM Landau. "X-ray structure of bacteriorhodopsin at 2.5 angstroms from microcrystals grown in lipidic cubic phases." (Science) 277(5332):1676-81 (1997).

Pereira, M M, M Santana, and M Teixeira. "A novel scenario for the evolution of haem–copper oxygen reductases." (Biochim Biophys Acta -Bioenergetics) vol. 1505, no. 2–3, pp. 185–208 (2001).

Quintas, Alexandre, Manuel Júdice Halpern, and Ana Ponces Freire. *Bioquímica- Organização Molecular da Vida.* Lidel, 2008.

Rahaman, A. "Correlations in the motion of atoms in liquid argon." (Phys Rev) 136A, 405-411 (1964).

Rapaport, D. C. *The Art of Molecular Dynamics Simulations.* New York: Cambridge University Press, 2004.

Roux, B. "Influence of the membrane potential on the free energy of an intrinsic protein." (Biophys J) 73(6): 2980–2989 (1997).

Ryckaert, J P, G Ciccotti, and H J C Berendsen. "Numerical integration of the Cartesian equations of motion of a system with constraints: molecular dynamics of n-alkanes." (J Comput Phys) 23(3):327 (1977).

Scaduro, R. C., and L. W. Grotyohann. "Measurement of mitochondrial membrane potential using fluorescent rhodamine derivatives." (Biophys J) 76, 469-477 (1999).

Schmid, N., et al. "Definition and testing of the GROMOS force-field versions 54A7 and 54B7." (Eur Biophys J) 40, 843-856 (2011).

Schutz, C N, and A Warshel. "What Are the Dielectric “Constants” of Proteins and How to Validate Electrostatic Models?" (Proteins: Struct, Funct, Bioinf) 44, 400–417 (2001).

Scott, W.R.P, et al. "The GROMOS biomolecular simulation program package." (J Phys Chem) 103: p. 3596-3607 (1999).

Shimokata, K, Y Katayama, H Murayama, M Suematsu, T Tsukihara, and et al. "The proton-pumping pathway of bovine heart cytochrome c oxidase." (Proc Natl Acad Sci USA) 104, 4200-4205 (2007).

Siletsky, Sergey A. "Steps of the coupled charge translocation in the catalytic cycle of cytochrome c oxidase." (Front Biosci) 18, 36-57 (2013).

Smith, J. C. "Potential-sensitive molecular probes in membranes of bioenergetics relevance." (Biochim Biophys Acta) 1016, 1-28 (1990).

Song, L., MA El-Sayed, and JK Lanyi. "Protein catalysis of the retinal subpicosecond photoisomerization in the primary process of bacteriorhodopsin photosynthesis." (Science) 13, 261(5123):891-4 (1993).

Svensson-Ek, M J Abramson, G Larsson, S Tornroth, P Brzezinski, and S Iwata. "The x-ray crystal structures of wild-type and EQ(I-286) mutant cytochrome c oxidases from Rhodobacter sphaeroides." (J Mol Biol) 321, 329-339 (2002).

Teixeira, V H, D Vila-Viçosa, A M Baptista, and M Machuqueiro. "Protonation of DMPC in a Bilayer Environment Using a Linear Response Approximation." (J Chem Theory Comput) 10, 2176-2184 (2014).

Teixeira, V H, et al. "On the Use of Different Dielectric Constants for Computing Individual and Pairwise Terms in Poisson-Boltzmann Studies of Protein Ionization Equilibrium." (J Phys Chem B) 109, 14691-14706 (2005).

Tironi, I. G., R. Sperb, P. E. Smith, and W. F. van Gunsteren. "A generalized reaction field method for molecular dynamics simulations." (J Chem Phys) 102, 13:5451-5459 (1995).

Tran, Q H, and G Unden. "Changes in the proton potential and the cellular energetics of Escherichia coli during growth by aerobic and anaerobic respiration or by fermentation." (Eur J Biochem) 251, 538-543 (1998).

van Gunsteren, W. F., and H. J. C. Beredndsen. "Computer simulation of molecular dynamics: Methodology, applications and perspectives in chemistry." (Angew Chem Int Ed Engl) 29:992-1023 (1990).

van Gunsteren, W. F., P. H. Hunenberger, A. E. Mark, P. E. Smith, and I. G. Tironi. "Computer-simulation of protein motion." (Comput Phys Commun) 91, 305-319 (1995).

Wikstrom, MKF. "Proton Pumps Coupled to Cytochrome-C Oxidase in Mitochondria." (Nature) 266, 271-273 (1977).

Woelke, A L, G Galstyan, A Galstyan, T Meyer, J Heberle, and E W Knapp. "Exploring the possible role of Glu286 in CcO by electrostatic energy computations combined with molecular dynamics." (J Phys Chem B) vol. 117, no. 41, pp. 12432–12441 (2013).

Xu, D, M Sheves, and K Schulten. "Molecular dynamics study of the M412 intermediate of bacteriorhodopsin." (Biophys J) 69(6):2745-60 (1995).

Yang, M, and WJ Brackenbury. "Membrane potential and cancer progression." (Front Phys) 4:185. doi:10.3389 (2013).

Yoshikawa, S, K Muramoto, and K Shinzawa-Ioth. "Proton-Pumping Mechanism of Cytochrome c oxidase." (Annu Rev Biophys) 40, 205-223 (2011).

Appendix A

This appendix contains the plots of all titrable residues in bR, in the presence of a membrane potential, at dielectric constants of 4, 6, 8 and 10. The color gradient represents the average protonation of the titrable sites, with 0 corresponding to the fully deprotonated state, and 1 to fully protonated state. On the title of each site is an indication (top/bot) of the side of the membrane to which the site was assigned to. For non-standard residues check the name on the abbreviation list.

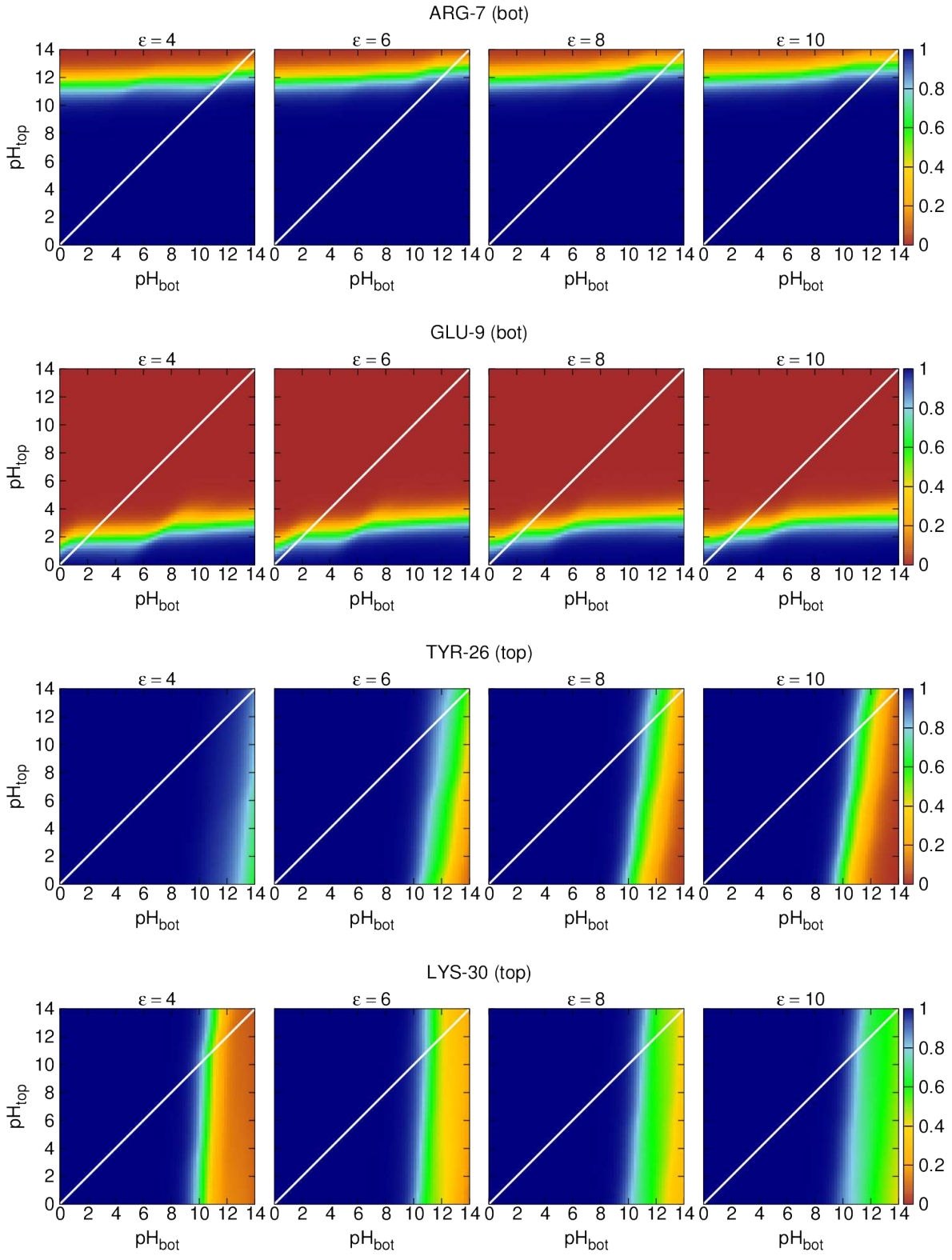
ARG-7 (bot)
GLU-9 (bot)
TYR-26 (top)
LYS-30 (top)
ε = 4
ε = 6
ε = 8
ε = 10
pH_top
pH_bot
0 2 4 6 8 10 12 14
0 0.2 0.4 0.6 0.8 1

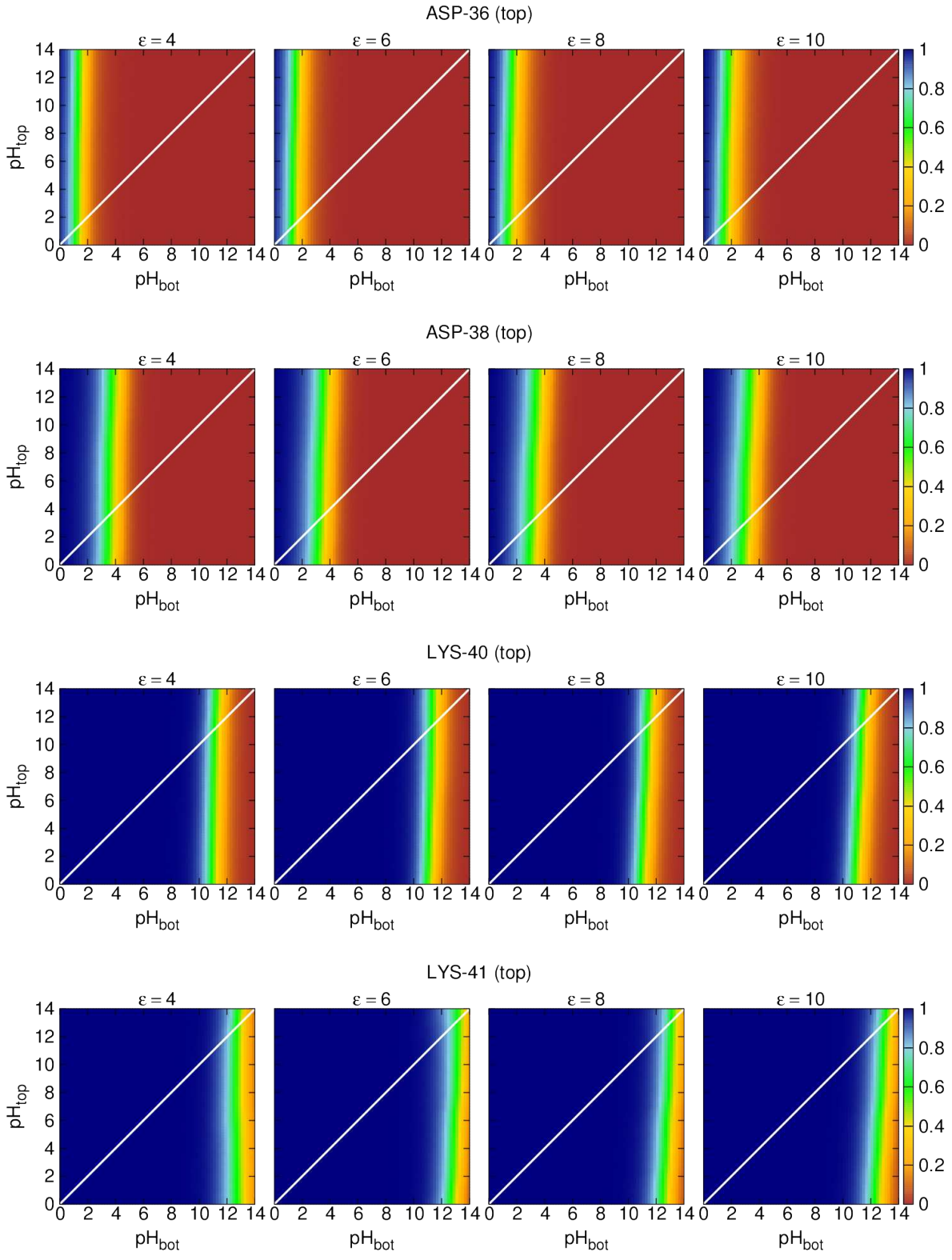
ASP-36 (top)
ε = 4
ε = 6
ε = 8
ε = 10
pH_top
pH_bot
ASP-38 (top)
LYS-40 (top)
LYS-41 (top)

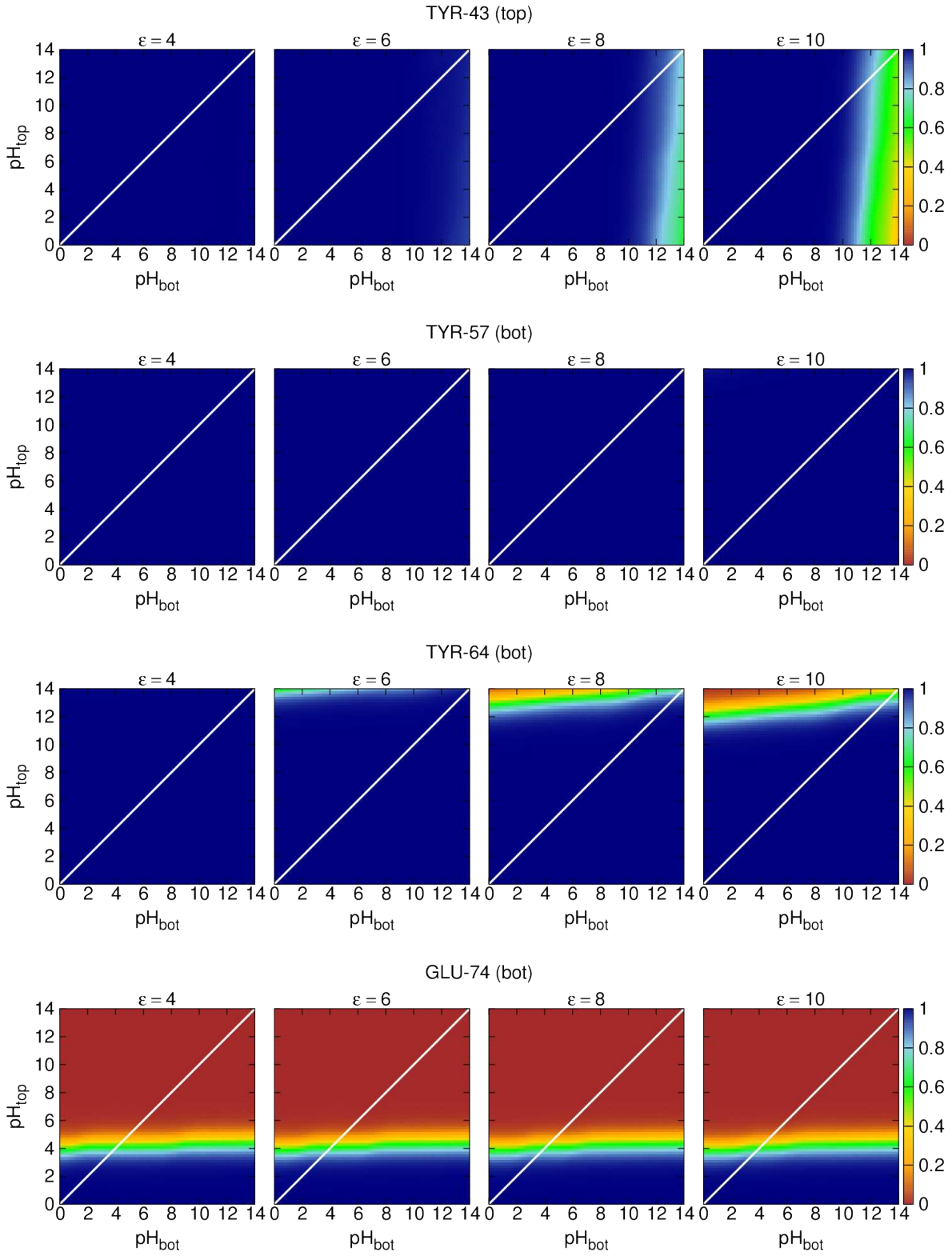
TYR-43 (top)
TYR-57 (bot)
TYR-64 (bot)
GLU-74 (bot)
ε = 4
ε = 6
ε = 8
ε = 10
pH_top
pH_bot
0 2 4 6 8 10 12 14
0 0.2 0.4 0.6 0.8 1

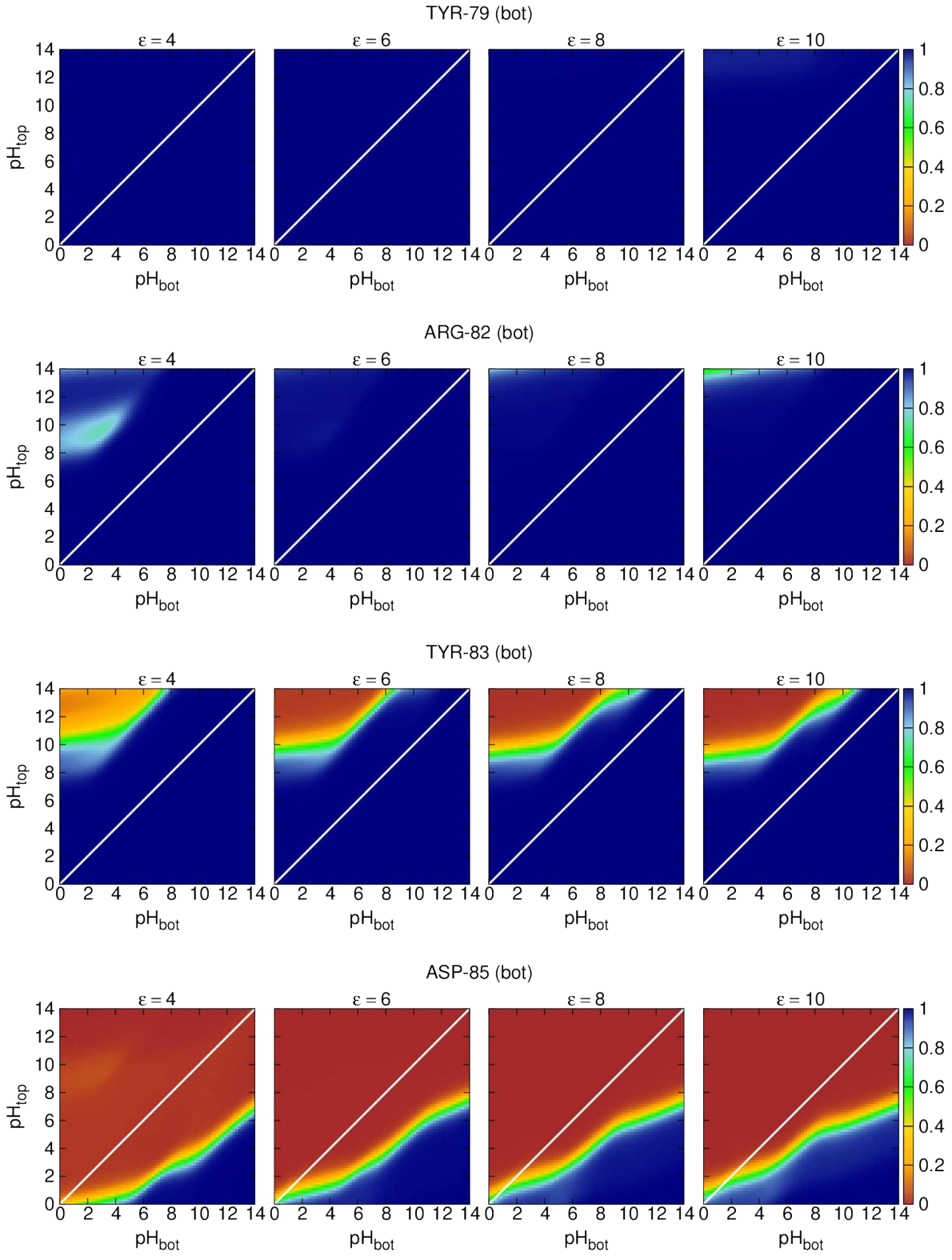
TYR-79 (bot)
ε = 4
ε = 6
ε = 8
ε = 10
pH_top
pH_bot
ARG-82 (bot)
TYR-83 (bot)
ASP-85 (bot)

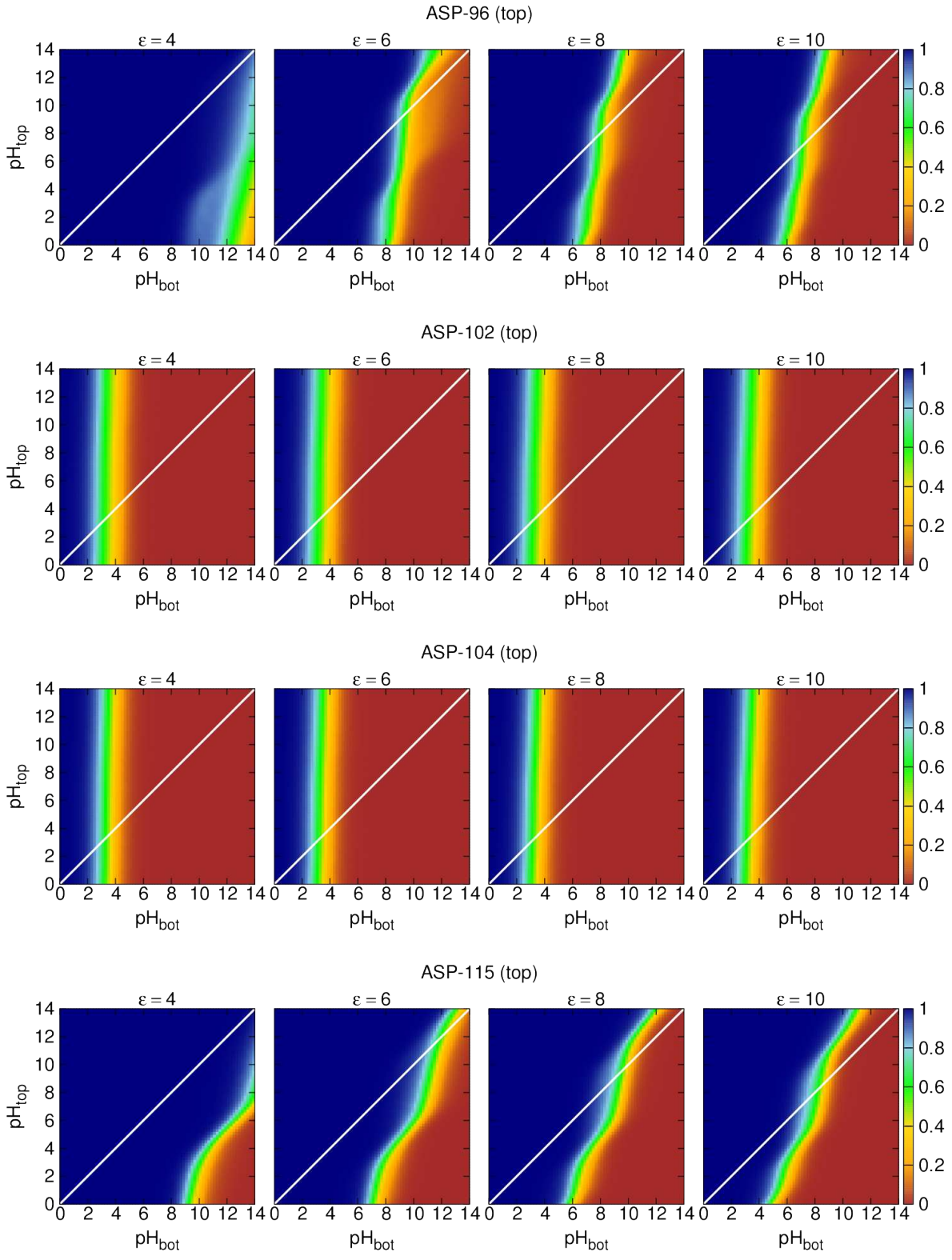
ASP-96 (top)
ASP-102 (top)
ASP-104 (top)
ASP-115 (top)
ε = 4
ε = 6
ε = 8
ε = 10
pH_top
pH_bot
0 2 4 6 8 10 12 14
1 0.8 0.6 0.4 0.2 0

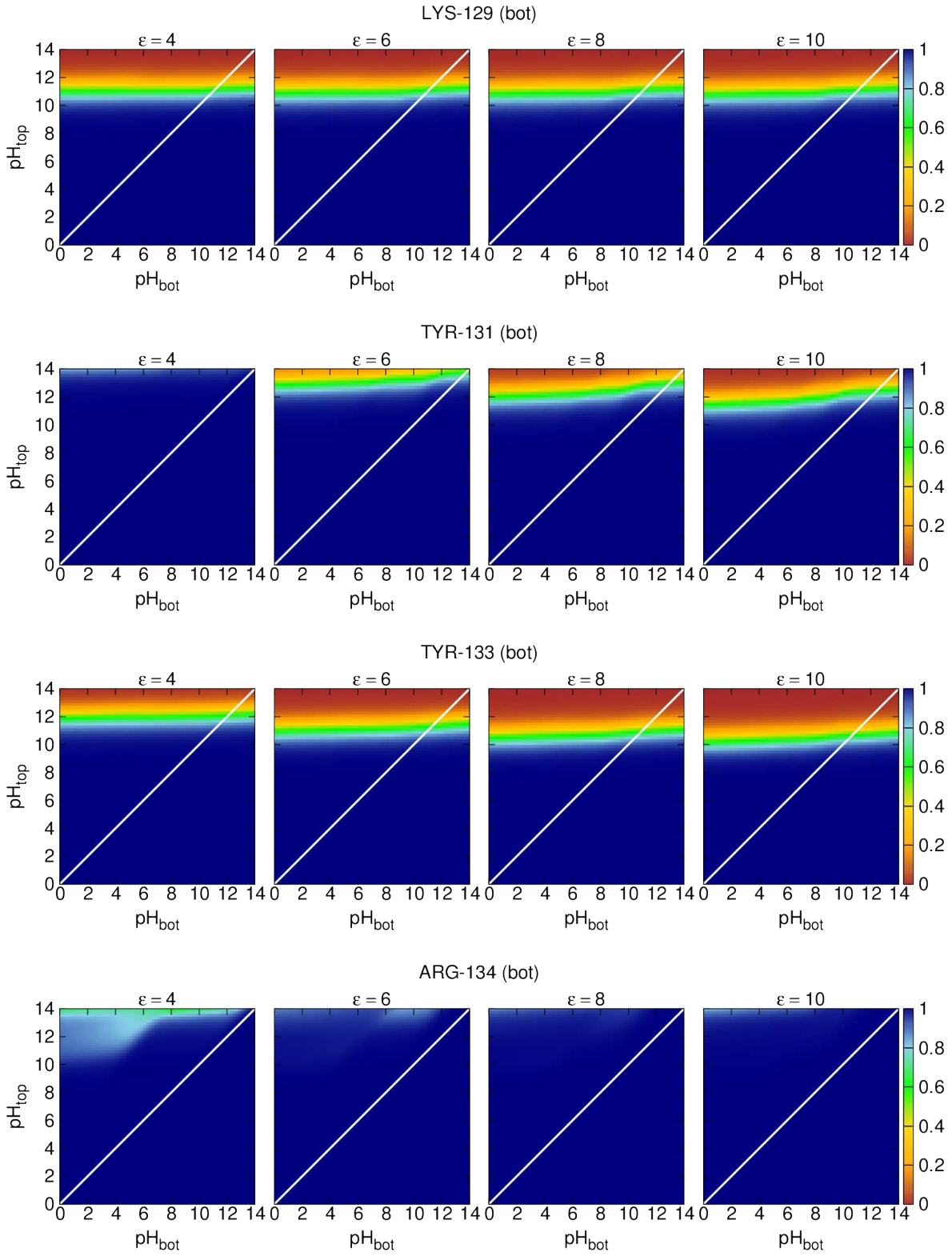
LYS-129 (bot)
TYR-131 (bot)
TYR-133 (bot)
ARG-134 (bot)
ε = 4
ε = 6
ε = 8
ε = 10
pH_top
pH_bot
0 2 4 6 8 10 12 14
1 0.8 0.6 0.4 0.2 0

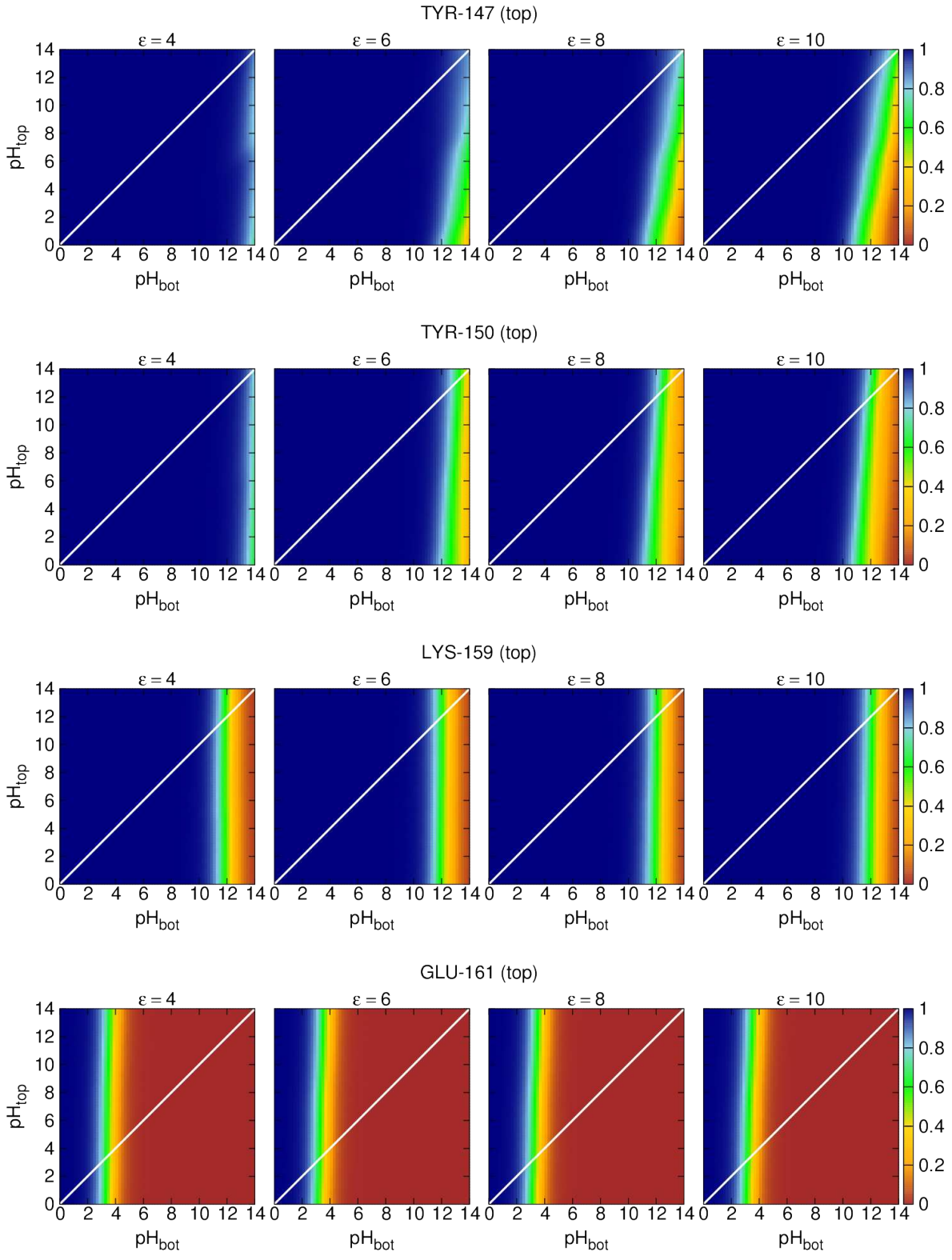
TYR-147 (top)
TYR-150 (top)
LYS-159 (top)
GLU-161 (top)
ε = 4
ε = 6
ε = 8
ε = 10
pH_top
pH_bot
0 2 4 6 8 10 12 14
1 0.8 0.6 0.4 0.2 0

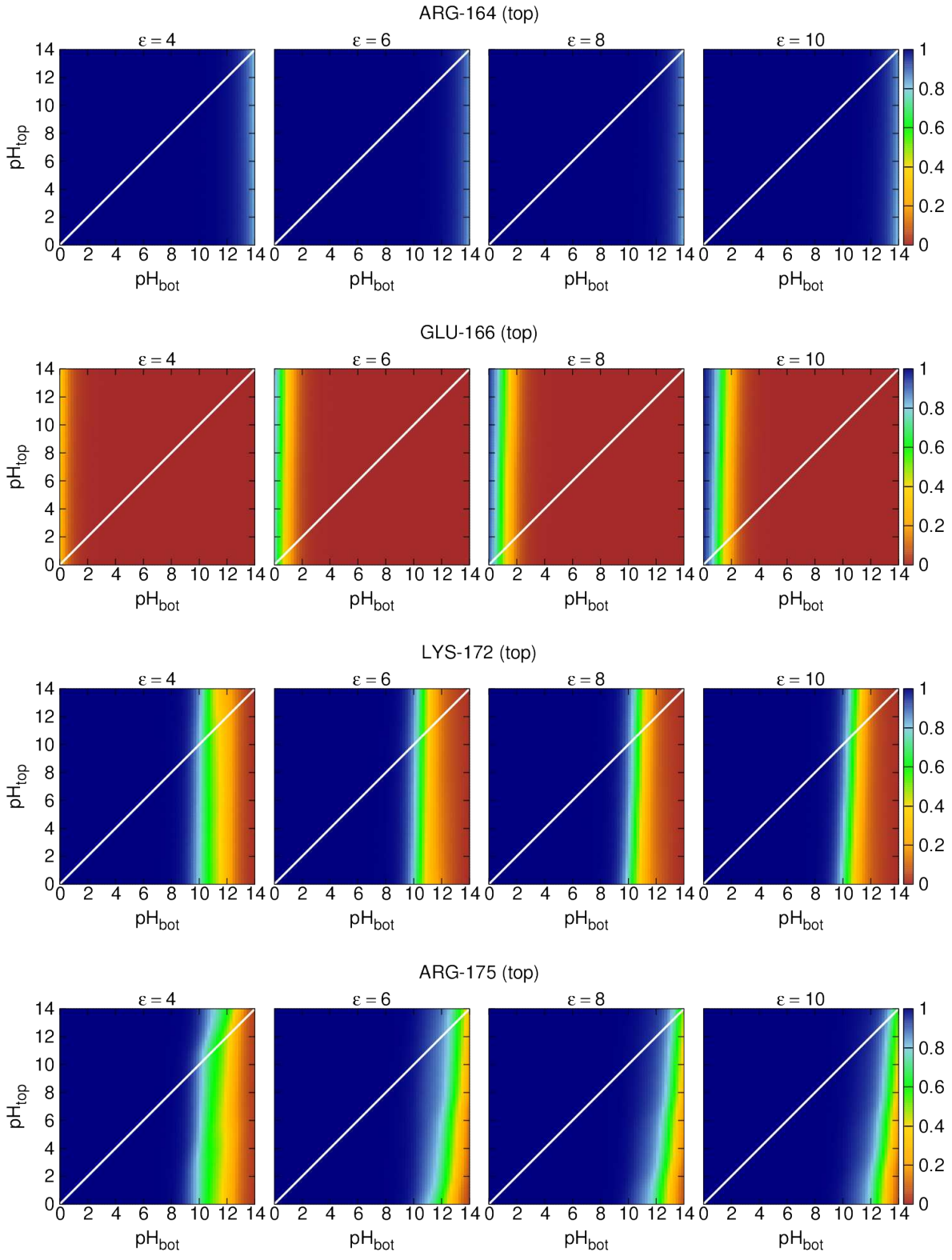
ARG-164 (top)
GLU-166 (top)
LYS-172 (top)
ARG-175 (top)
ε = 4
ε = 6
ε = 8
ε = 10
pH_top
pH_bot
0 2 4 6 8 10 12 14
0 0.2 0.4 0.6 0.8 1

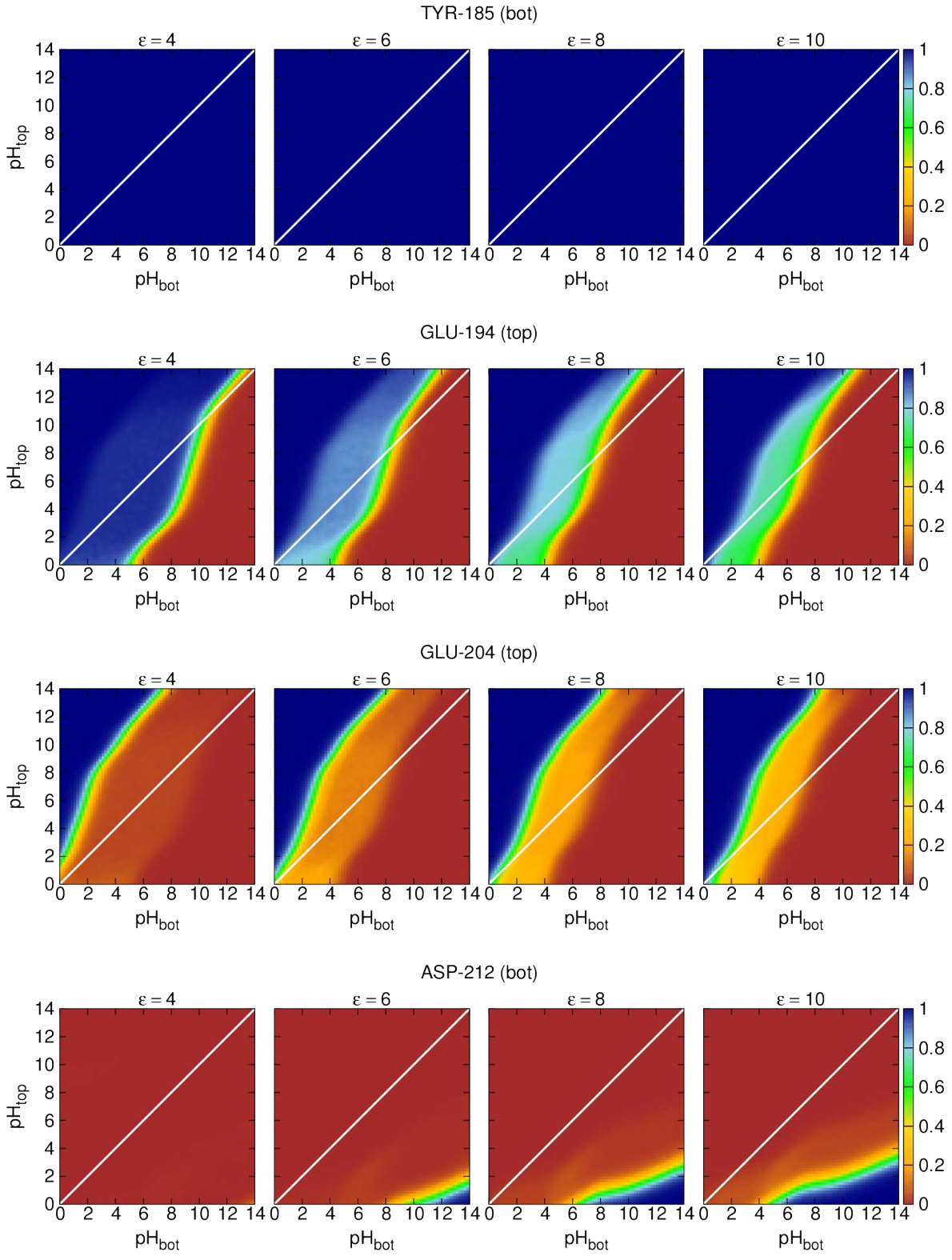
TYR-185 (bot)
GLU-194 (top)
GLU-204 (top)
ASP-212 (bot)
ε = 4
ε = 6
ε = 8
ε = 10
pH_top
pH_bot
0 2 4 6 8 10 12 14
1 0.8 0.6 0.4 0.2 0

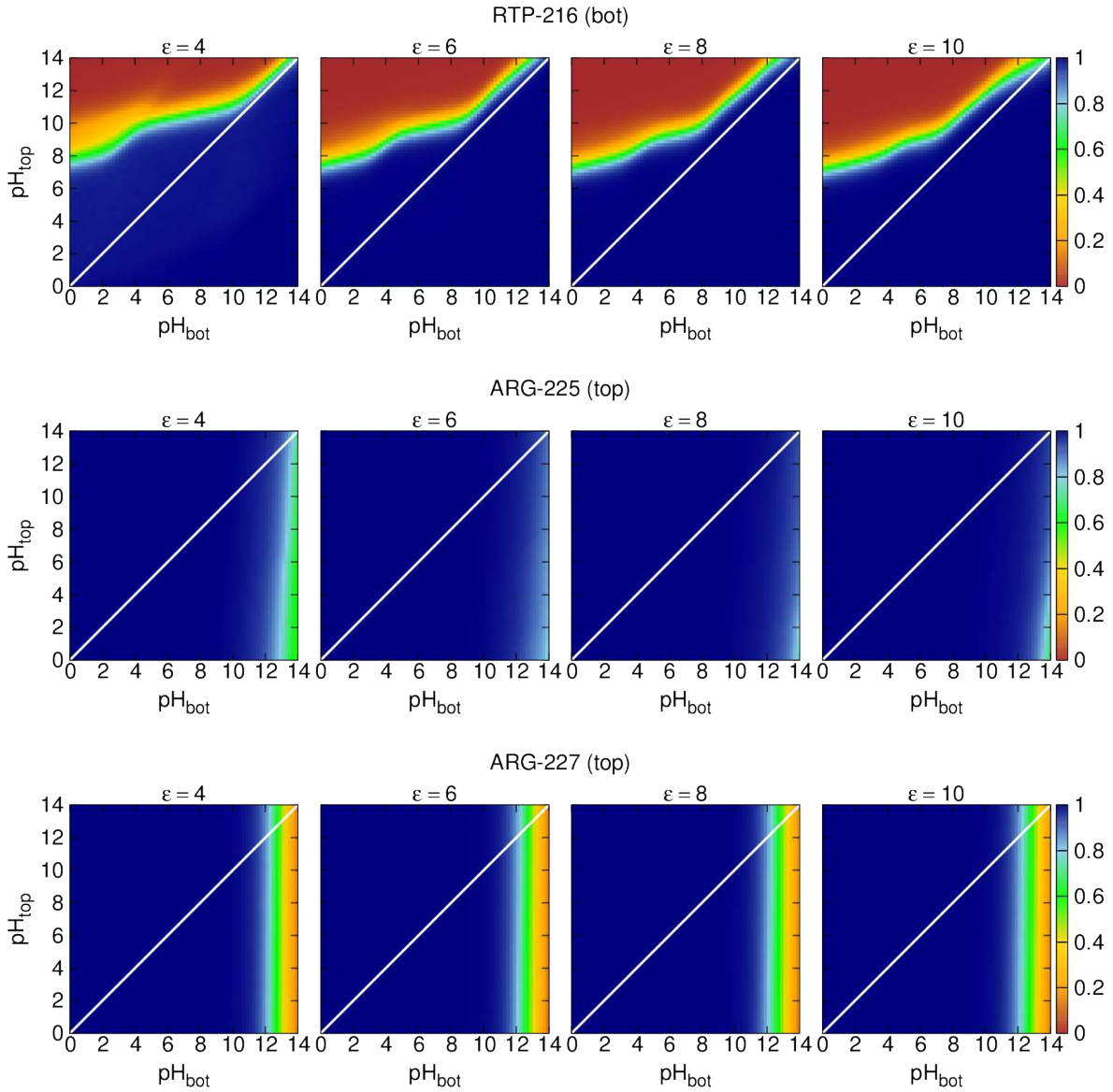
RTP-216 (bot)
ε = 4
ε = 6
ε = 8
ε = 10
pH_top
pH_bot
ARG-225 (top)
ε = 4
ε = 6
ε = 8
ε = 10
pH_top
pH_bot
ARG-227 (top)
ε = 4
ε = 6
ε = 8
ε = 10
pH_top
pH_bot

Appendix B

This appendix contains the plots of all titrable residues in Ccox, in the presence of a membrane potential at dielectric constant of 10 and using the pmf values of 150 mV and 200 mV. The color gradient represents the average protonation of the titrable sites, with 0 corresponding to the fully deprotonated state, and 1 to fully protonated state. On the title of each site is an indication (top/bot) of the side of the membrane to which the site was assigned to. For non-standard residues check the name on the abbreviation list.

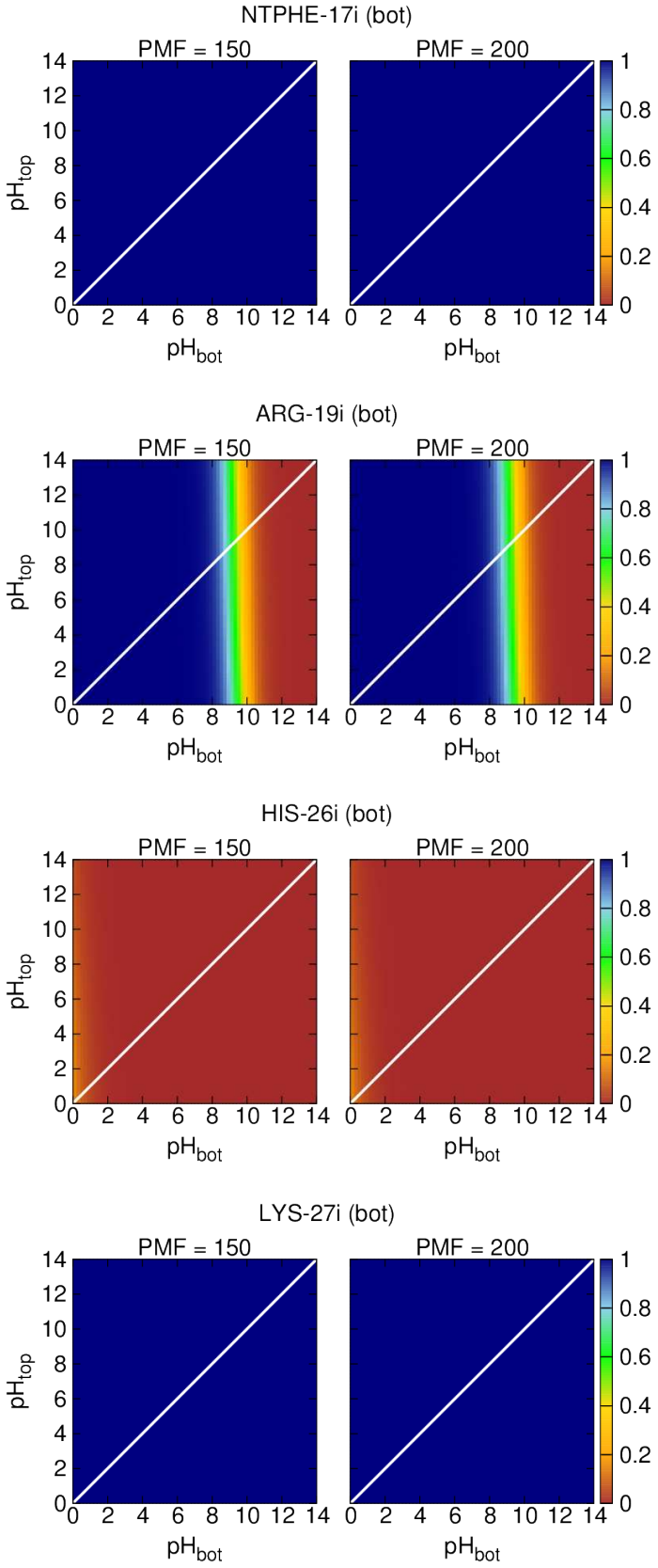
NTPHE-17i (bot)
PMF = 150
PMF = 200
ARG-19i (bot)
PMF = 150
PMF = 200
HIS-26i (bot)
PMF = 150
PMF = 200
LYS-27i (bot)
PMF = 150
PMF = 200
pH_top
pH_bot
0 2 4 6 8 10 12 14
0 0.2 0.4 0.6 0.8 1

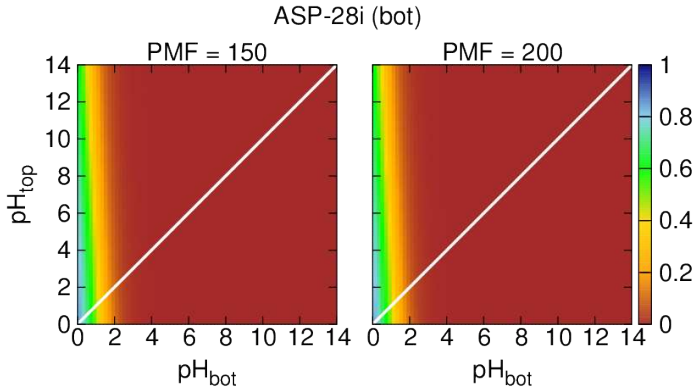
ASP-28i (bot)
PMF = 150
PMF = 200
pH_top
pH_bot
0 2 4 6 8 10 12 14
1 0.8 0.6 0.4 0.2 0

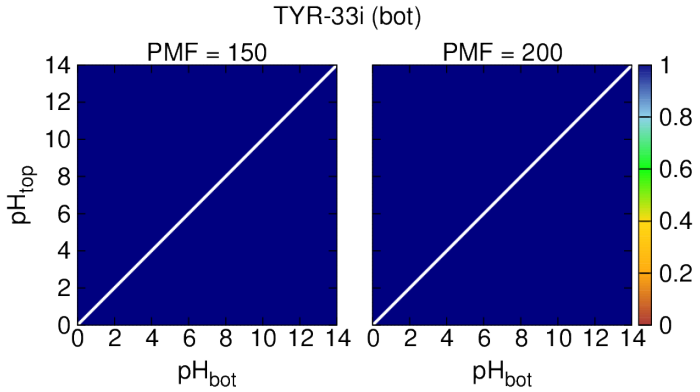
TYR-33i (bot)
PMF = 150
PMF = 200
pH_top
pH_bot
0 2 4 6 8 10 12 14
1 0.8 0.6 0.4 0.2 0

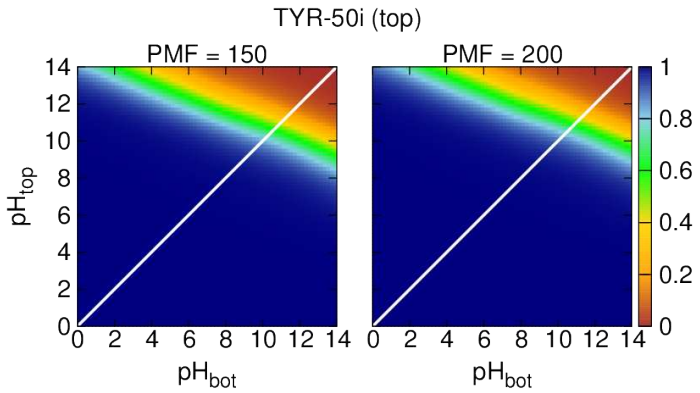
TYR-50i (top)
PMF = 150
PMF = 200
pH_top
pH_bot
0 2 4 6 8 10 12 14
1 0.8 0.6 0.4 0.2 0

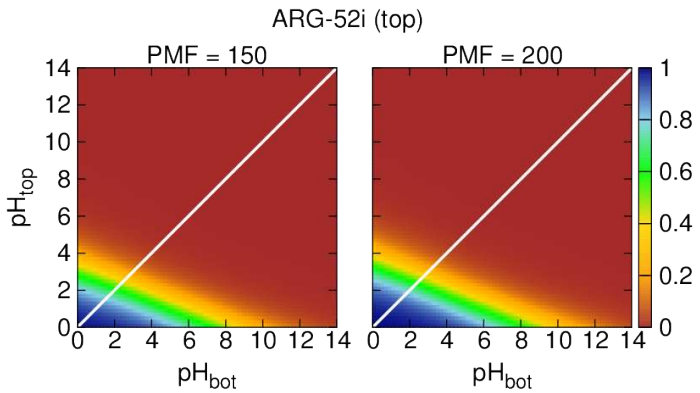
ARG-52i (top)
PMF = 150
PMF = 200
pH_top
pH_bot
0 2 4 6 8 10 12 14
1 0.8 0.6 0.4 0.2 0

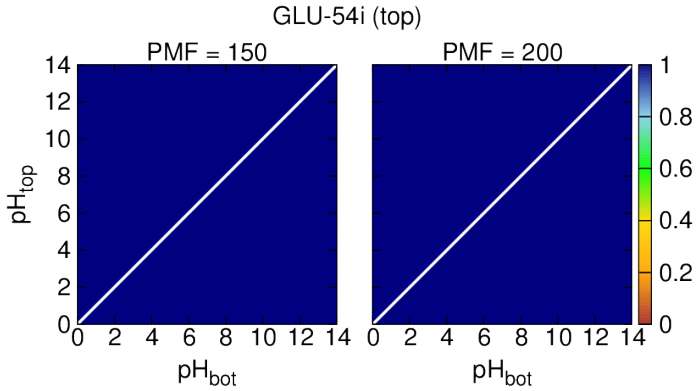
GLU-54i (top)
PMF = 150
PMF = 200
pH_top
pH_bot
0 2 4 6 8 10 12 14
0 0.2 0.4 0.6 0.8 1

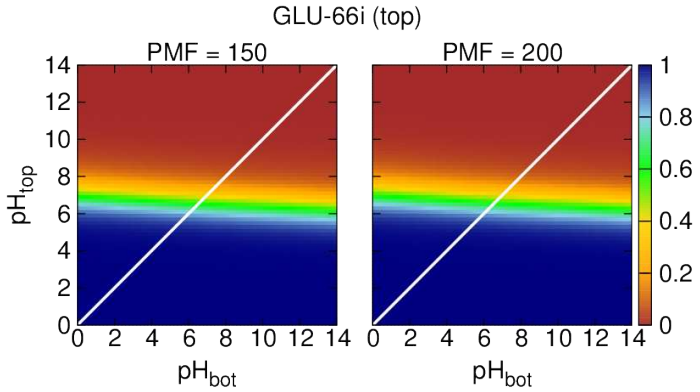
GLU-66i (top)
PMF = 150
PMF = 200
pH_top
pH_bot
0 2 4 6 8 10 12 14
0 0.2 0.4 0.6 0.8 1

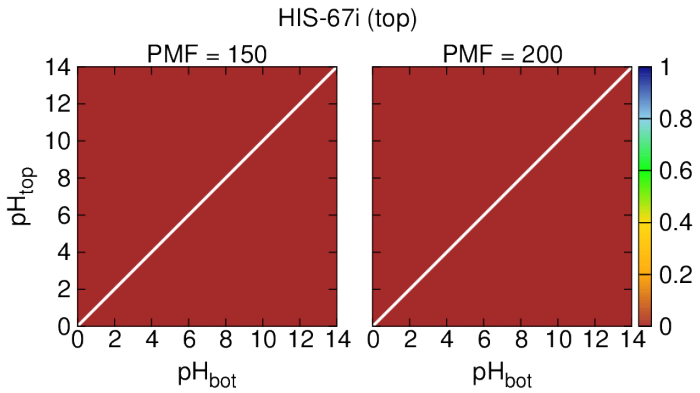
HIS-67i (top)
PMF = 150
PMF = 200
pH_top
pH_bot
0 2 4 6 8 10 12 14
0 0.2 0.4 0.6 0.8 1

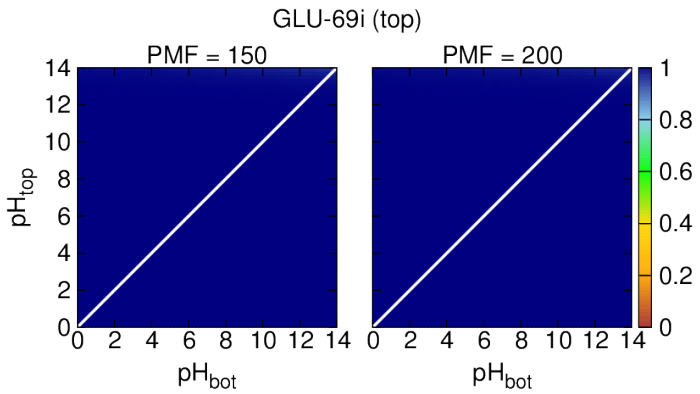
GLU-69i (top)
PMF = 150
PMF = 200
pH_top
pH_bot
0 2 4 6 8 10 12 14
0 0.2 0.4 0.6 0.8 1

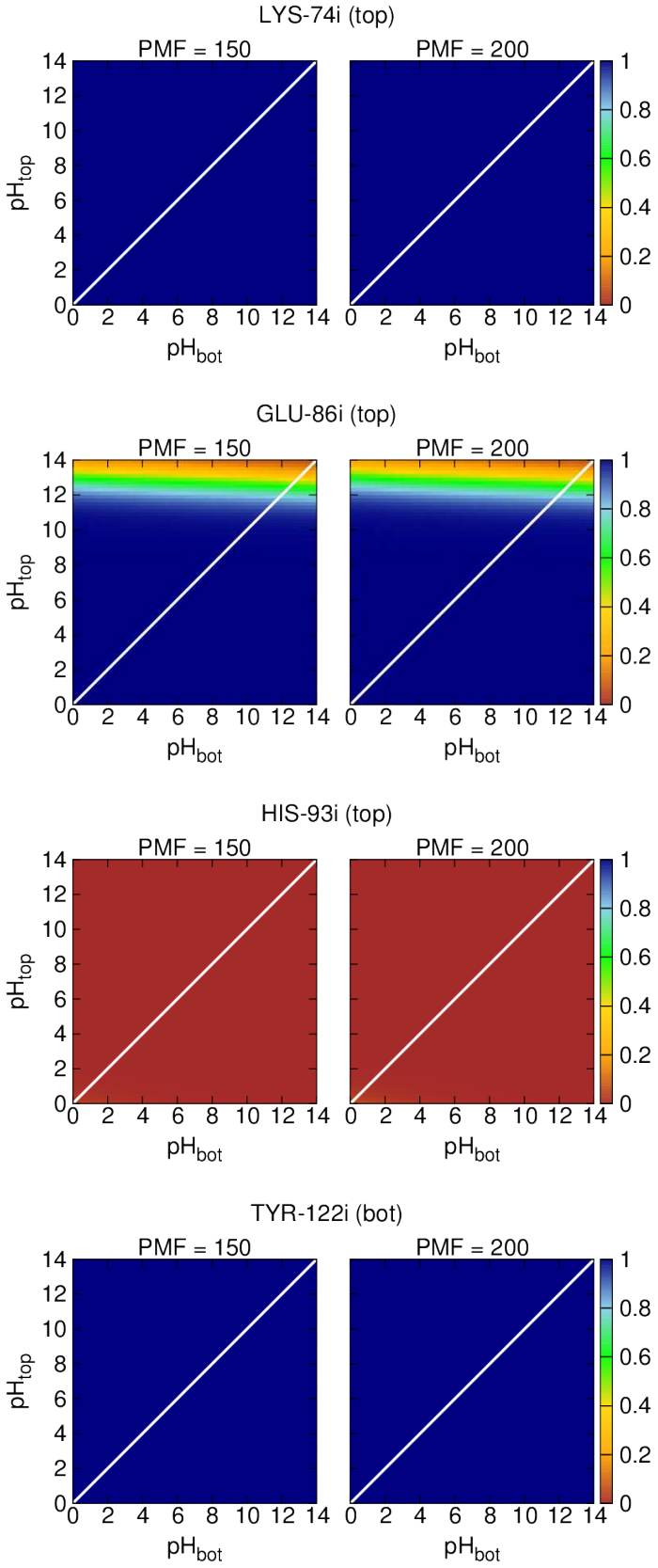
LYS-74i (top)
PMF = 150
PMF = 200
GLU-86i (top)
PMF = 150
PMF = 200
HIS-93i (top)
PMF = 150
PMF = 200
TYR-122i (bot)
PMF = 150
PMF = 200
pH_top
pH_bot
0 2 4 6 8 10 12 14
0 0.2 0.4 0.6 0.8 1

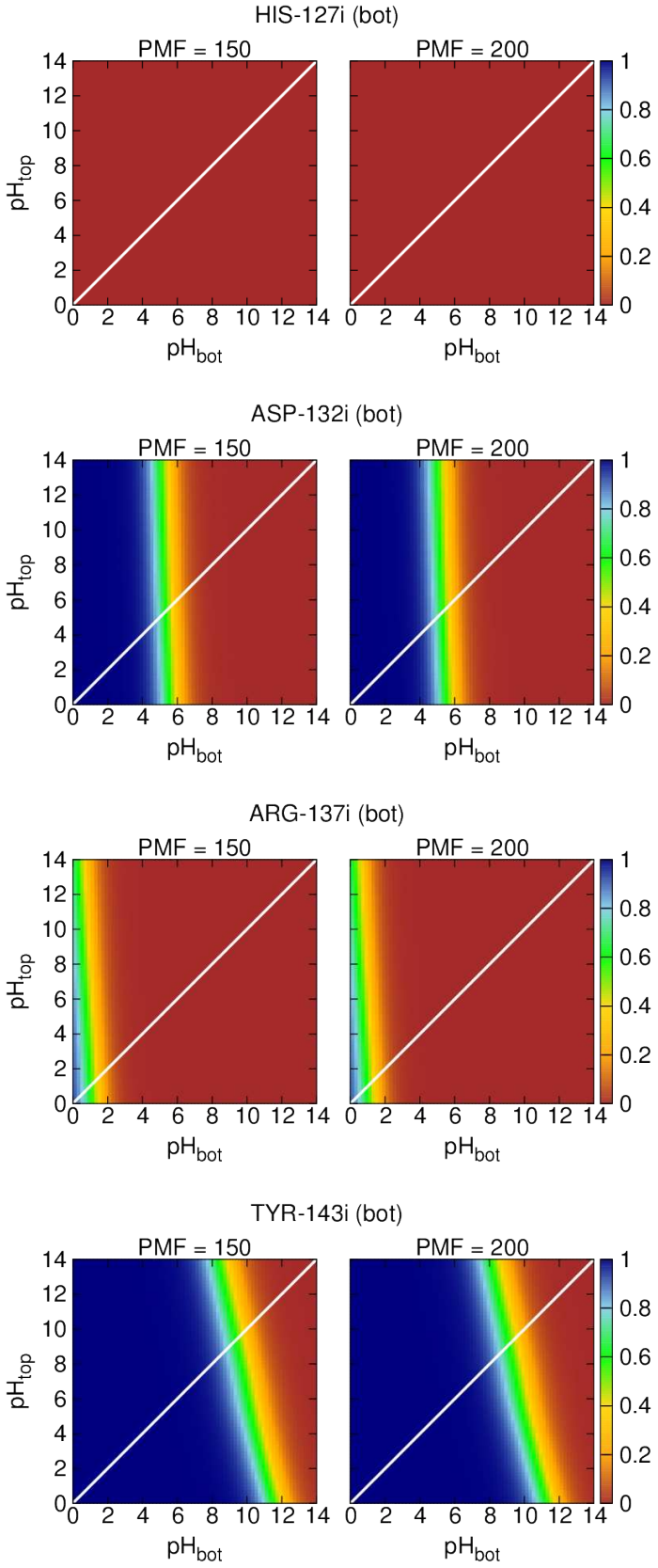
HIS-127i (bot)
PMF = 150
PMF = 200
ASP-132i (bot)
PMF = 150
PMF = 200
ARG-137i (bot)
PMF = 150
PMF = 200
TYR-143i (bot)
PMF = 150
PMF = 200
pH_top
pH_bot
0 2 4 6 8 10 12 14
0 0.2 0.4 0.6 0.8 1

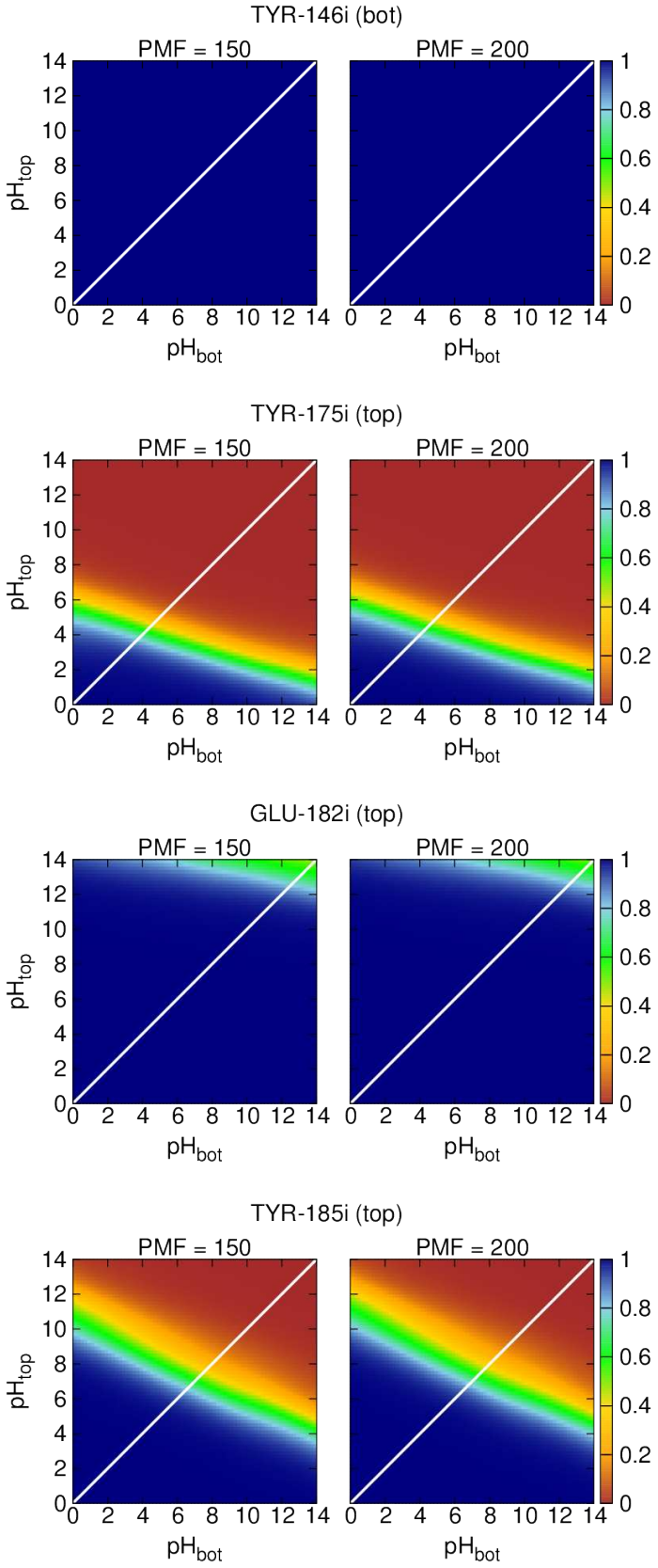
TYR-146i (bot)
PMF = 150
PMF = 200
TYR-175i (top)
PMF = 150
PMF = 200
GLU-182i (top)
PMF = 150
PMF = 200
TYR-185i (top)
PMF = 150
PMF = 200
pH_top
pH_bot
0 2 4 6 8 10 12 14
1 0.8 0.6 0.4 0.2 0

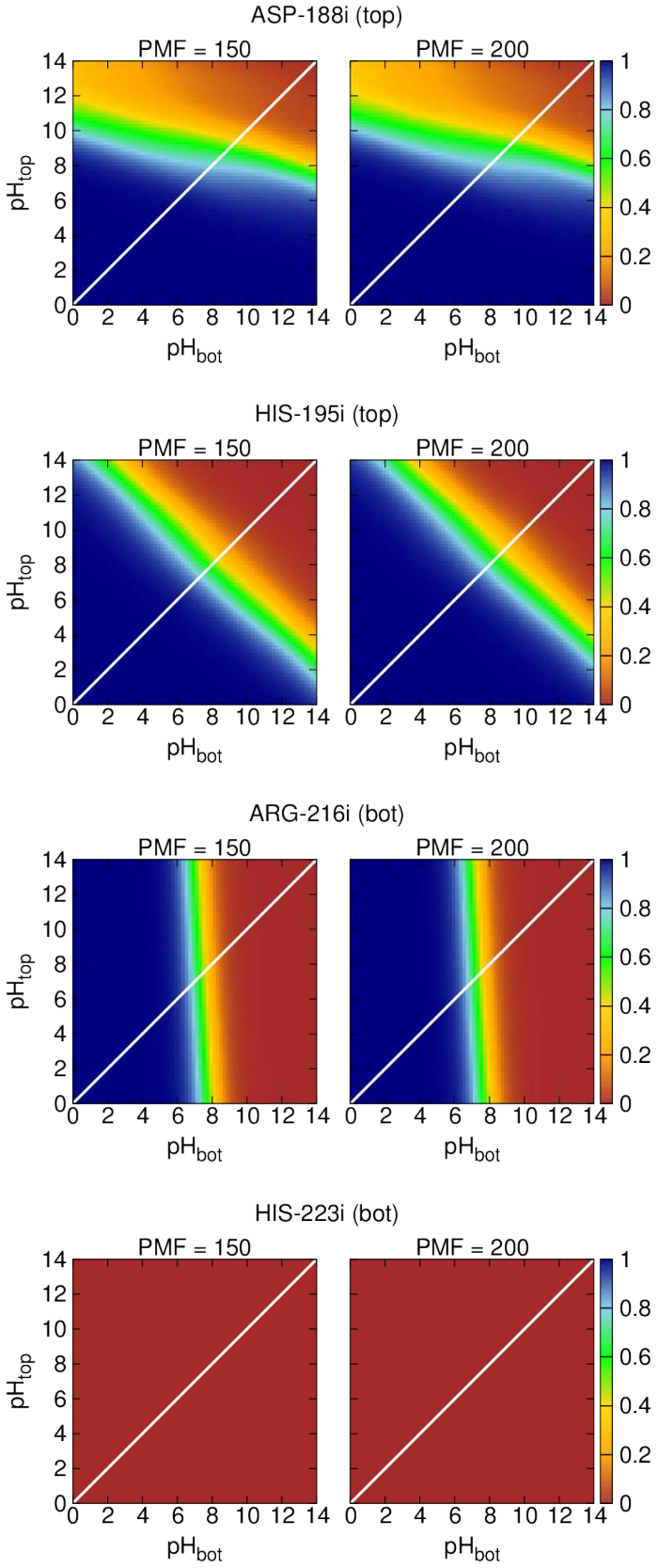
ASP-188i (top)
PMF = 150
PMF = 200
HIS-195i (top)
PMF = 150
PMF = 200
ARG-216i (bot)
PMF = 150
PMF = 200
HIS-223i (bot)
PMF = 150
PMF = 200
pH_top
pH_bot
0 2 4 6 8 10 12 14
0 0.2 0.4 0.6 0.8 1

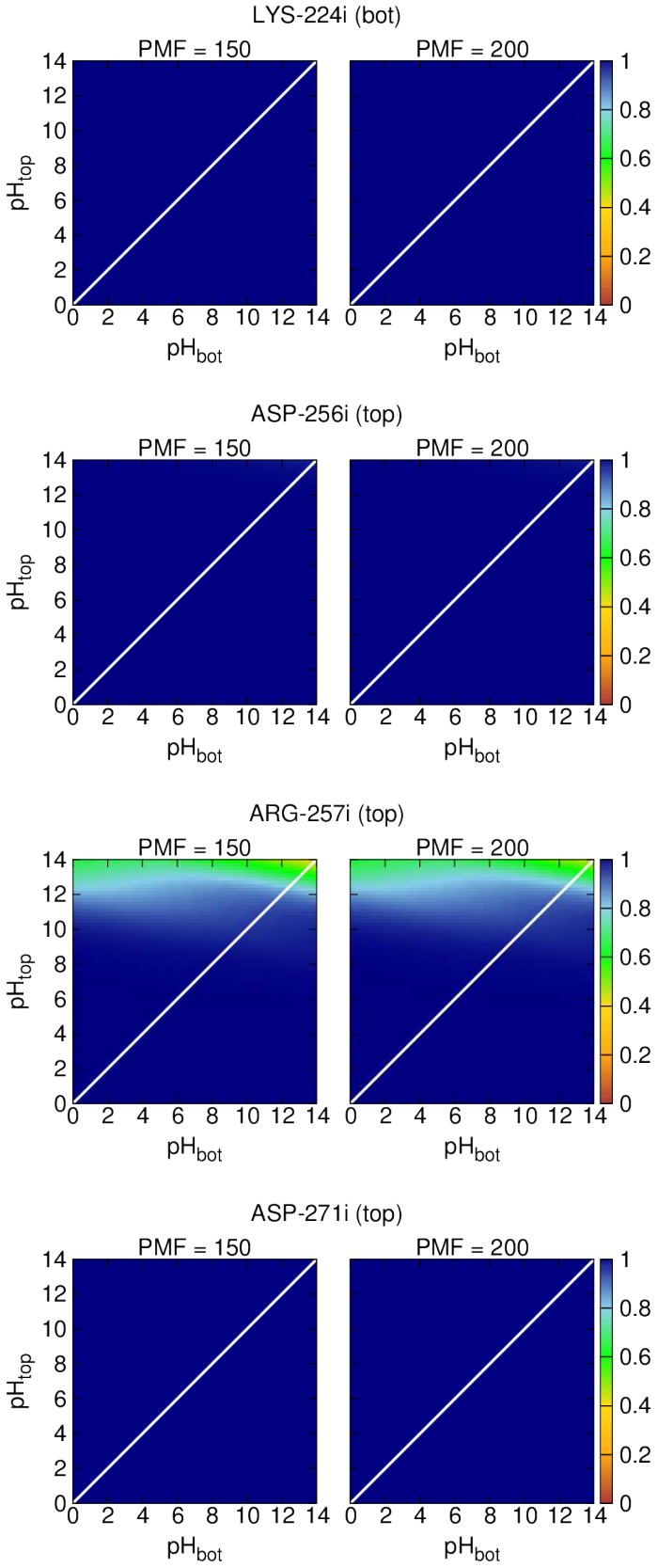
LYS-224i (bot)
PMF = 150
PMF = 200
ASP-256i (top)
PMF = 150
PMF = 200
ARG-257i (top)
PMF = 150
PMF = 200
ASP-271i (top)
PMF = 150
PMF = 200
pH_top
pH_bot
0 2 4 6 8 10 12 14
0 0.2 0.4 0.6 0.8 1

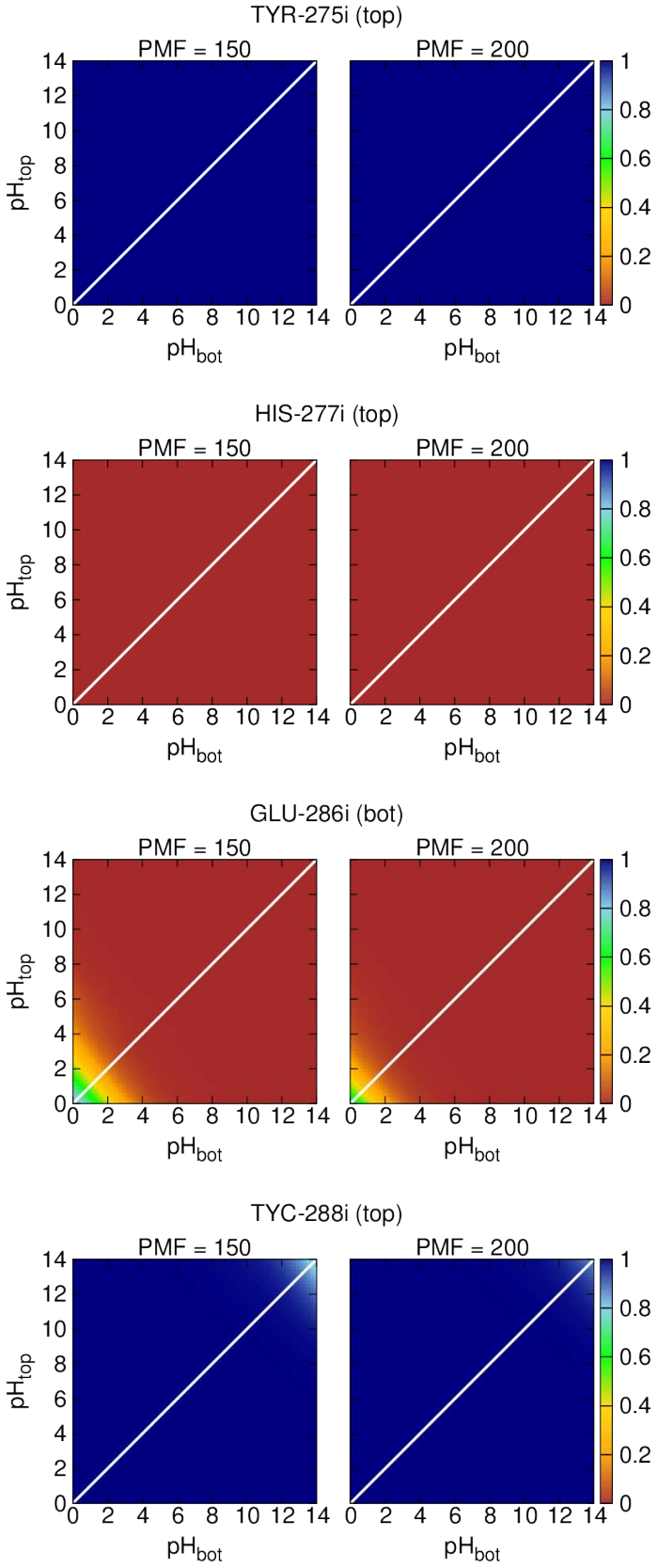
TYR-275i (top)
PMF = 150
PMF = 200
HIS-277i (top)
PMF = 150
PMF = 200
GLU-286i (bot)
PMF = 150
PMF = 200
TYC-288i (top)
PMF = 150
PMF = 200
pH_top
pH_bot
0 2 4 6 8 10 12 14
0 0.2 0.4 0.6 0.8 1

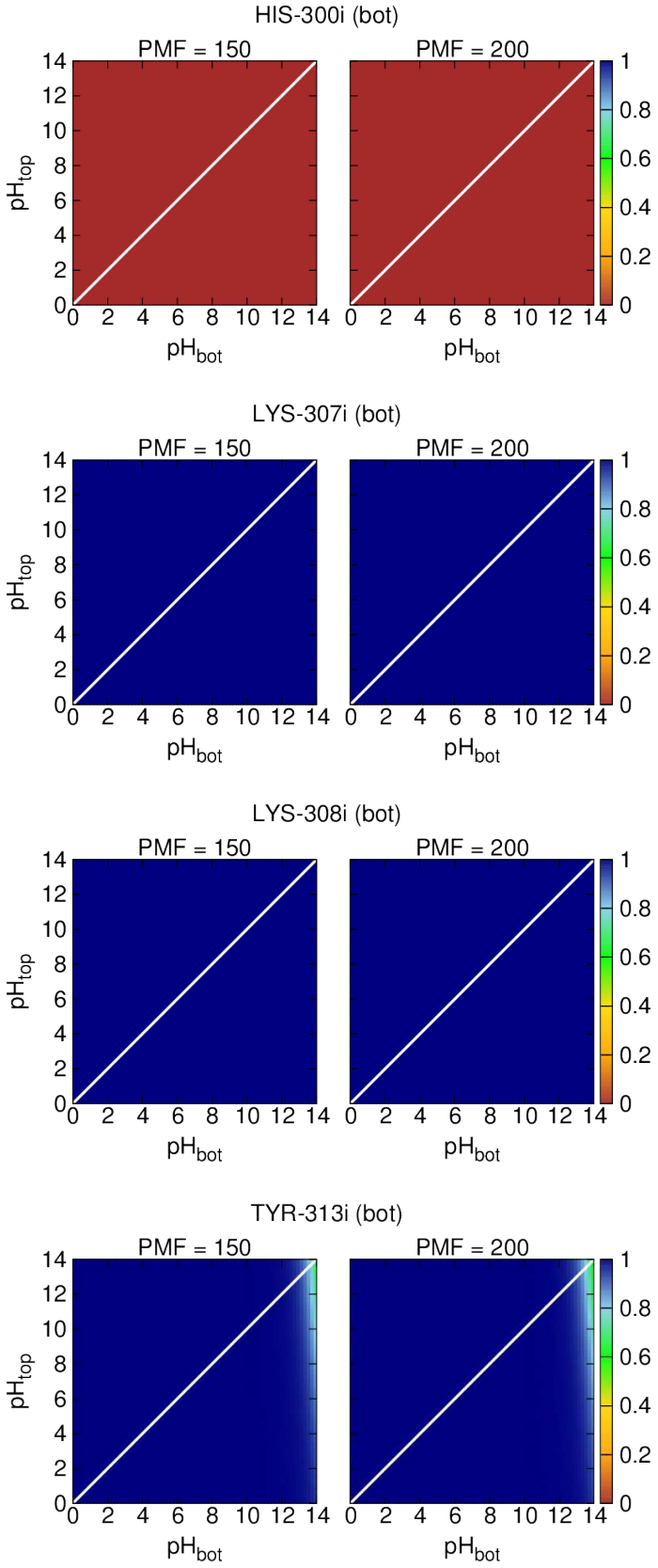
HIS-300i (bot)
PMF = 150
PMF = 200
LYS-307i (bot)
PMF = 150
PMF = 200
LYS-308i (bot)
PMF = 150
PMF = 200
TYR-313i (bot)
PMF = 150
PMF = 200
pH_top
pH_bot
0 2 4 6 8 10 12 14
0 0.2 0.4 0.6 0.8 1

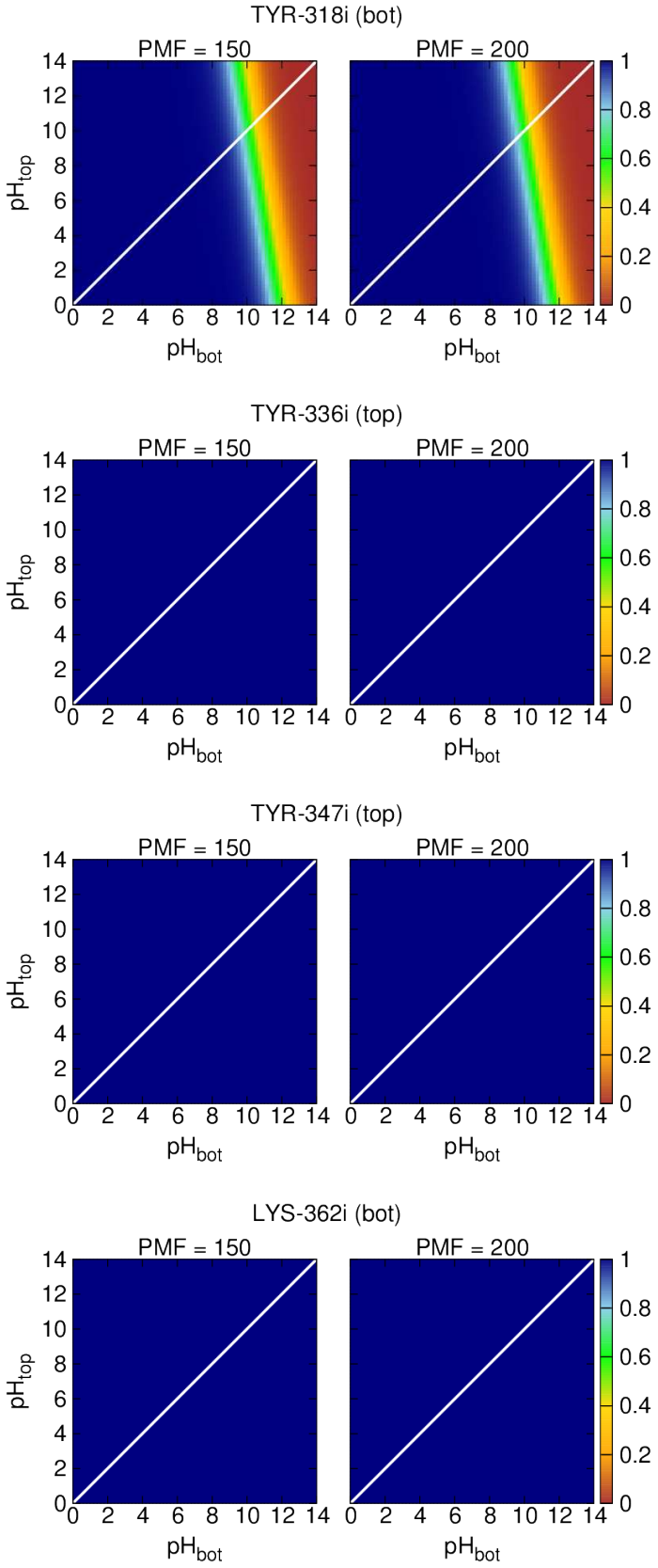
TYR-318i (bot)
PMF = 150
PMF = 200
TYR-336i (top)
PMF = 150
PMF = 200
TYR-347i (top)
PMF = 150
PMF = 200
LYS-362i (bot)
PMF = 150
PMF = 200
pH_top
pH_bot
0 2 4 6 8 10 12 14
1 0.8 0.6 0.4 0.2 0

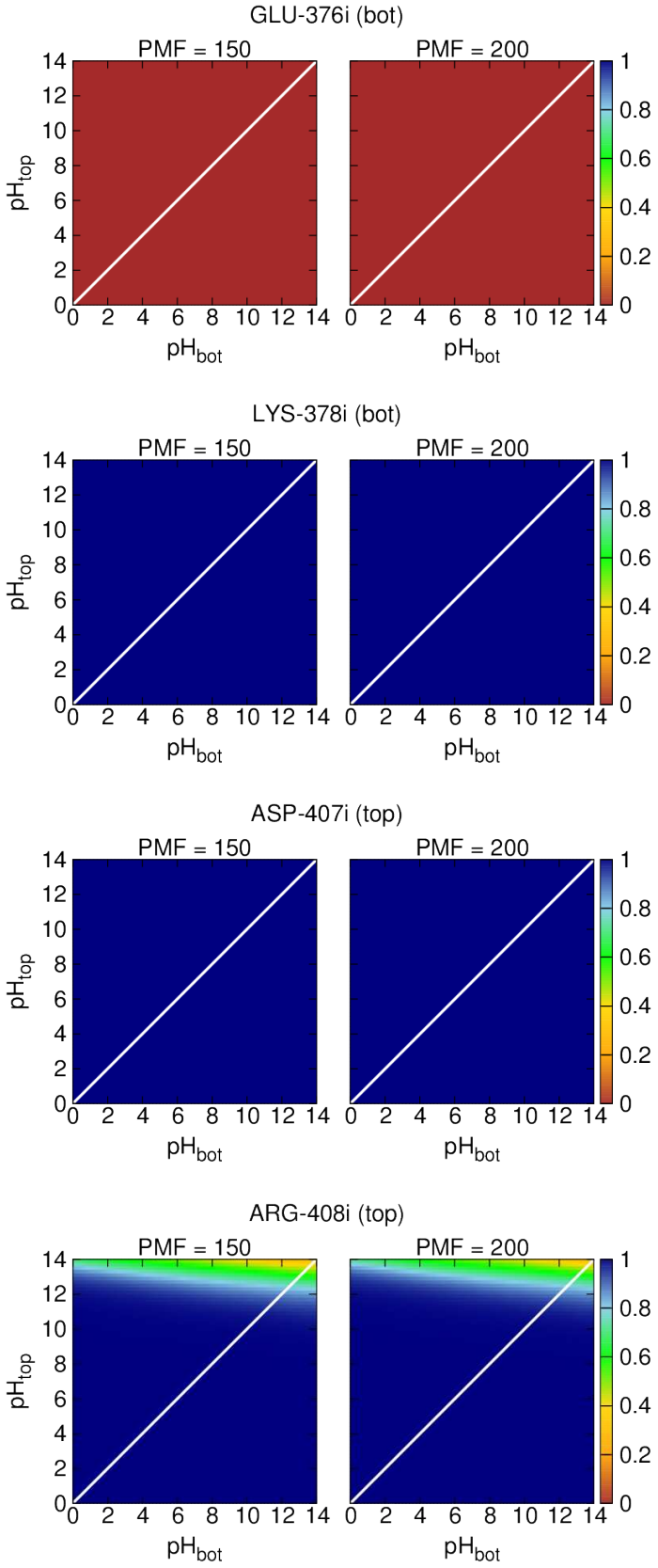
GLU-376i (bot)
PMF = 150
PMF = 200
LYS-378i (bot)
PMF = 150
PMF = 200
ASP-407i (top)
PMF = 150
PMF = 200
ARG-408i (top)
PMF = 150
PMF = 200
pH_top
pH_bot
0 2 4 6 8 10 12 14
0 0.2 0.4 0.6 0.8 1

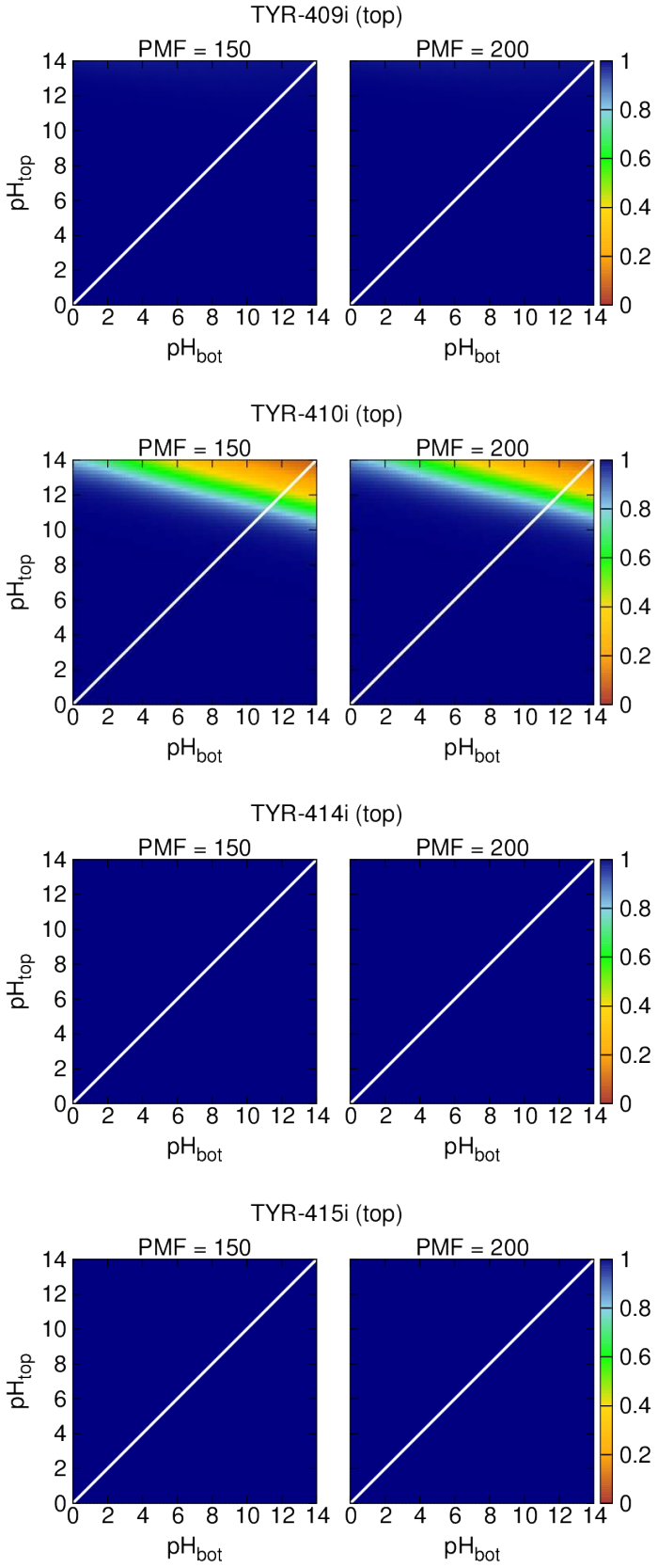
TYR-409i (top)
PMF = 150
PMF = 200
TYR-410i (top)
PMF = 150
PMF = 200
TYR-414i (top)
PMF = 150
PMF = 200
TYR-415i (top)
PMF = 150
PMF = 200
pH_top
pH_bot
0 2 4 6 8 10 12 14
0 0.2 0.4 0.6 0.8 1

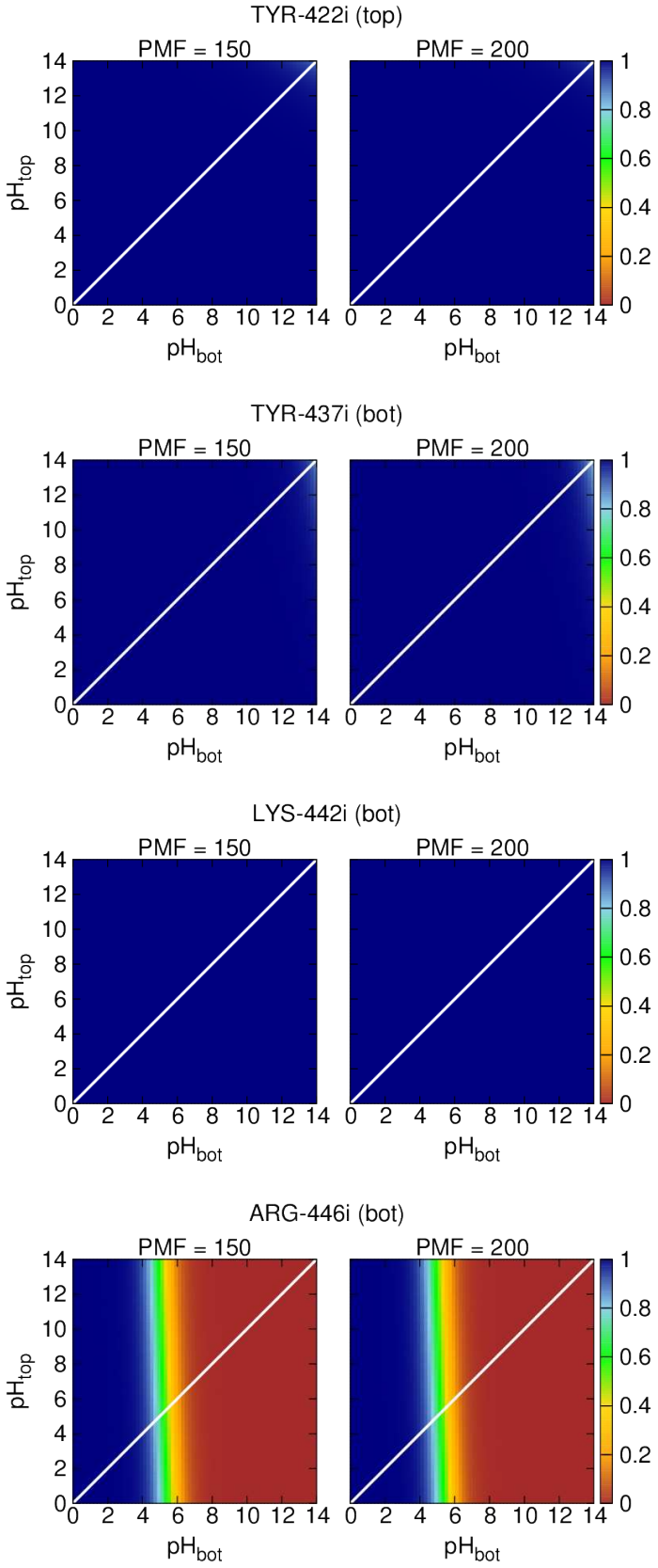
TYR-422i (top)
PMF = 150
PMF = 200
TYR-437i (bot)
PMF = 150
PMF = 200
LYS-442i (bot)
PMF = 150
PMF = 200
ARG-446i (bot)
PMF = 150
PMF = 200
pH_top
pH_bot
0 2 4 6 8 10 12 14
0 0.2 0.4 0.6 0.8 1

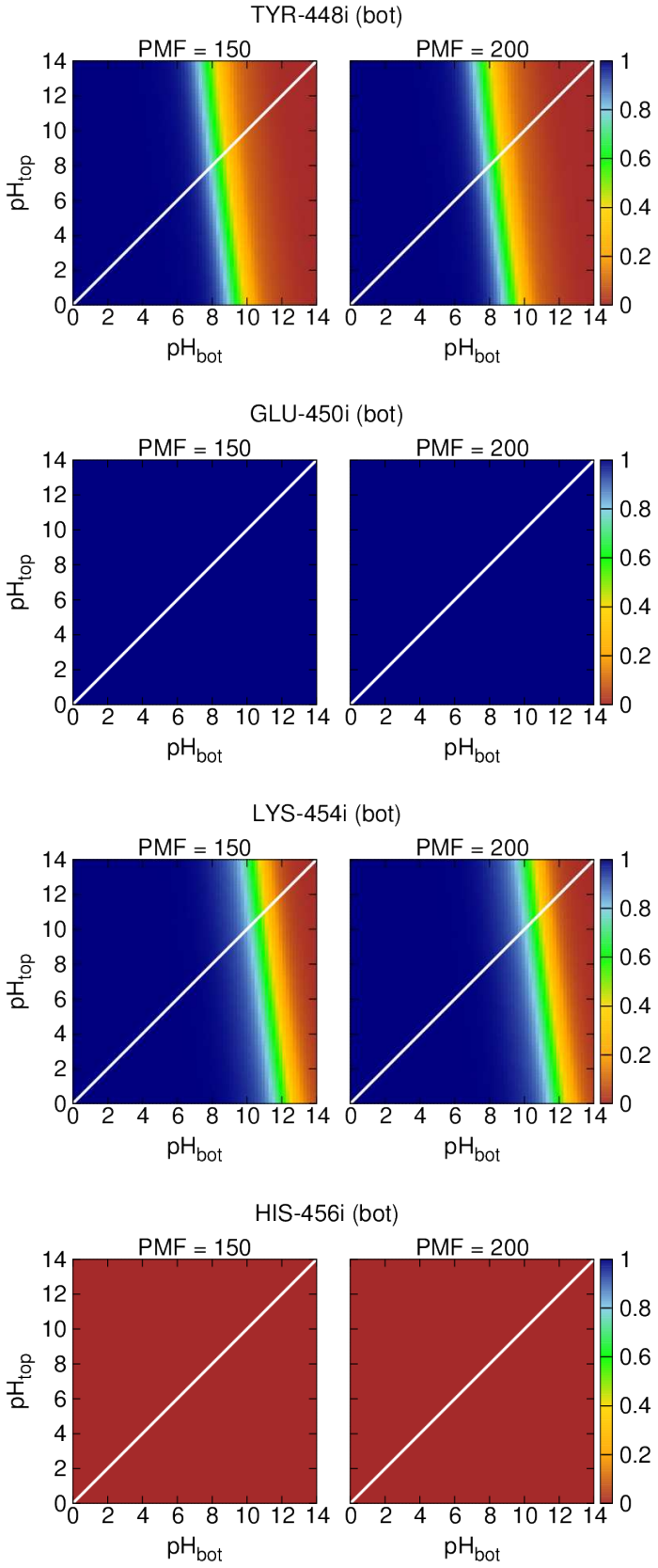
TYR-448i (bot)
PMF = 150
PMF = 200
GLU-450i (bot)
PMF = 150
PMF = 200
LYS-454i (bot)
PMF = 150
PMF = 200
HIS-456i (bot)
PMF = 150
PMF = 200
pH_top
pH_bot
0 2 4 6 8 10 12 14
0 0.2 0.4 0.6 0.8 1

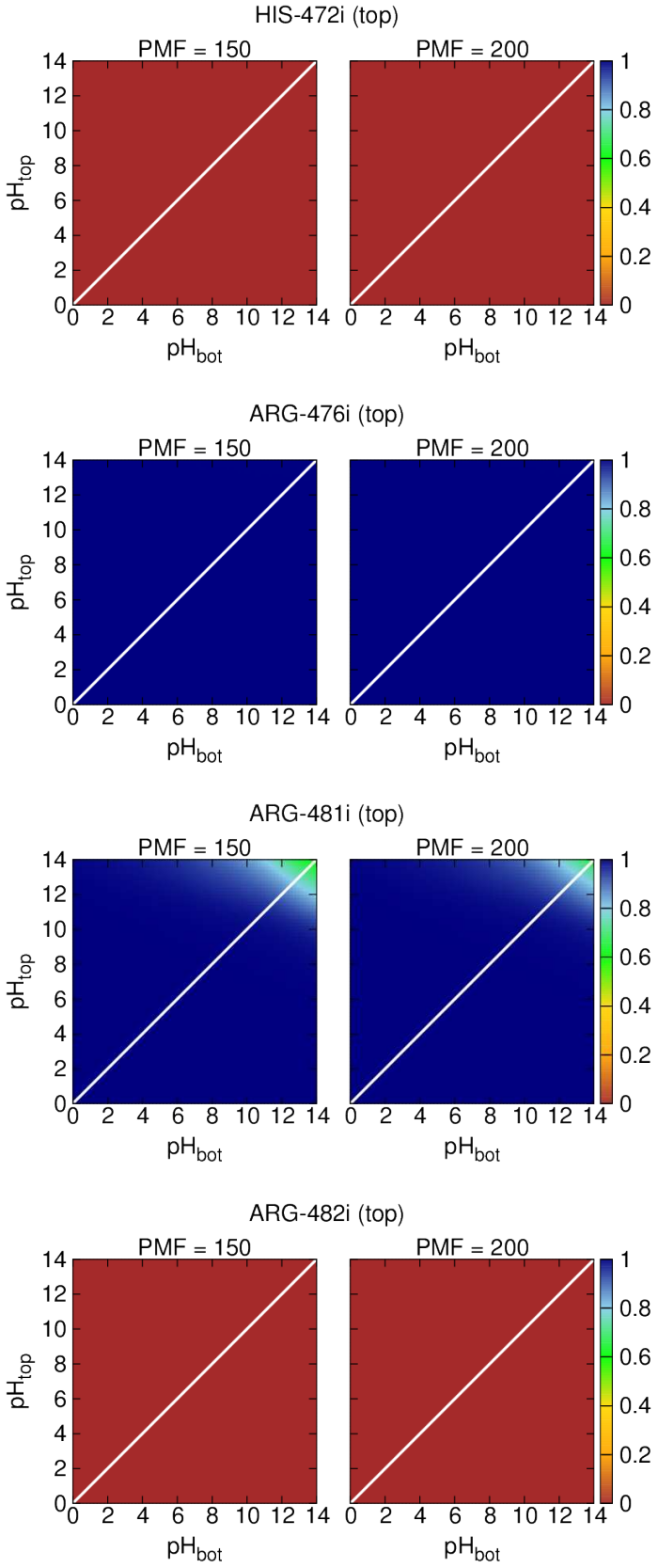
HIS-472i (top)
PMF = 150
PMF = 200
ARG-476i (top)
PMF = 150
PMF = 200
ARG-481i (top)
PMF = 150
PMF = 200
ARG-482i (top)
PMF = 150
PMF = 200
pH_top
pH_bot
0 2 4 6 8 10 12 14
0 0.2 0.4 0.6 0.8 1

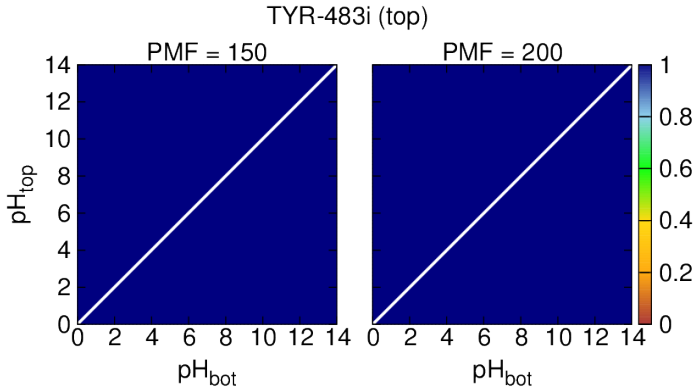
TYR-483i (top)
PMF = 150
PMF = 200
pH_top
pH_bot
0 2 4 6 8 10 12 14
1 0.8 0.6 0.4 0.2 0

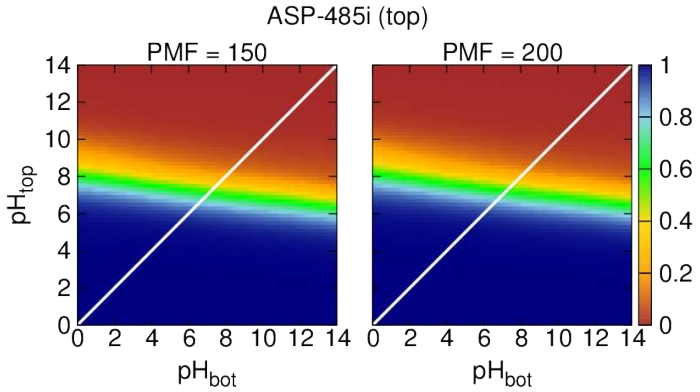
ASP-485i (top)
PMF = 150
PMF = 200
pH_top
pH_bot
0 2 4 6 8 10 12 14
1 0.8 0.6 0.4 0.2 0

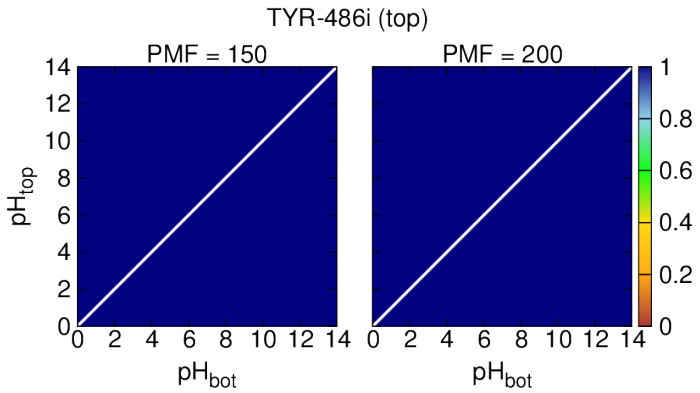
TYR-486i (top)
PMF = 150
PMF = 200
pH_top
pH_bot
0 2 4 6 8 10 12 14
1 0.8 0.6 0.4 0.2 0

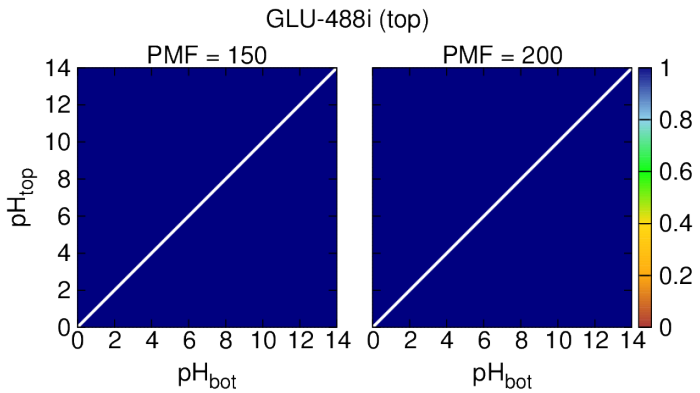
GLU-488i (top)
PMF = 150
PMF = 200
pH_top
pH_bot
0 2 4 6 8 10 12 14
1 0.8 0.6 0.4 0.2 0

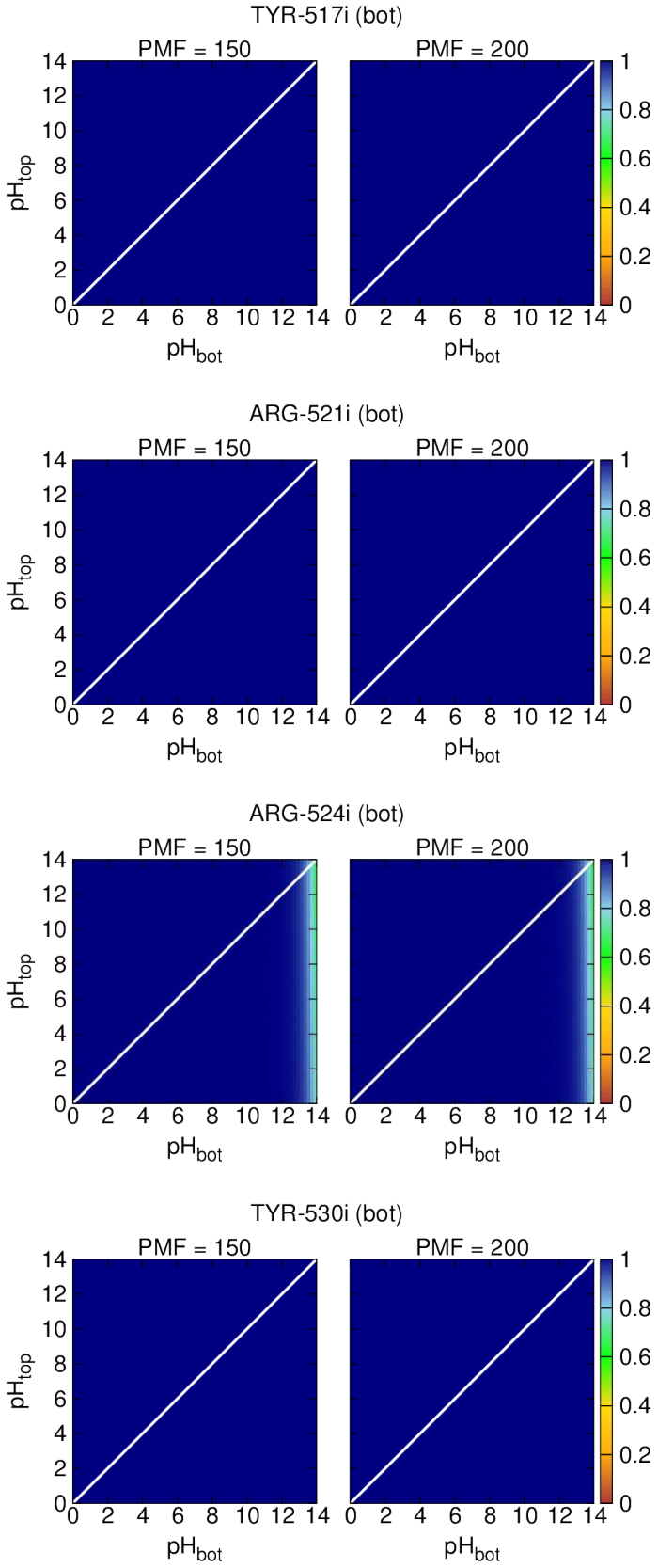
TYR-517i (bot)
PMF = 150
PMF = 200
ARG-521i (bot)
PMF = 150
PMF = 200
ARG-524i (bot)
PMF = 150
PMF = 200
TYR-530i (bot)
PMF = 150
PMF = 200
pH_top
pH_bot
0 2 4 6 8 10 12 14
0 0.2 0.4 0.6 0.8 1

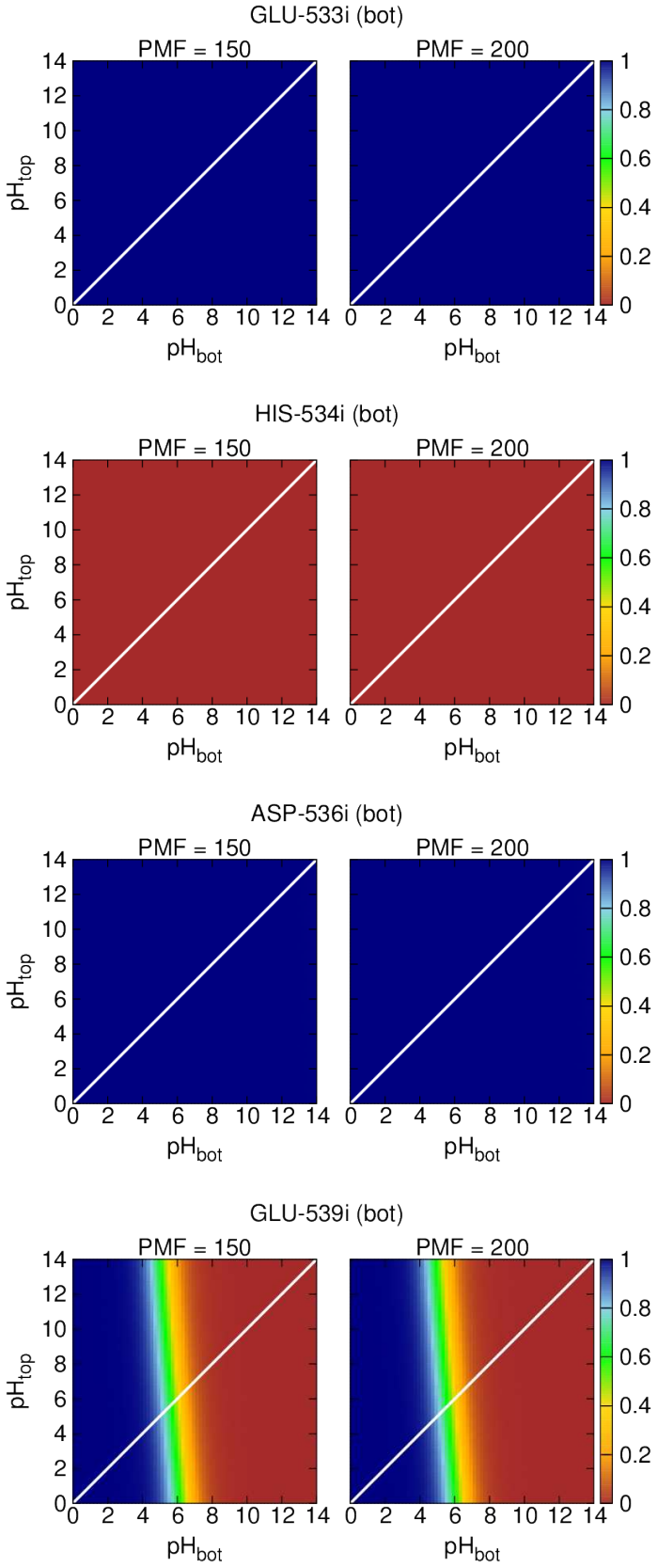
GLU-533i (bot)
PMF = 150
PMF = 200
HIS-534i (bot)
PMF = 150
PMF = 200
ASP-536i (bot)
PMF = 150
PMF = 200
GLU-539i (bot)
PMF = 150
PMF = 200
pH_top
pH_bot
0 2 4 6 8 10 12 14
0 0.2 0.4 0.6 0.8 1

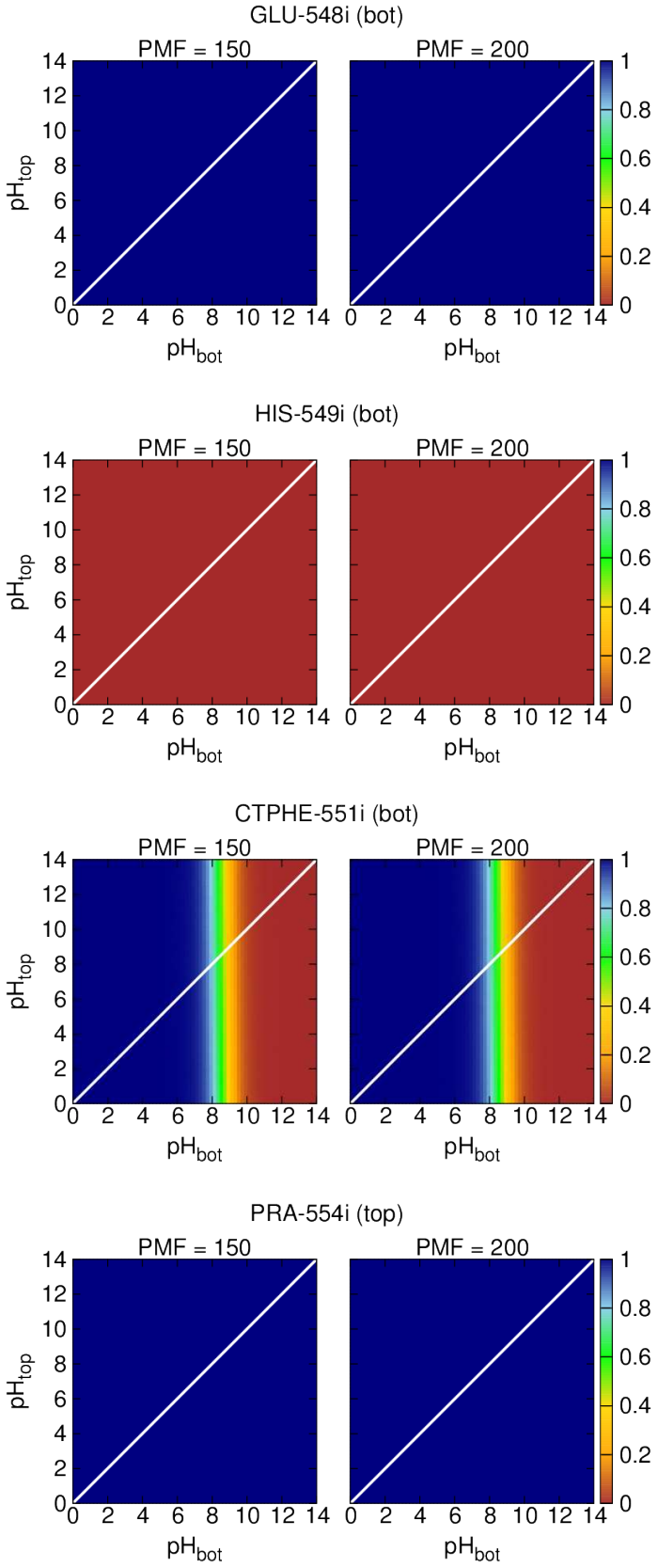
GLU-548i (bot)
PMF = 150
PMF = 200
HIS-549i (bot)
PMF = 150
PMF = 200
CTPHE-551i (bot)
PMF = 150
PMF = 200
PRA-554i (top)
PMF = 150
PMF = 200
pH_top
pH_bot
0 2 4 6 8 10 12 14
0 0.2 0.4 0.6 0.8 1

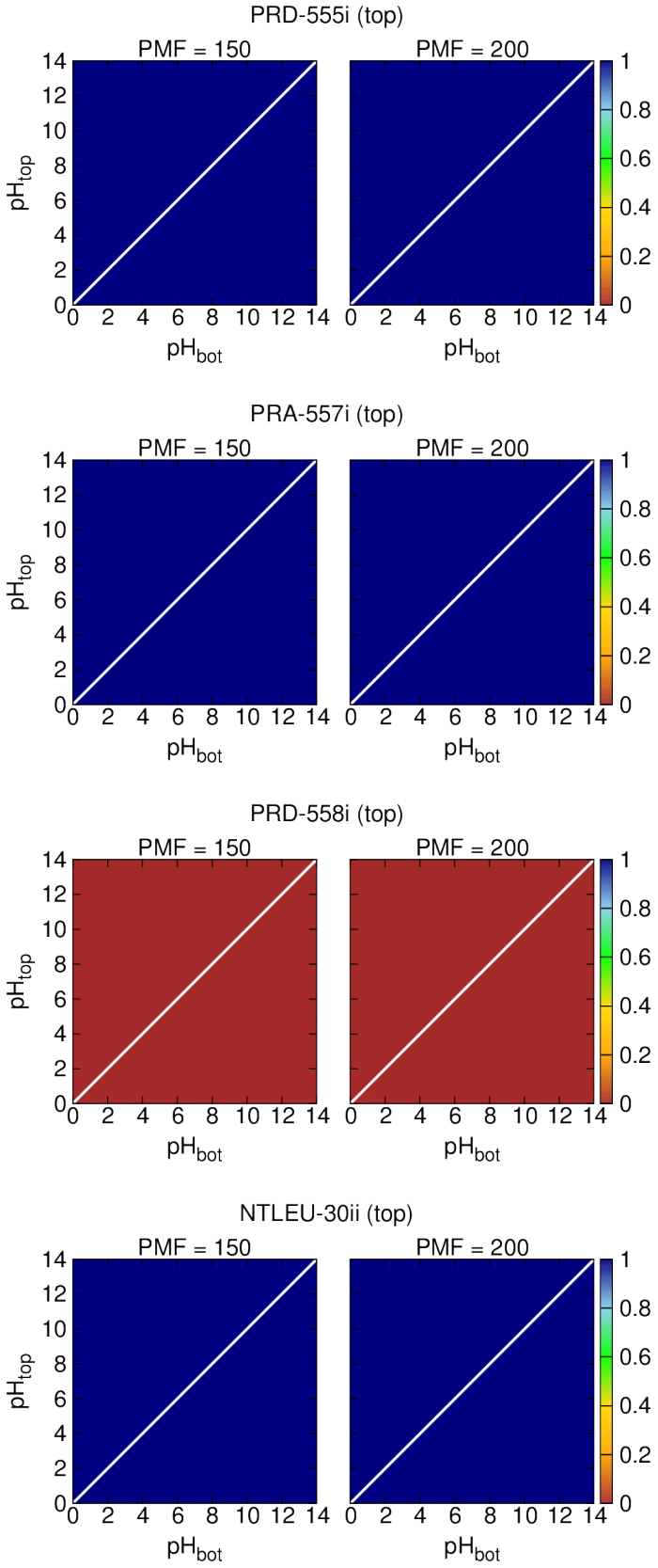
PRD-555i (top)
PMF = 150
PMF = 200
PRA-557i (top)
PMF = 150
PMF = 200
PRD-558i (top)
PMF = 150
PMF = 200
NTLEU-30ii (top)
PMF = 150
PMF = 200
pH_top
pH_bot
0 2 4 6 8 10 12 14
0 0.2 0.4 0.6 0.8 1

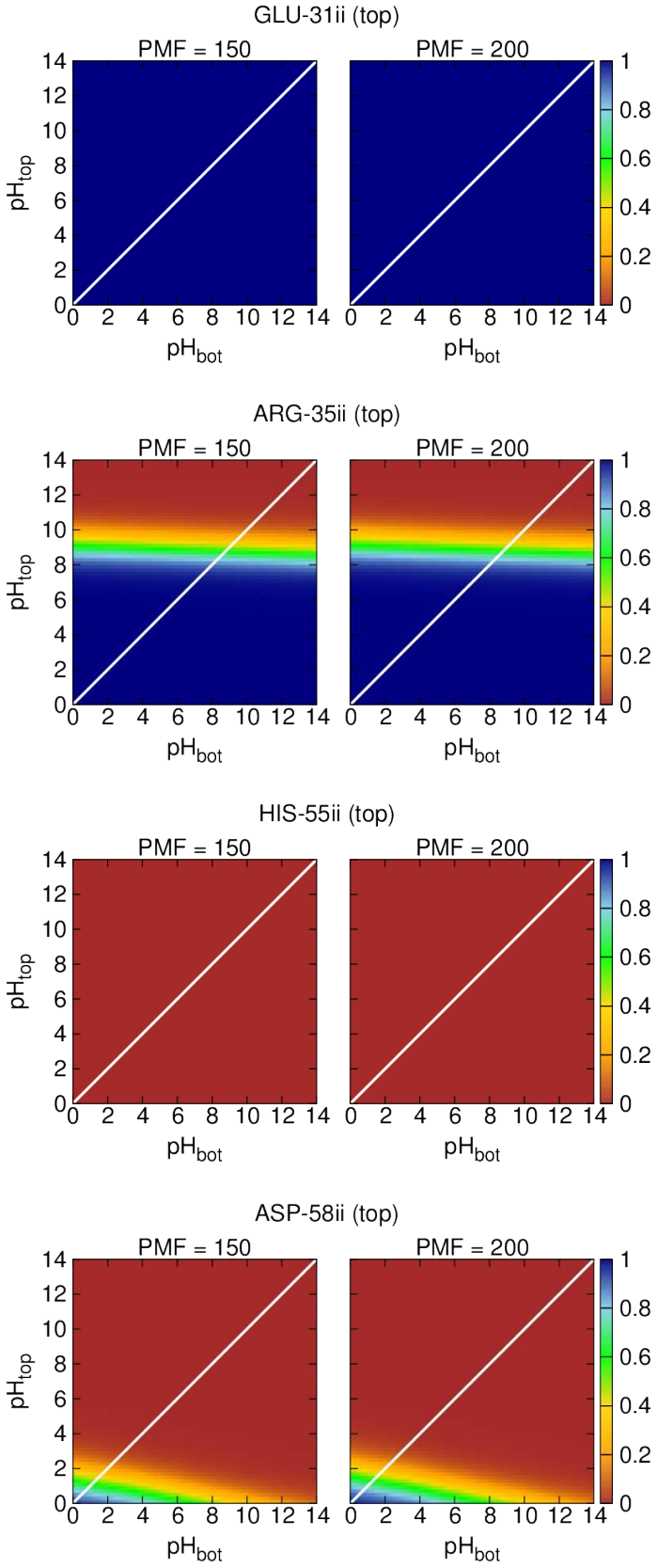
GLU-31ii (top)
PMF = 150
PMF = 200
ARG-35ii (top)
PMF = 150
PMF = 200
HIS-55ii (top)
PMF = 150
PMF = 200
ASP-58ii (top)
PMF = 150
PMF = 200
pH_top
pH_bot
0 2 4 6 8 10 12 14
0 0.2 0.4 0.6 0.8 1

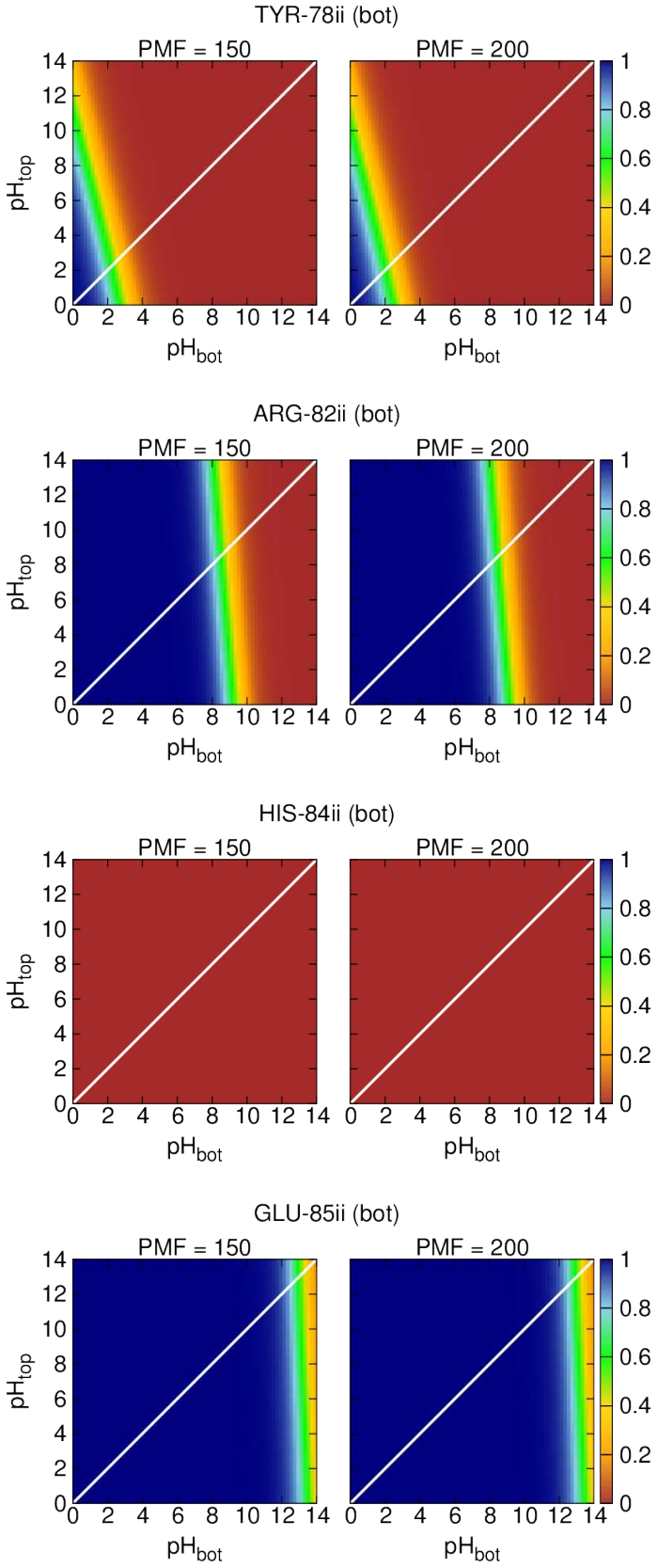
TYR-78ii (bot)
PMF = 150
PMF = 200
ARG-82ii (bot)
PMF = 150
PMF = 200
HIS-84ii (bot)
PMF = 150
PMF = 200
GLU-85ii (bot)
PMF = 150
PMF = 200
pH_top
pH_bot
0 2 4 6 8 10 12 14
0 0.2 0.4 0.6 0.8 1

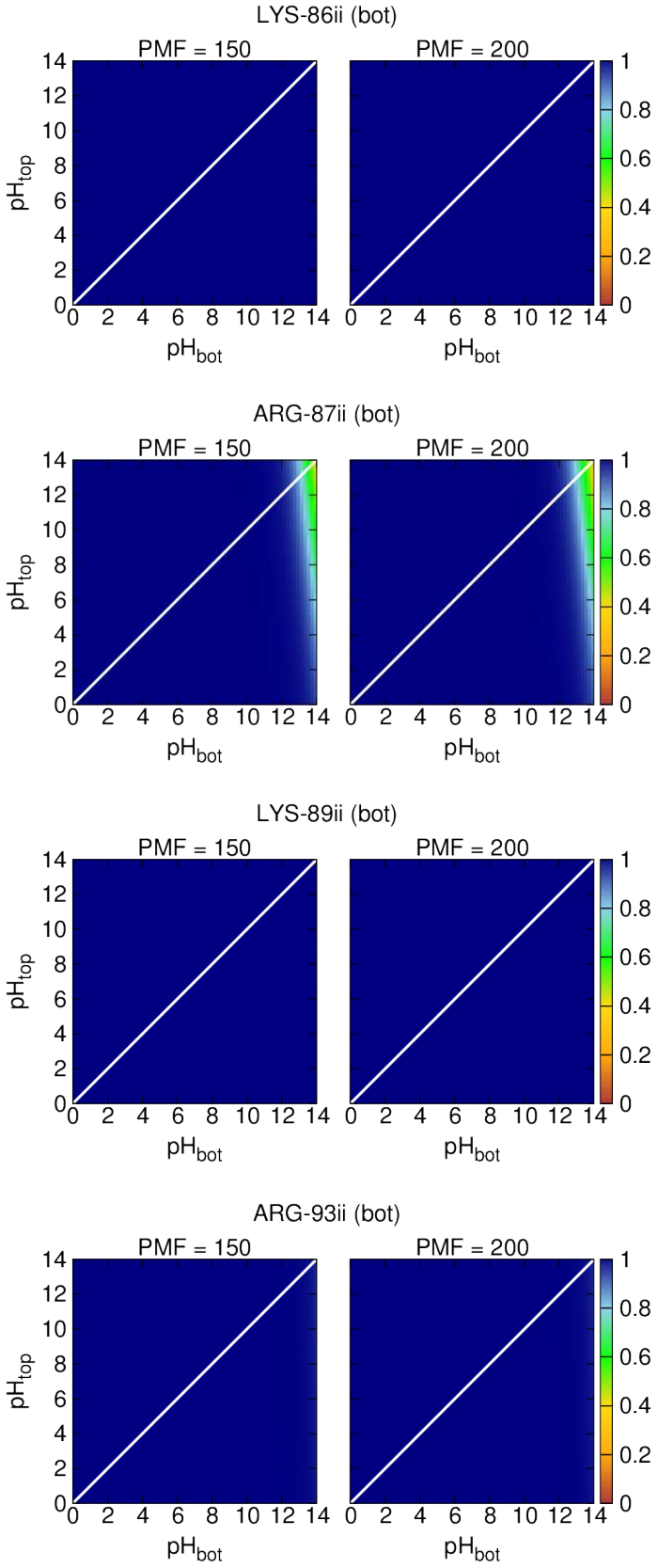
LYS-86ii (bot)
PMF = 150
PMF = 200
ARG-87ii (bot)
PMF = 150
PMF = 200
LYS-89ii (bot)
PMF = 150
PMF = 200
ARG-93ii (bot)
PMF = 150
PMF = 200
pH_top
pH_bot
0 2 4 6 8 10 12 14
0 0.2 0.4 0.6 0.8 1

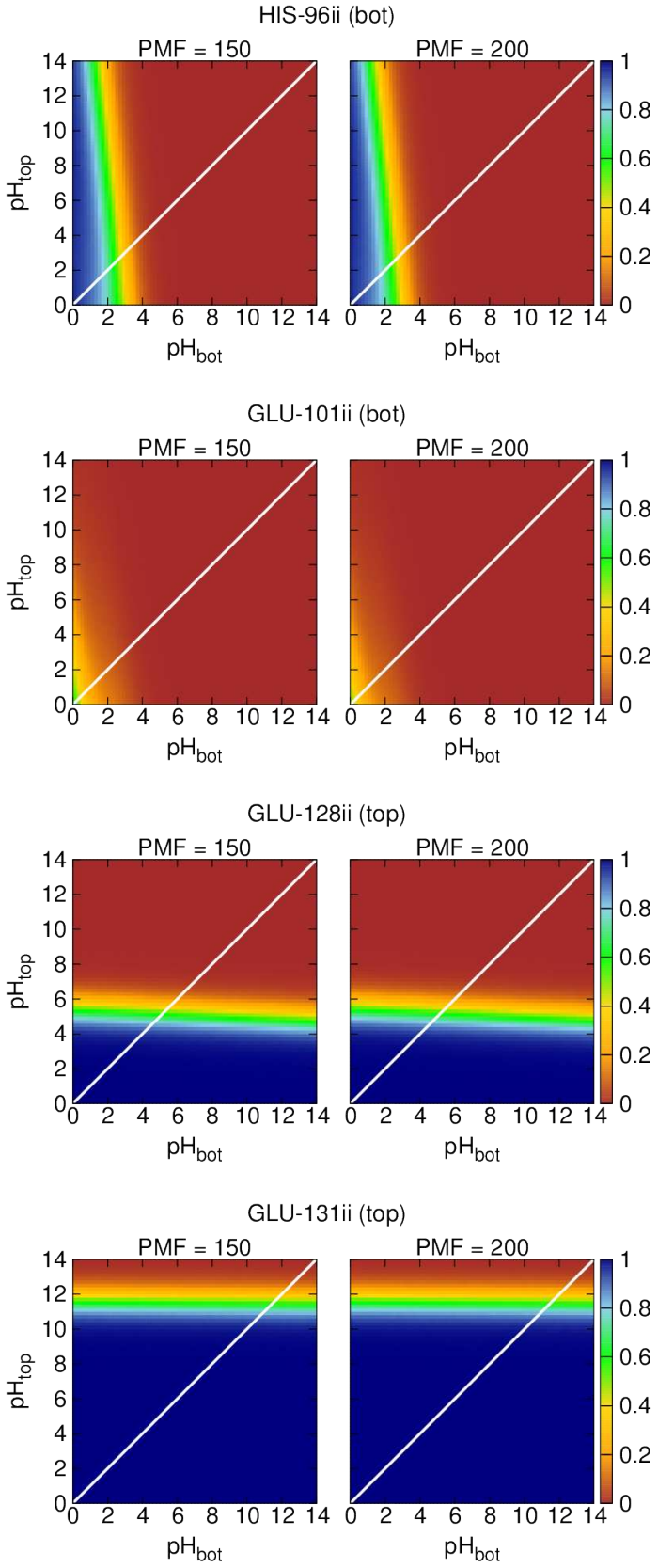
HIS-96ii (bot)
PMF = 150
PMF = 200
GLU-101ii (bot)
PMF = 150
PMF = 200
GLU-128ii (top)
PMF = 150
PMF = 200
GLU-131ii (top)
PMF = 150
PMF = 200
pH_top
pH_bot
0 2 4 6 8 10 12 14
1 0.8 0.6 0.4 0.2 0

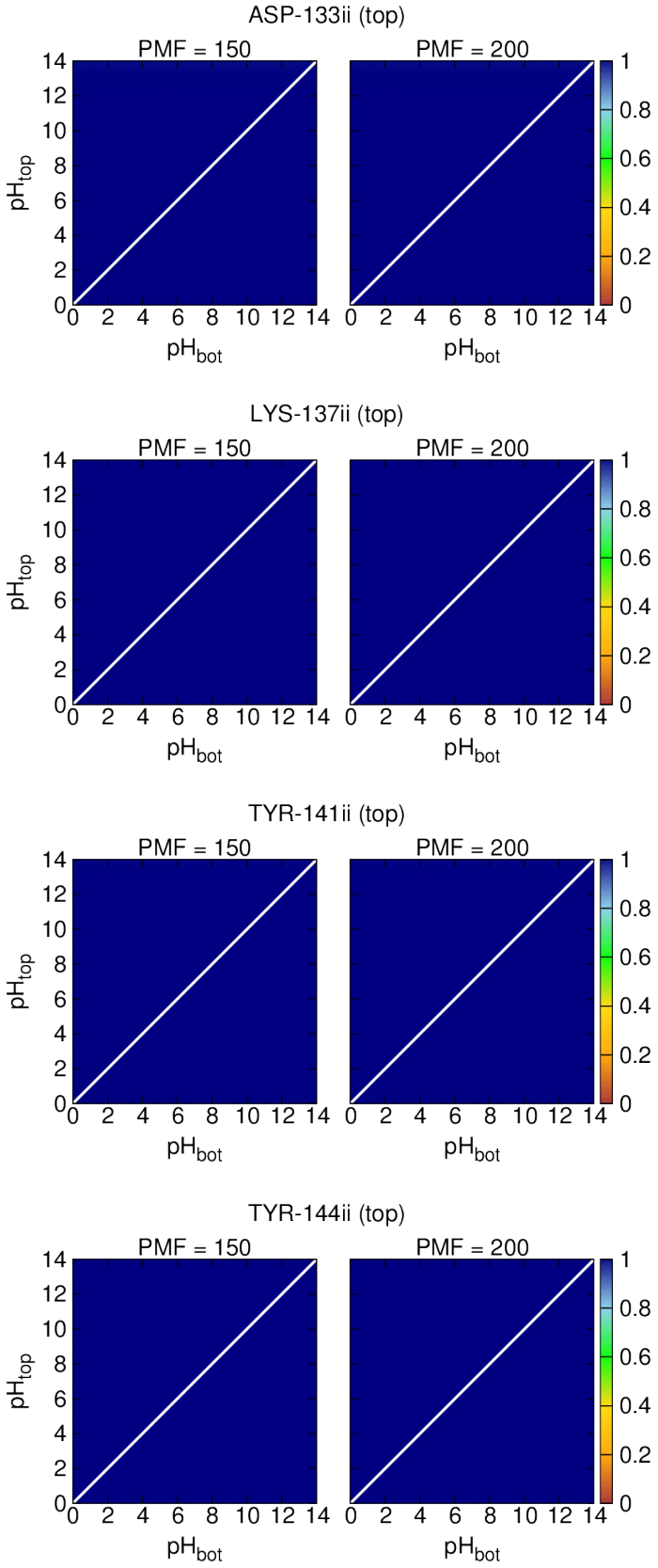
ASP-133ii (top)
PMF = 150
PMF = 200
LYS-137ii (top)
PMF = 150
PMF = 200
TYR-141ii (top)
PMF = 150
PMF = 200
TYR-144ii (top)
PMF = 150
PMF = 200
pH_top
pH_bot
0 2 4 6 8 10 12 14
0 0.2 0.4 0.6 0.8 1

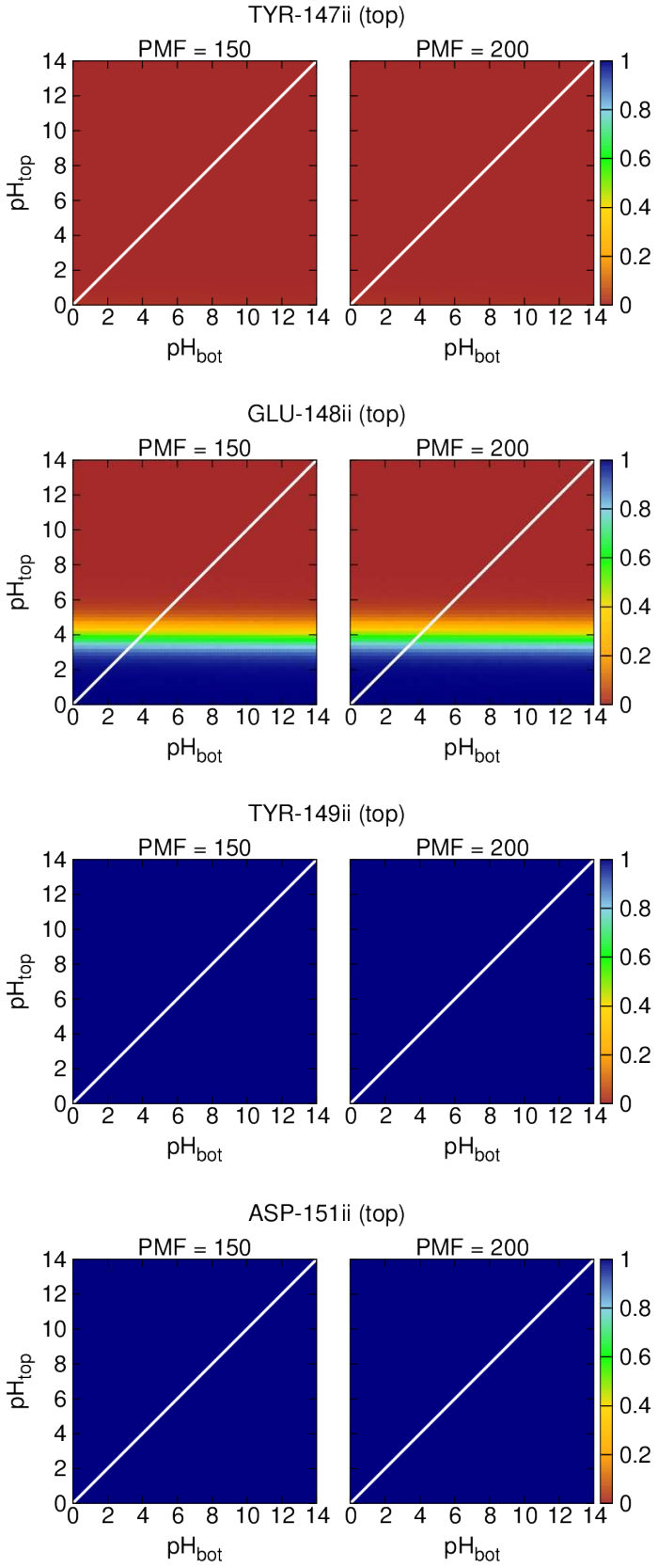
TYR-147ii (top)
PMF = 150
PMF = 200
GLU-148ii (top)
PMF = 150
PMF = 200
TYR-149ii (top)
PMF = 150
PMF = 200
ASP-151ii (top)
PMF = 150
PMF = 200
pH_top
pH_bot
0 2 4 6 8 10 12 14
0 0.2 0.4 0.6 0.8 1

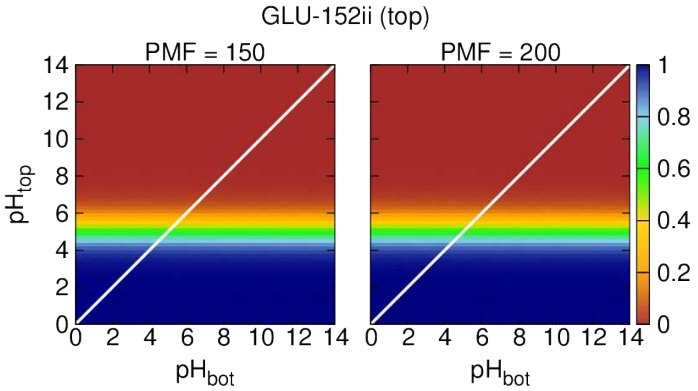
GLU-152ii (top)
PMF = 150
PMF = 200
pH_top
pH_bot
0 2 4 6 8 10 12 14
1 0.8 0.6 0.4 0.2 0

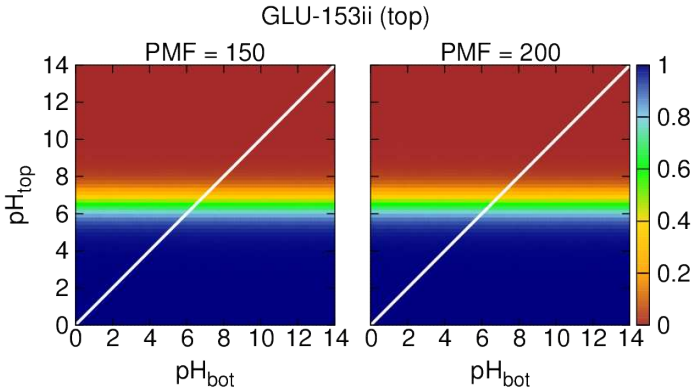
GLU-153ii (top)
PMF = 150
PMF = 200
pH_top
pH_bot
0 2 4 6 8 10 12 14
1 0.8 0.6 0.4 0.2 0

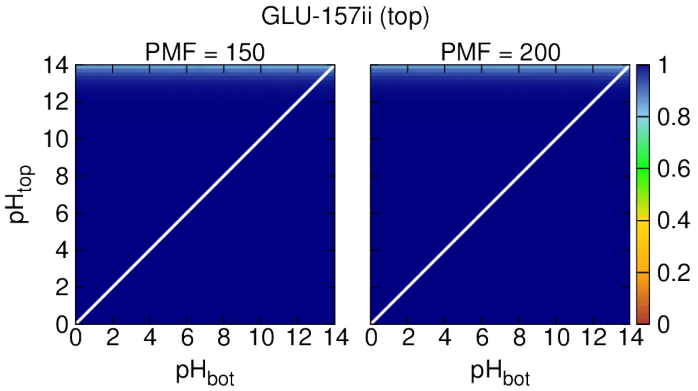
GLU-157ii (top)
PMF = 150
PMF = 200
pH_top
pH_bot
0 2 4 6 8 10 12 14
1 0.8 0.6 0.4 0.2 0

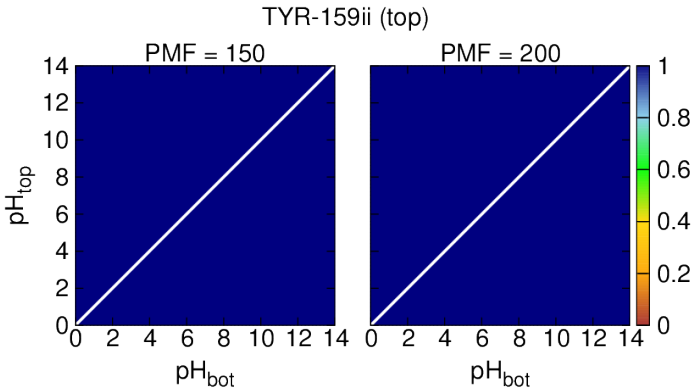
TYR-159ii (top)
PMF = 150
PMF = 200
pH_top
pH_bot
0 2 4 6 8 10 12 14
1 0.8 0.6 0.4 0.2 0

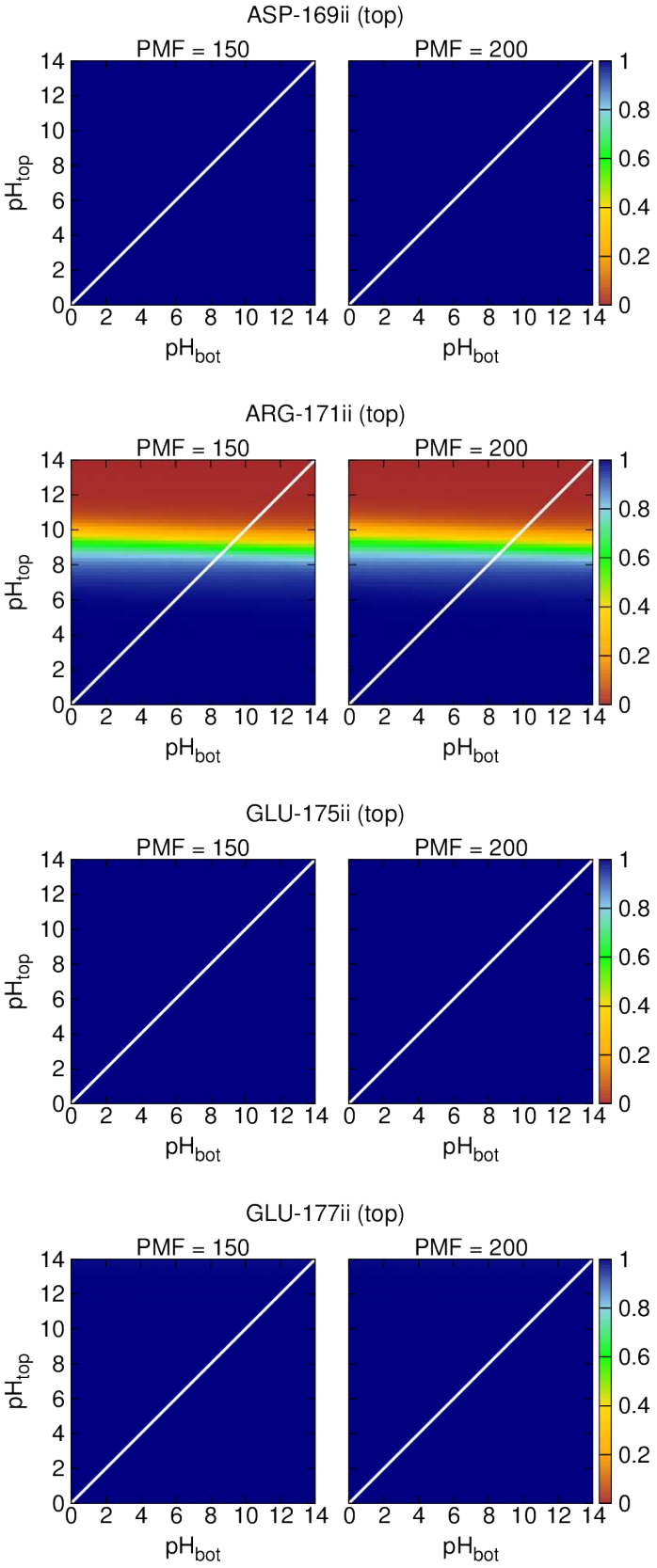
ASP-169ii (top)
PMF = 150
PMF = 200
ARG-171ii (top)
PMF = 150
PMF = 200
GLU-175ii (top)
PMF = 150
PMF = 200
GLU-177ii (top)
PMF = 150
PMF = 200
pH_top
pH_bot
0 2 4 6 8 10 12 14
0 0.2 0.4 0.6 0.8 1

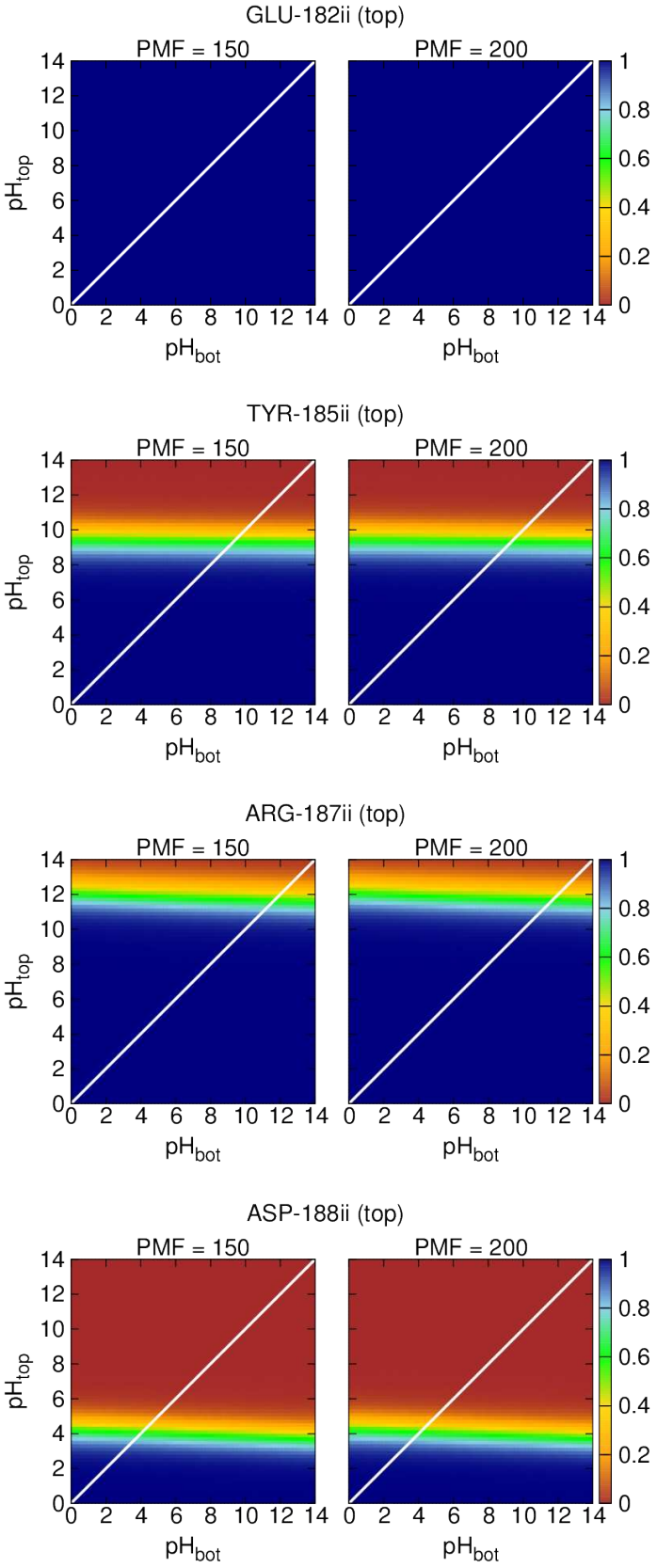
GLU-182ii (top)
PMF = 150
PMF = 200
TYR-185ii (top)
PMF = 150
PMF = 200
ARG-187ii (top)
PMF = 150
PMF = 200
ASP-188ii (top)
PMF = 150
PMF = 200
pH_top
pH_bot
0 2 4 6 8 10 12 14
0 0.2 0.4 0.6 0.8 1

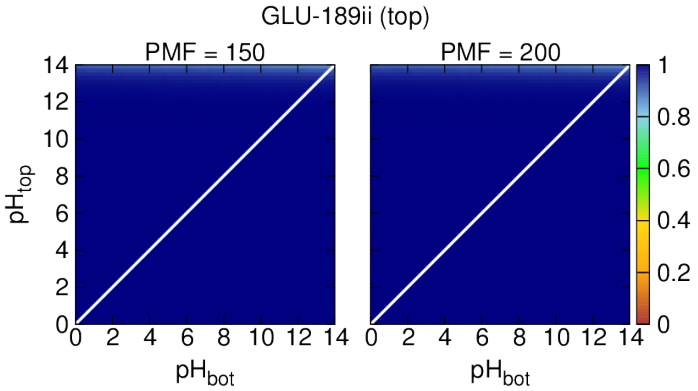
GLU-189ii (top)
PMF = 150
PMF = 200
pH_top
pH_bot
0 2 4 6 8 10 12 14
0 0.2 0.4 0.6 0.8 1

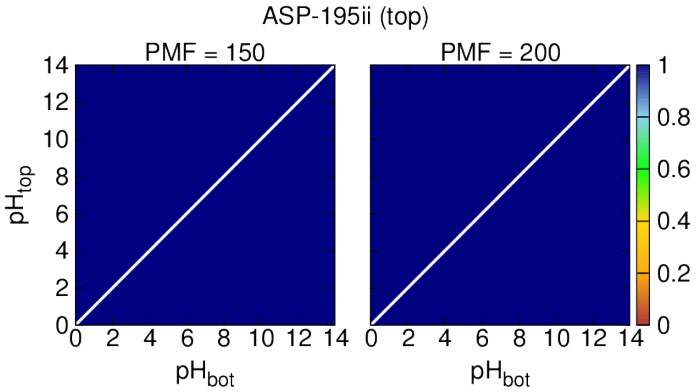
ASP-195ii (top)
PMF = 150
PMF = 200
pH_top
pH_bot
0 2 4 6 8 10 12 14
0 0.2 0.4 0.6 0.8 1

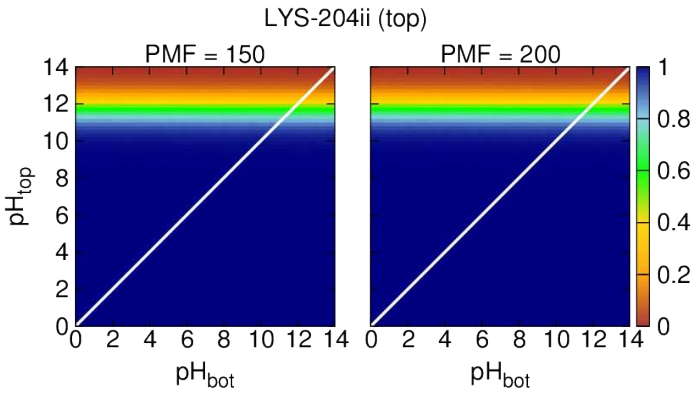
LYS-204ii (top)
PMF = 150
PMF = 200
pH_top
pH_bot
0 2 4 6 8 10 12 14
0 0.2 0.4 0.6 0.8 1

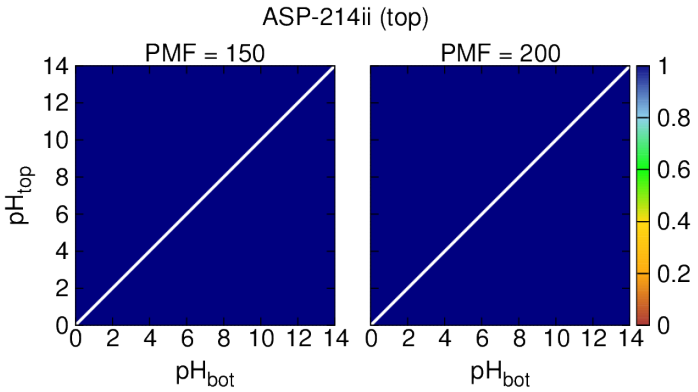
ASP-214ii (top)
PMF = 150
PMF = 200
pH_top
pH_bot
0 2 4 6 8 10 12 14
0 0.2 0.4 0.6 0.8 1

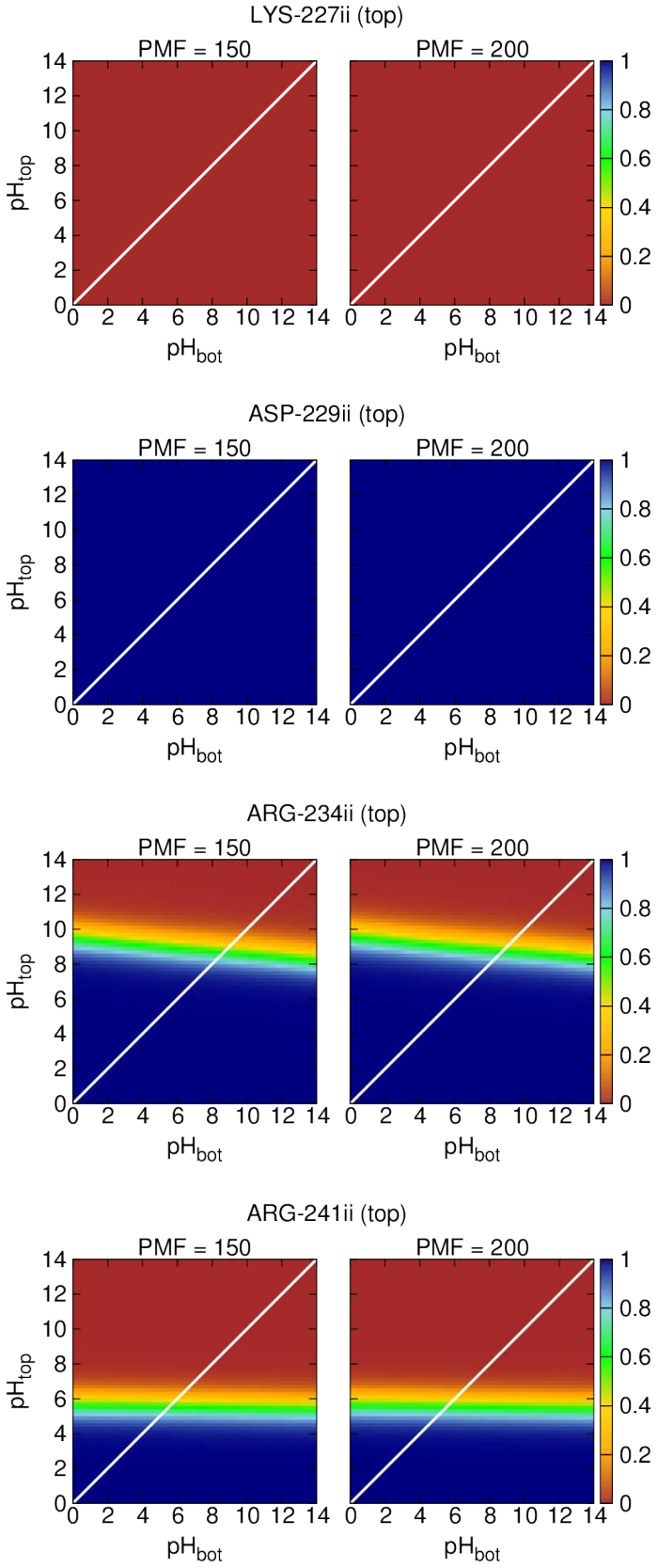
LYS-227ii (top)
PMF = 150
PMF = 200
ASP-229ii (top)
PMF = 150
PMF = 200
ARG-234ii (top)
PMF = 150
PMF = 200
ARG-241ii (top)
PMF = 150
PMF = 200
pH_top
pH_bot
0 2 4 6 8 10 12 14
0 0.2 0.4 0.6 0.8 1

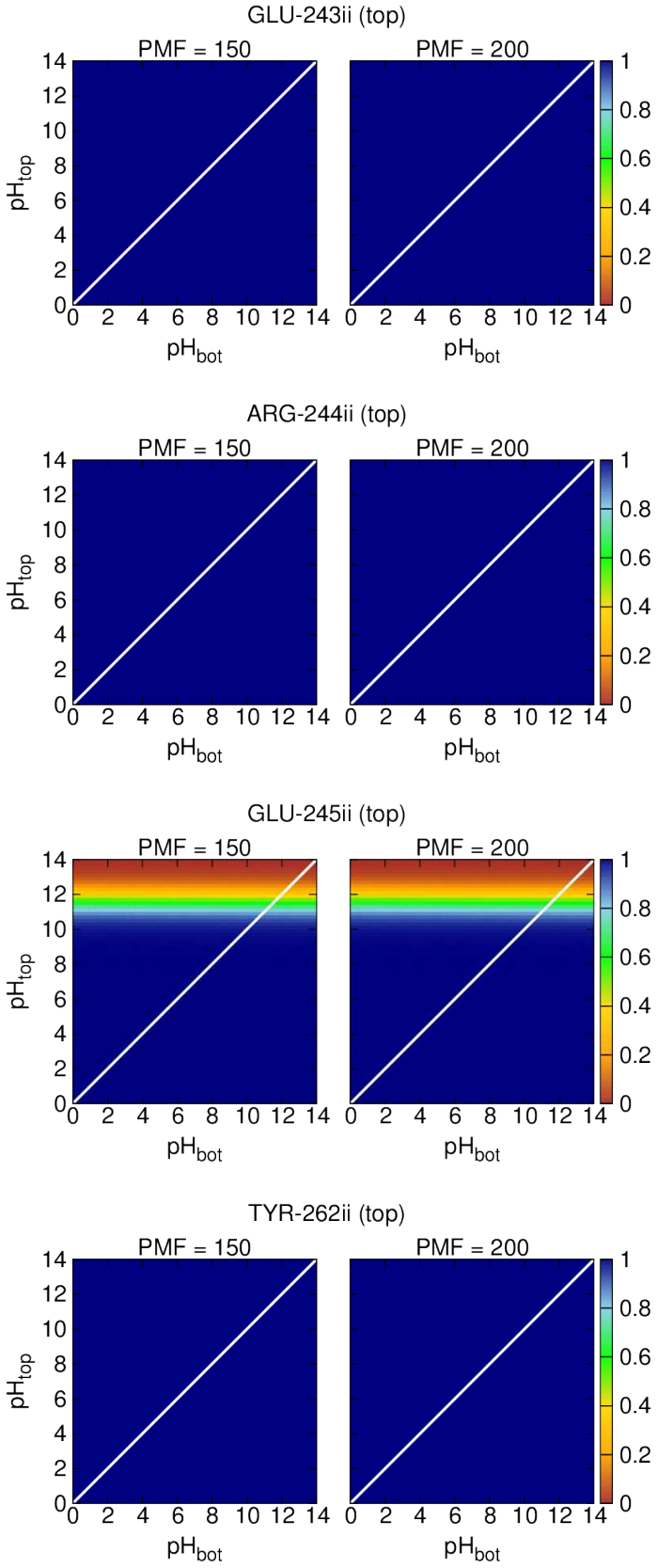
GLU-243ii (top)
PMF = 150
PMF = 200
pH_top
pH_bot
0 2 4 6 8 10 12 14
0 0.2 0.4 0.6 0.8 1
ARG-244ii (top)
PMF = 150
PMF = 200
pH_top
pH_bot
GLU-245ii (top)
PMF = 150
PMF = 200
pH_top
pH_bot
TYR-262ii (top)
PMF = 150
PMF = 200
pH_top
pH_bot

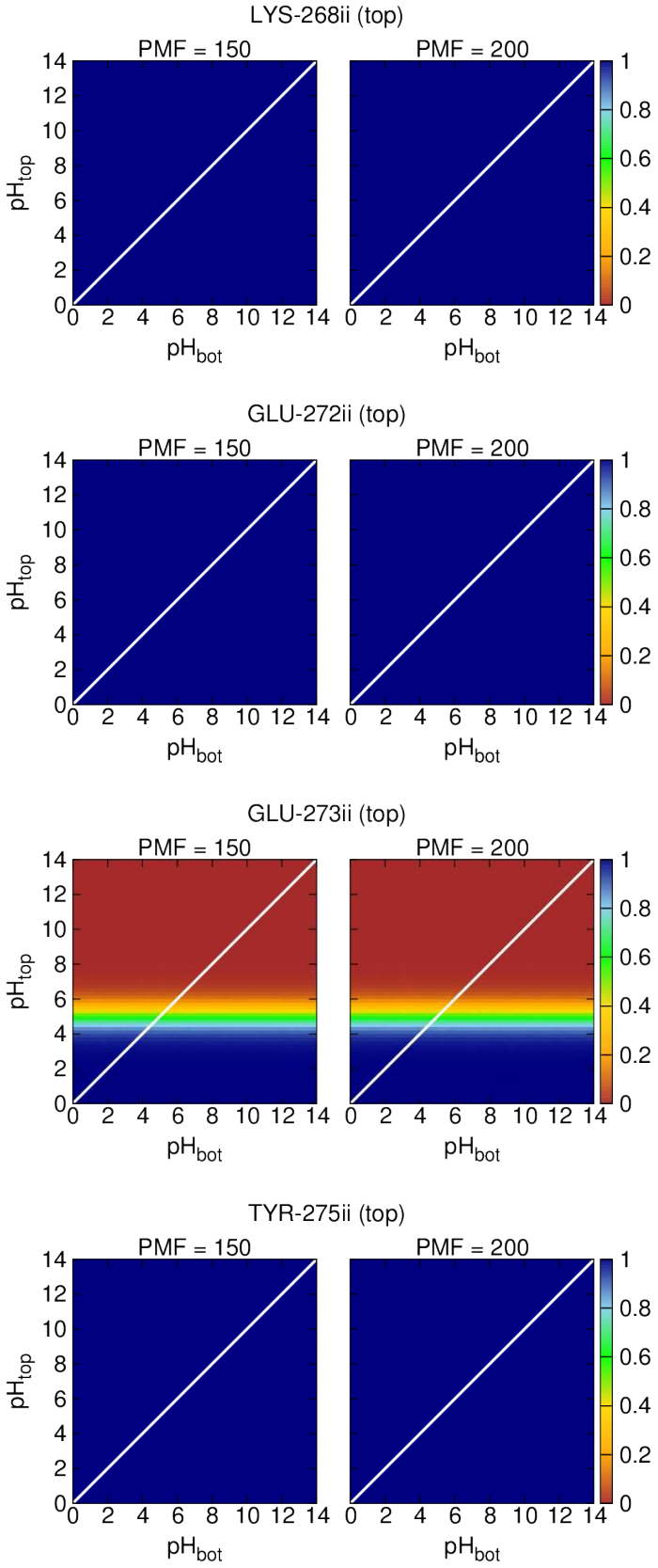
LYS-268ii (top)
PMF = 150
PMF = 200
GLU-272ii (top)
PMF = 150
PMF = 200
GLU-273ii (top)
PMF = 150
PMF = 200
TYR-275ii (top)
PMF = 150
PMF = 200
pH_top
pH_bot
0 2 4 6 8 10 12 14
0 0.2 0.4 0.6 0.8 1

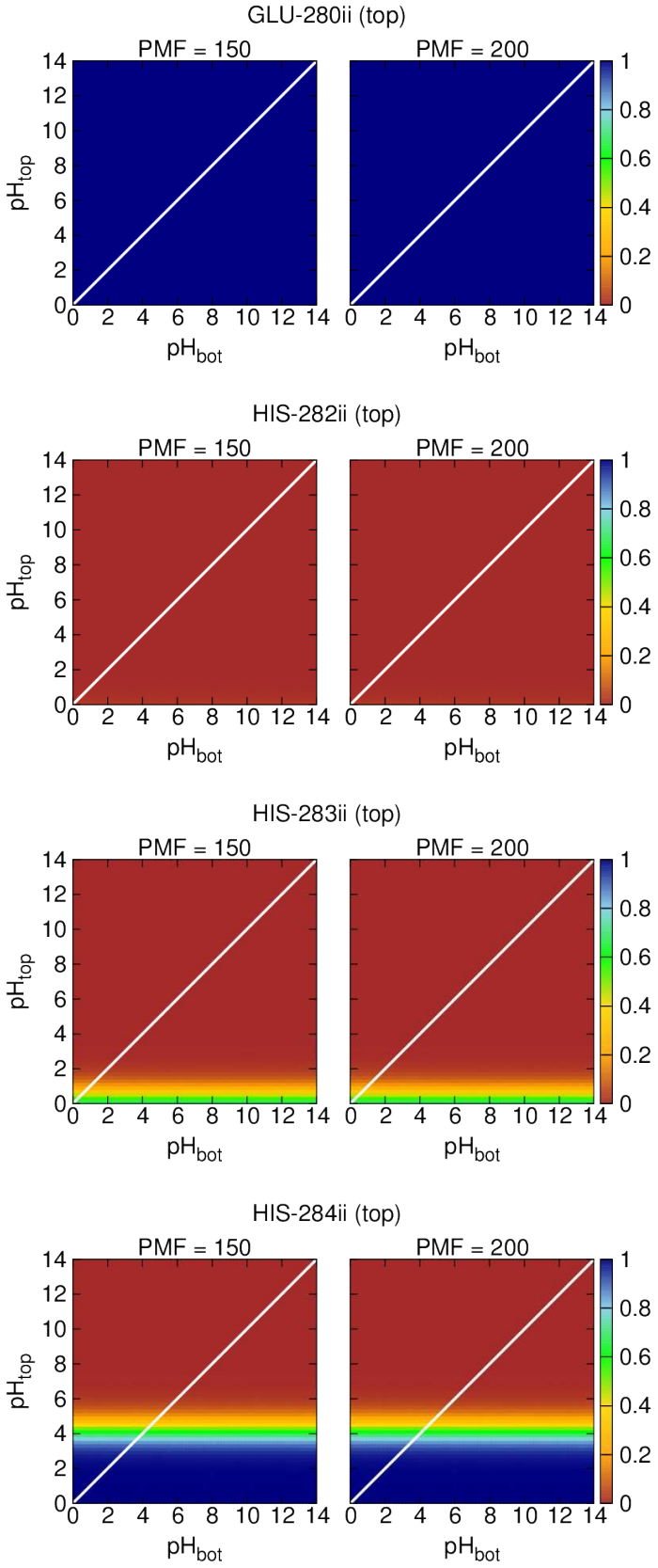
GLU-280ii (top)
PMF = 150
PMF = 200
HIS-282ii (top)
PMF = 150
PMF = 200
HIS-283ii (top)
PMF = 150
PMF = 200
HIS-284ii (top)
PMF = 150
PMF = 200
pH_top
pH_bot
0 2 4 6 8 10 12 14
0 0.2 0.4 0.6 0.8 1

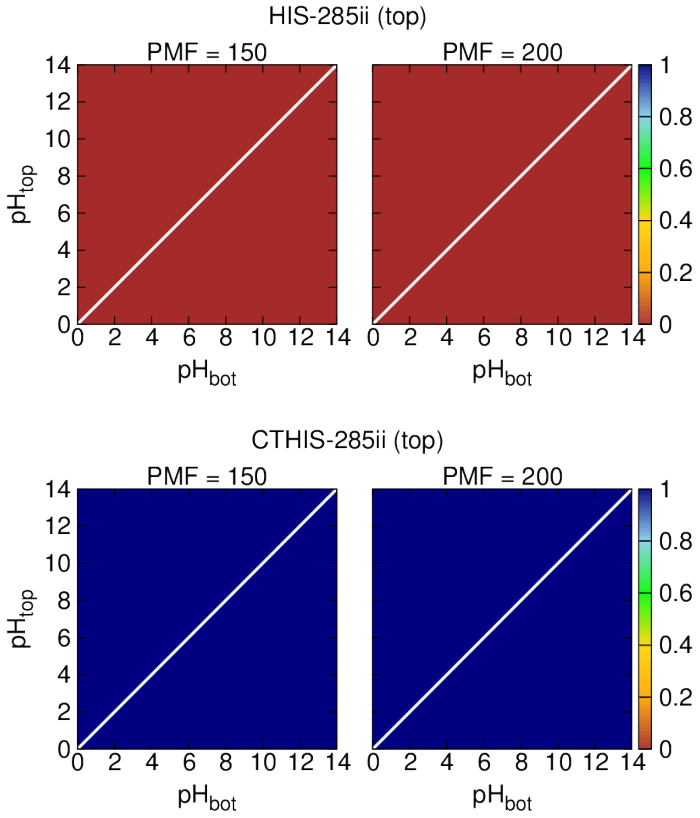
HIS-285ii (top)
PMF = 150
PMF = 200
pH_top
pH_bot
0 2 4 6 8 10 12 14
1
0.8
0.6
0.4
0.2
0
CTHIS-285ii (top)
PMF = 150
PMF = 200
pH_top
pH_bot
0 2 4 6 8 10 12 14
1
0.8
0.6
0.4
0.2
0